Real-Time, *in-situ* Detection of Pathogenic Bacteria on Food Surfaces Using a Surface-Scanning Coil Detector and Phage-Based Magnetoelastic Biosensors

by

Yating Chai

A dissertation submitted to the Graduate Faculty of
Auburn University
in partial fulfillment of the
requirements for the Degree of
Doctor of Philosophy

Auburn, Alabama
May 3, 2014

Keywords: magnetoelastic biosesnsor, surface-scanning coil detector, phage, pathogenic bacteria, food safety

Approved by

Bryan A. Chin, Chair, Professor of Materials Engineering
Zhongyang Cheng, Professor of Materials Engineering
Dong-Joo Kim, Associate Professor of Materials Engineering
Valery A. Petrenko, Professor of Pathobiology
Sang-Jin Suh, Associate Professor of Biological Sciences

Abstract

This research uses wireless magnetoelastic (ME) biosensors combined with a surface-scanning coil detector for the direct, real-time detection of *Salmonella* Typhimurium on fresh food surfaces. The ME biosensor consists of an ME resonator as the sensor platform and E2 phage as the bio-recognition element. For *in-situ* detection of surface bacterial contaminants, a surface-scanning coil detector was designed and its performance was evaluated. The designed coil was used to excite the ME biosensor and then measure the biosensor's signal in response to the potential presence of bacteria. A model of the sensor's longitudinal vibration and an equivalent electrical circuit of the detection system were constructed to theoretically evaluate the coil design and its effect on signal amplitude and detection distance. In order to explain the reason for the different signal amplitudes, a theory of mutual inductive coupling between a vibrating sensor and the coil detector was proposed. Two types of coil detectors were evaluated for design and comparison: solenoid and planar spiral coils. Based on the sensor's longitudinal vibration and the structure of the coils, the planar spiral coil detector was found to be more sensitive and to give a much larger signal amplitude at resonance. Furthermore, the ability to simultaneously measure multiple sensors on surfaces with the planar spiral coil has been demonstrated.

A gradual change of the resonant frequency was observed over time during the reaction between an E2 phage-coated ME biosensor and *S.* Typhimurium on fresh food surfaces. The effects of a humid environment were researched and the limit of detection

was statistically determined. This new technique eliminates the time-consuming and costly sample selection and preparation steps previously required.

Acknowledgments

I would like to thank my advisor Dr. Bryan Chin's expert guidance and persistent help during my five years' research at Auburn University. Without Dr. Chin's wisdom, patience and encouragement, this dissertation would not have been possible. I am also indebted to all my committee members, Dr. Zhongyang Cheng, Dr. Dong-Joo Kim, Dr. Valery A. Peternko and Dr. Sang-Jin Suh for their sincere help and support. Special thanks go to Dr. Zhongyang Cheng, who has helped me improve my scientific thought and research attitude. I am grateful to Charles Ellis, who has helped me with the coil's microfabrication and I-Hsuan Chen, who has provided all the biological samples and shared a great deal of biological knowledge.

I am thankful for all the support from Dr. Shin Horikawa, Dr. Suiqiong Li, Dr. Howard C. Wikle, Steve Best, Zhenyu Wang, Leslie C. Mathison, Dr. Kanchana Weerakoon, Dr. John Shu, Dr. Shichu Huang, Dr. Wen Shen, Dr. M-K Park, Dr. Lin Zhang, Dr. Peixuan Wu, Dr. Kewei Zhang, Zhizhi Sheng, Parick Bass, Naved Siddiqui, John Andress and Amanda Neer. I especially would like to give thanks to Dr. Shin Horikawa, who has shared with me countless discussions and given me lots of help on experiments.

Last but not least, I have immense gratitude for my family's love and understanding, for my Auburn friends' support, and for the encouragement from my friends' in China. Special thanks go to Dr. Dongye Zhao's family, Dr. Kai H. Chang's family, and Dr. Zhongyang Cheng's family; they treated me warmly as a part of their own family.

Table of Contents

List of Figures

List of Tables

List of Abbreviations

AFM	Atomic force microscopy
AUDF	the Auburn University Detection and Food Safety Center
BSA	Bovine serum albumin
CAD	Computer-aided design
CDC	the Centers for Disease Control and Prevention
CFU	Colony-forming unit
DC	Dielectric constant
DNA	Deoxyribonucleic acid
ELISA	Enzyme-linked immunosorbent assay
FDA	Food and Drug Administration
IDT	Interdigital transducer
LLMDA	Lawrence Livemore Microbial Detection Array
LOD	Limit of detection
MDG	Millennium Development Goals
ME	Magnetoelastic
PAHO	Pan American Health Organization
PC	Photonic crystal
PCR	Polymerase chain reaction
QCM	Quartz-crystal microbalance

MQCM Multichannel quartz-crystal microbalance

RH Relative humidity

RNA Ribonucleic acid

SAW Surface acoustic wave

SEM Scanning electron microscopy

SNR Signal-to-noise ratio

SPR Surface Plasmon Resonance

TBS Tris-buffered saline

USDA United States Department of Agriculture

WHO World Health Organization

Chapter 1

Introduction

1.1 Background and need

1.1.1 The challenge of foodborne illness and global public health

Bacteria and viruses are widely found in nature and in the environment, such as in food, soil, water and the intestinal tracts of humans and animals [1]. Foodborne diseases are caused by ingestion of contaminated foods and include a broad group of illnesses [2]. The foods and food products can be contaminated at different points in the food production and preparation process. It is estimated that infectious diseases cause about 40% of the total annual deaths world-wide [1]. The Centers for Disease Control and Prevention (CDC) estimate that each year roughly 1 in 6 Americans (or 48 million people) get sick, 128,000 are hospitalized, and 3,000 die of foodborne diseases [3, 4]. Estimating illnesses, hospitalizations, and deaths for various types of diseases is a common and important public health practice [5]. The following food groups have been identified as potential causes of foodborne illnesses:

1. Fresh vegetables have recently become recognized in the USA as the leading vehicle of illnesses associated with recent foodborne outbreaks. A recent case is the outbreak of Shiga toxin-producing *Escherichia coli* O157:H7 infections

linked to ready-to-eat salads in November 2013. In the past decade, fresh leafy produce has been responsible for more than 16 outbreaks of illness [6].

2. Reports of foods such as peanut butter and commercially canned food being contaminated with pathogens have also recently occurred. The outbreak of *Salmonella enterica* serovar Typhimurium infections linked to peanut butter included 714 cases in 46 states from 2008 to 2009. A recent outbreak resulted in 42 people being infected with *S.* Bredeney from peanut butter in November 2012 [7].
3. Microwavable products and ready-to-cook pizzas have recently been associated with outbreaks of *E. coli* O157:H7 infections and *Salmonellae* contamination [8].
4. Poultry, eggs and meat products are still important vehicles of bacterial pathogens. More than 60% of pathogen outbreak reports in the previous five years are associated with poultry and meat products. Between 1998 and 2008, poultry, fish and beef were consistently responsible for the greatest proportion of foodborne illness outbreaks. Considering the emphasis that reducing pathogen contamination of poultry and meat products has received, relatively little progress has been made in reducing the incidence of human disease during the past decade [9, 10].

The problems about food safety and public health in under-developed countries are always combined with poverty and hunger. The international Millennium Development Goals (MDG) aimed to reduce the burden of foodborne diseases in

developing countries, which is also related to children and the poor (Figure 1.1).

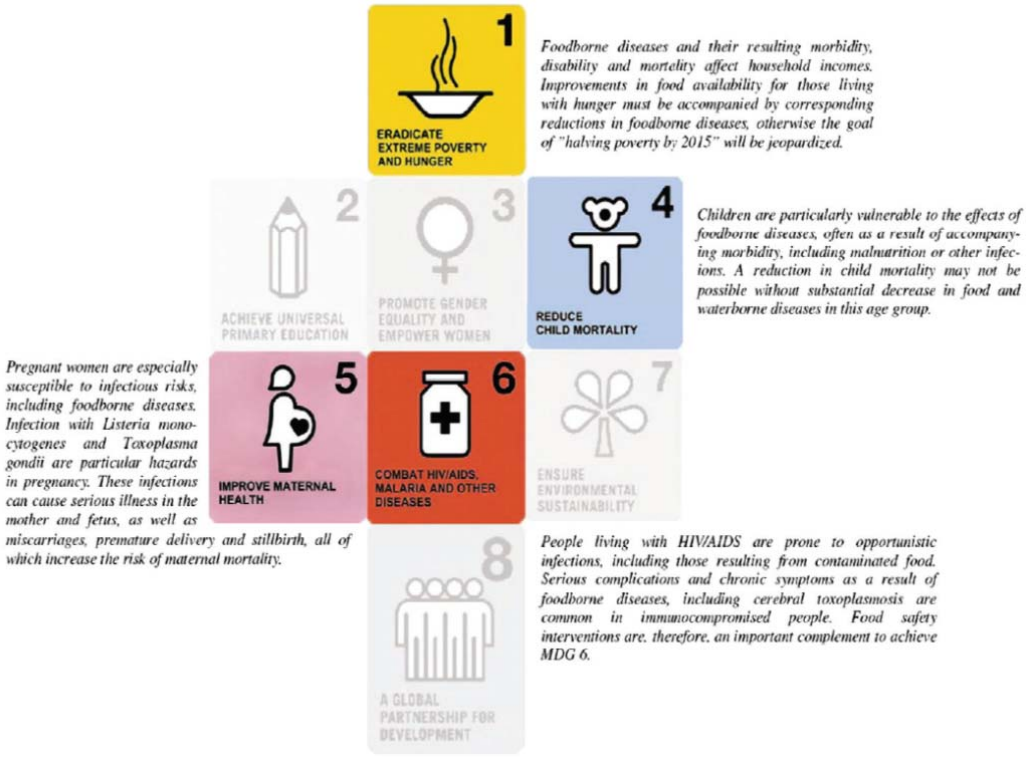

Figure 1.1 Foodborne disease and the millennium development goals [15].

Meanwhile, globalization is no longer a philosophy but a description of commerce. Growing international trade, migration and travel accelerate and widen the spread of dangerous pathogens and contaminants in food [5]. What once were only local foodborne disease outbreaks have now become a potential threat to the entire globe in this interconnected and interdependent world. For instance, 80% to 90% of the incidence of Salmonellosis in Scandinavian countries is attributed to international travels [5]. A recent estimate suggests that approximately 30% of all new globally emerging infections over the past 60 years included pathogens commonly transmitted

through food [14].

Because of globalization, the problems of foodborne illness have become more complex: new pathogens emerge and established pathogens appear in unexpected new food vehicles. Consumer tastes and requirements change, populations age and migrate, and the technologies and trade that go into the products continue to evolve. The past decade has been recognized for having more microbiological food safety challenges for the food industry than ever before. Many of these microbial threats were not new but rather presented themselves under unanticipated circumstances [23]. Emerging and reemerging pathogens have become greater foodborne threats in past years. More and more newly recognized and un-established foodborne pathogens challenge public health. Medical costs and productivity losses from foodborne illness are in the range of 6.6 billion to 37.1 billion U.S dollars [11]. The annual economic losses caused by the food-borne illnesses are estimated to be 2.9 billion to 6.7 billion U.S. dollars according to the United States Department of Agriculture (USDA) [12]. The full extent of the burden and cost of unsafe food is currently still unknown but its impact on global health, trade and development is likely to be profound. The surveillance and prevention of food risk and biological terrorism are of central importance all over the world.

Therefore, food safety and public health become a global mission and need worldwide cooperation.

1.1.2 Bioterrorism and biodefense

Foodborne illness is not the only problem that poses a severe risk to public safety. The events of September 11, 2001 reinforced the need to enhance the security of the U.S., and Congress responded by passing the Public Health Security and Bioterrorism Preparedness and Response Act of 2002 (the Bioterrorism Act) [16]. A bioterrorism attack is the deliberate release of viruses, bacteria, or other germs to cause illness or death [17]. These germs are often found in nature, but they can sometimes be made more harmful by increasing their ability to cause disease, spread, or resist medical treatment. Bioterrorism, which makes use of bacteria, viruses, fungi, and/or toxins as a bio-weapon, has been publicly recognized as an emerging danger [18]. The CDC has, thus far, identified 35 potential bioterrorism agents and classified them into three categories [19]. The highest priority Category A agents include organisms that pose a risk to national security because they can be easily disseminated or transmitted from person to person, result in high mortality rates and have the potential for a major public health impact, cause public panic and social disruption, and require special action for public health preparedness.

Biodefense uses medical measures to protect people against bioterrorism. The goal of biodefense is to integrate the sustained efforts of national and homeland security, and public health, intelligence, diplomatic, and law enforcement communities. In fact, the funding for civilian biodefense dramatically increased after the 2001 anthrax attacks, and over $4 billion of funding has been maintained since 2002 [20-22]. The budget transition clearly indicates that there is a need for

comprehensive biodefense systems that enable the nationwide surveillance and prevention of bioterrorism. As part of the ongoing efforts to secure the safety of food as well as to guard against possible bioterrorism, the role of pathogen detection technologies has become vital. Recently, much research has been focused on developing label-free biosensors, which are meant to be low-cost, rapid, user-friendly, and adequate for on-site pathogen detection for both food safety and biosecurity.

1.1.3 Surveillance systems

When an established pathogen appears in a new food vehicle, many questions arise. The most important question is how to improve control and prevention. Figure 1.2 shows the cycle of public health prevention and control [15]. When a problem of foodborne illness arises, an epidemiological investigation may clarify its etiology, source and impact. For well-understood pathogens, the established process of prevention and control measures can be directly applied. For unknown pathogens, applied research is needed to answer questions and produce treatment information. The results of this research can then be used to develop the prevention and control measures which are related to the special target. The documents and experiences of prevention and control measures can be summarized for surveillance. With a successive and high-efficiency circle, the infection decreases and the prevention is more successful. However, assembling this information is time-consuming and may take decades.

Figure 1.2 The cycle of public health prevention and control [15].

Passive surveillance systems collect information on outbreaks depending on the public's willingness to report illnesses and the public health authorities to investigate and submit reports. In the U.S., the passive Foodborne-Disease Outbreak Surveillance System, managed by the Centers for Disease Control and Prevention, is designed to investigate foodborne outbreaks and establish both short-term control measures and long-term improvements to prevent similar outbreaks in the future [23, 24]. On the other hand, FoodNet is one of the operative surveillance systems in the USA. FoodNet is the collaboration between the CDC, the US Food and Drug Administration (FDA), and the U.S. Department of Agriculture (USDA). FoodNet was created in 1996 to conduct population-based, active surveillance for foodborne infections in the USA [5]. The main objectives of FoodNet include the determination of the epidemiology of foodborne diseases, and the investigation of the link between certain foods and the proportion of foodborne disease. FoodNet conducts surveillance for *E. coli* O157:H7, *Campylobacter* spp., *Listeria* spp., *Salmonella* serovars, *Shigella* spp.,

Yersinia spp., *Vibrio* spp., *Cryptosporidium*, and *Cyclospora*. This has been successful in monitoring, tracking trends, and defining risk factors for causes of foodborne illnesses, and in estimating the burden of foodborne illnesses in the USA [15, 24].

Surveillance systems for foodborne disease vary in capacity by country. There is not an outstanding system that could serve as a model for different countries or different conditions. In general, the developed countries have more funding for their surveillance programs. In order to build a successive and high efficiency surveillance system, there are three suggestions for surveillance system improvement:

1. The evaluation system for an outbreak investigation can be modeled as a three-dimensional food safety box. An outbreak investigation is usually caused by a specific pathogen to a specific food. However, in the first case of *E. coli* O157: H7, the same organism was identified in two separate outbreaks at the same restaurant chain. For some pathogens, the process can be complex and difficult to detect. As global food transportation and various sources and vehicles for foodborne illness increase, attribution of outbreaks become more complex [25]. Therefore, the problem can be considered in three dimensions: the range of pathogens, the range of transmission routes and vehicles, and the flow of the food from production on farm to final consumption. In this way, a particular issue in food safety can be localized in all three dimensions.

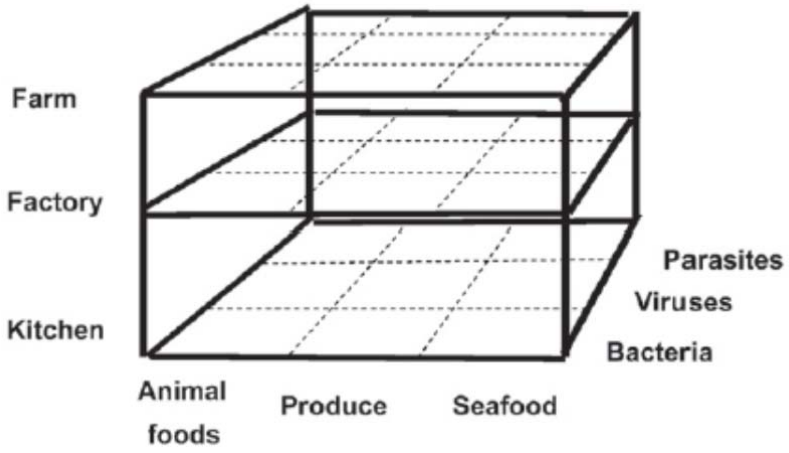

Figure 1.3 The food safety box in which problems and solutions can be localized, along with the dimensions of pathogen, food vehicle of transmission and level of processing [15].

2. The international coordination in surveillance system is becoming more and more important. The information and data can be rapidly and efficiently shared. The data documents of foodborne disease can be transmitted through the food supply chain and to the place where the food production was contaminated. The international organizations (WHO, PAHO) are building networks in different parts of the world that cooperate with several governments to detect pathogens, prevent outbreaks and organize the international food supply chain.
3. A new, rapid, and robust pathogen detection technique should be developed for all steps of the food supply chain and be suited in different detection environments [26]. As the current pathogen detection and illness certification are accurate but time-consuming, a rapid, “first-line” food safety test is

necessary and significant. The requirements of the detection method are fast-response, low-cost, stable in various environments, highly efficient and technically friendly.

1.2 Motivation and objectives of this research

Typical microbiological methods for pathogen detection, such as culturing, immunoassay, and PCR offer very high sensitivities [27, 28]. However, they require pre-analytical sample preparation, which generally includes sample collection, separation of a target pathogen from food, increasing pathogen concentration, and achieving a desired analysis volume from a large amount of samples before detection. These processes are time-consuming, leading to delays in obtaining screening results. More importantly, food samples have to be delivered to laboratories for culture preparation and analysis. Label-free biosensors are available in today's market [29]. However, they also require sample preparation prior to the actual testing (i.e., sampling from fresh produce, purification and concentration of the collected samples, and injection of the purified/concentrated samples into a flow system where a biosensor resides). Due to the complexity of these test procedures and requirements for expensive equipments and highly trained personnel, current food safety controls mainly rely on control of worker/environment hygiene in the food processing industry, rather than direct pathogen detection.

Food can be contaminated by pathogenic bacteria at any stage of a food cycle: production, packaging, transport, and consumption [30]. In order to test the food

safety at each stage of the food cycle, a rapid, user-friendly, and low-cost detection method is required. The goal of this research is to design, develop, and demonstrate an accurate, easy-to-use, and inexpensive biosensor for the detection of *Salmonella* contamination on globe fruits and vegetables. In the agricultural field, globe fruits and vegetables (e.g., watermelons and tomatoes) will be picked and placed in a disposable plastic bag that serves as a portable test chamber. The ME biosensors will then be placed directly on the surface of the food, the bag sealed, and the biosensors interrogated wirelessly to determine whether the surface of the produce is contaminated with *Salmonella*. The biosensors will then be retrieved with an electromagnet. The tested tomato and plastic bag will then be properly disposed. Figure 1.4 shows the envisioned method of *Salmonella* detection on tomatoes. The detection sequence and estimated time for each step are:

1) Place a tomato in a test bag. Distribute biosensors onto the tomato. Seal the bag and allow binding with *Salmonella* to occur.
2) Measure biosensors wirelessly and simultaneously.
3) Monitor resonant frequency shifts of the biosensors.
4) Retrieve biosensors with an electromagnet and dispose of the bag and tomato.

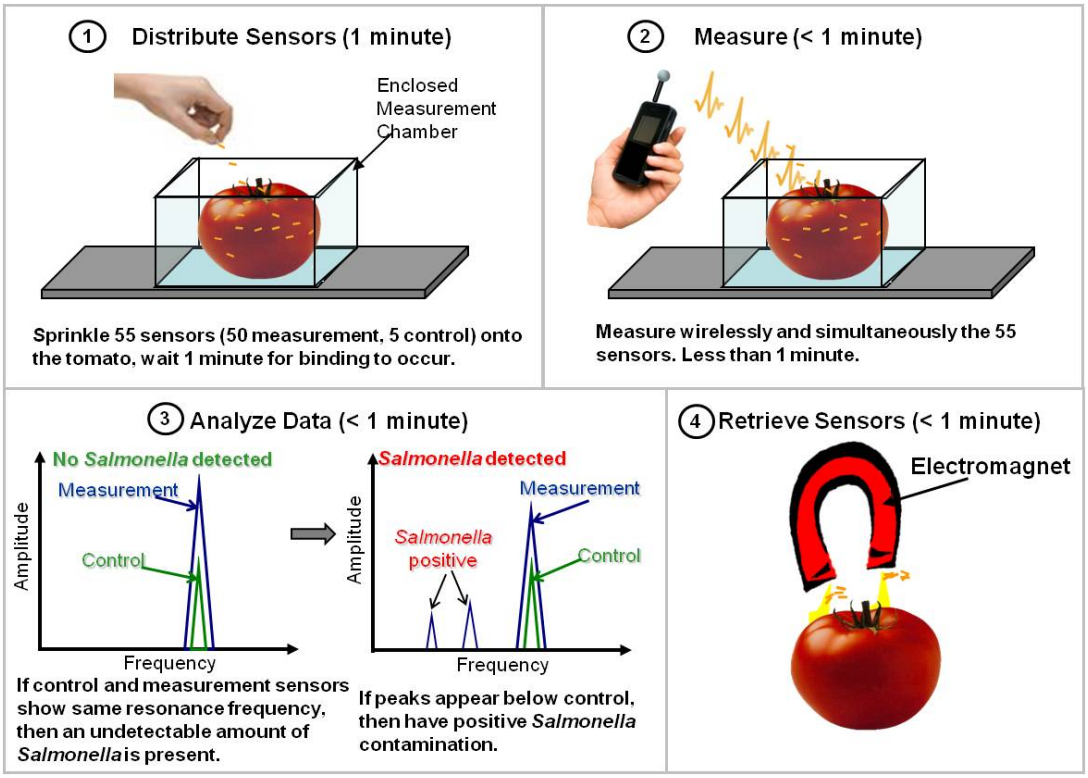

Figure 1.4 The vision of direct bacteria detection on food surfaces.

The study of ME biosensors for bacterial pathogen detection has been discussed for several years. In previous work, the ME biosensors required placement inside the solenoid coil for the frequency measurement, and then they were moved out of the coil for exposure to bacteria on the food surface [31-34]. Hence, this detection was cumbersome and not in real-time. In order to pursue real-time *in situ* bacteria detection directly on food surfaces, the primary objective of this research is to design and fabricate different surface-scanning coil detectors for use with phage-coated ME biosensors for the wireless, "extracoil" detection of foodborne pathogens. To accomplish the objective, this research focuses mainly on the following three topics:

1. Specific binding between E2 phage and *Salmonella* Typhimurium on fresh food surfaces.
2. Design and microfabrication of surface-scanning coil detectors for ME biosensors and comparison of different coil structures for signal optimization.
3. Using the designed coil detector and ME biosensors for direct, real-time *S.* Typhimurium detection on food surfaces.

1.3 Dissertation organization

In this chapter, the need for high-performance biosensors for on-site pathogen detection was described, and the objectives of the present research were stated. The rest of this dissertation is organized as follows:

Chapter 2 briefly reviews major bacterial detection methods and discusses reasons for the current shift towards the development of label-free biosensors and surface-scanning coil detectors.

Chapter 3 describes the fundamentals, detection principle, and fabrication methods of phage-based ME biosensors in depth.

Chapter 4 presents the possibility of *S.* Typhimurium detection on fresh food surfaces. Multiple ME biosensors are utilized for the detection in different bacterial solutions. Control biosensors without phage were also used to compensate for environmental effects and non-specific binding.

Chapter 5 presents the theoretical research on detection technique with coil detector and ME biosensors. A theory of the sensor's mutual inductance with the

measurement coil is proposed. The simulation results of magnetic flux change and the experiment data of frequency signal are discussed and compared.

Chapter 6 investigates a new design of microfabricated planar coil detector. A comparison of a planar-spiral coil and a solenoid coil is discussed about the signal amplitude, detection distance, and the working space. Based on the sensor's longitudinal vibration and the structure of the coils, the planar spiral coil detector was found to be more sensitive at detecting the coupled magnetic flux changes. In addition, both numerical simulation data and experimental results demonstrate that the planar coil detector dramatically improves the detection distance, which is significant for surface scanning, especially with large curvature or rough surfaces.

Chapter 7 uses the ME biosensors for the real-time *in situ* bacteria detection on food surfaces. A gradual change of the resonant frequency was observed over time during the reaction between an E2 phage-coated ME biosensor and *S.* Typhimurium on a tomato surface. The LOD was statistically determined to be lower than 1.5×10^3 CFU/mm^2 with a confidence level of difference higher than 95 % ($p < 0.05$).

Finally, Chapter 8 presents an overall summary and conclusions of this dissertation.

Bibliography

1. CDC Estimates of Foodborne illness in the United States, http://www.cdc.gov/foodborneburden/
2. http://www.cdc.gov/features/dsfoodborneoutbreaks/
3. http://www.cdc.gov/salmonella/outbreaks.html
4. http://health.mo.gov/data/btsurveillance/
5. E.C., Todd. Challenges to global surveillance of disease patterns, *Marine Pollution Bulletin* 53: 569-578, 2006.
6. http://www.cdc.gov/ecoli/2013/O157H7-11-13/index.html
7. http://www.cdc.gov/salmonella/typhimurium/index.html
8. http://ag.udel.edu/abc/epdr.html
9. http://www.foodsafetynews.com/2013/06/20-years-of-foodborne-illness-data-show-poultry-fish-beef-continue-to-be-leading-sources-of-outbreaks/
10. http://extension.missouri.edu/publications/DisplayPub.aspx?P=G8904
11. E.C. Todd. Cost of acute bacterial foodborne disease in Canada and the United States, *International Journal of Food Microbiology* 9: 313-326, 1989.
12. http://www.ers.usda.gov/Data/FoodborneIllness/
13. http://www.actionbioscience.org/newfrontiers/davis.html
14. W., Jongen. *Improving the Safety of Fresh Fruit and Vegetables*, Woodhead Publishing Limited, Cambridge. 2005.

15. R.V., Tauxe, M.P., Doyle, T., Kuchenmuller, J., Schlundt, C.E., Stein, Evolving public health approaches to the global challenge of foodborne infections, *International Journal of Food Microbiology* 139: S16-S28, 2010.
16. http://emergency.cdc.gov/agent/agentlist-category.asp
17. http://en.wikipedia.org/wiki/Biodefense
18. http://www.homelandsecuritynewswire.com/topics/bioterrorism-biosecurity
19. http://doh.dc.gov/service/bioterrorism-surveillance
20. http://www.cbp.gov/xp/cgov/trade/trade_programs/is_initiatives/bioterrorism/
21. http://www.aana.com/resources2/Pages/Bioterrorism-Information-and-Resources-Links-.aspx
22. http://www.sciencedaily.com/articles/b/bioterrorism.htm
23. http://www.bt.cdc.gov/agent/anthrax/faq/.
24. http://www.fsis.usda.gov/wps/portal/fsis/topics/recalls-and-public-health-alerts/recall-case-archive
25. http://www.medscape.com/viewarticle/474667
26. http://www.fda.gov/Food/FoodSafety/ProductSpecificInformation/EggSafety/ucm24158.htm
27. T.W., Alexander, T., Reuter, E., Okine, R., Sharma, and T.A., McAllister. Conventional and real-time polymerase chain reaction assessment of the fate of transgenic DNA in sheep fed Roundup Ready (R) rapeseed meal, *British Journal of Nutrition* 96(6): 997-1005, 2006.

28. K., Lind, A., Stahiberg, N., Zoric, and M., Kubista. Combining sequence-specific probes and DNA binding dyes in real-time PCR for specific nucleic acid quantification and melting curve analysis, *Biotechniques*, 40(3): 315-319, 2006.

29. S. Li, Y. Li, H. Chen, S. Horikawa, W. Shen, A. Simonian and B.A. Chin. Direct detection of *Salmonella* Typhimurium on fresh produce using phage-based magnetoelastic biosensors, *Biosensor and Bioelectronic* 26 (4): 1313-1319, 2010.

30. http://www.ers.usda.gov/Briefing/FoodSafety/

31. R.S. Lakshmanan, R. Guntupalli, J. Hu, D.-J. Kim, V.A. Petrenko, J. M. Barbaree, and B.A. Chin. Phage immobilized magnetoelastic sensor for the detection of *Salmonella typhimurium*, *Journal of Microbiological Methods* 71(1): 55-60, 2007.

32. S. Huang, H. Yang, R.S. Lakshmanan, M.L. Johnson, J. Wan, I.-H. Chen, H.C. Wikle, V.A. Petrenko, J.M. Barbaree and B.A. Chin. Sequential detection of *Salmonella* Typhimurium and *Bacillus anthracis* spores using magnetoelastic biosensors, *Biosensors and Bioelectronics* 24: 1730-1736, 2009.

33. S. Li, Y. Li, H. Chen, S. Horikawa, W. Shen, A. Simonian and B.A. Chin. Direct detection of *Salmonella* Typhimurium on fresh produce using phage-based magnetoelastic biosensors, *Biosensor and Bioelectronic* 26 (4): 1313-1319, 2010.

34. M. Park, H.C. Wikle, Y. Chai, S. Horikawa, W. Shen, and B.A. Chin. The

effect of incubation time for *Salmonella* Typhimurium binding to phage-based magnetoelastic biosensors, *Food Control* 26(2): 539-545, 2012.

Chapter 2

Review of the Literature on Bacterial Detection Methods

2.1 Conventional detection methods

Traditional methods for enumerating bacteria are based on the ability of bacteria in a sample to grow into visible colonies on a defined nutrient medium. Theoretically, a colony is derived from a single bacterial cell which provides the identification of a very small number of bacterial pathogens. However, in a culture-based method, cumbersome and lengthy experimental steps, such as pre-enrichment, selective enrichment, biochemical screening, and serological confirmation, are required. This may take up to 5 to 7 days to complete, depending on the target organisms [1].

The polymerase chain reaction (PCR) method, which is currently considered by many to be the golden standard for microbial detection, amplifies small quantities of genetic material to determine the presence of bacteria [2]. It requires rigorous sample preparation, complex reactive components of limited shelf life, precise temperature regulation, a complex detection process and trained personnel. Similar to the culture-based method, PCR is labor-intensive and time-consuming. The recent advances in PCR technologies, such as the real-time PCR [3], digital PCR [4], and microfluidic PCR [5], could provide better performance in terms of assay time, reagent volume, and cost. However, these PCR variants additionally require the use of

reporter dyes and/or fluorescent-labeled probes, resulting in an increase in total assay cost and complexity [5]. Thus, these PCR methods cannot meet general performance criteria for on-site detection of bacterial pathogens.

As an alternative, the enzyme-linked immunosorbent assay (ELISA) has been developed and widely used for the determination of food safety [6-8]. The ELISA is an immunological technique that employs two kinds of antibodies with an enzyme. After a target antigen is captured by a primary antibody immobilized on an ELISA plate and linked with the enzyme by a secondary antibody, optical signals can be generated through biochemical reactions between the enzyme and a chromogenic substrate that is subsequently added [9]. Although the ELISA can reduce assay time and cost, it still takes hours of assays. Hence, there will be much work to do before the ELISA becomes a real alternative.

2.2 Biosensor techniques

The biosensor industry is rapidly expanding with relatively low-cost and rapid detection methods. According to the market analysis of biosensors, the annual growth rate is 4.5% with a total market value of $563 million [10]. A biosensor is an analytical device incorporating a biological sensing element into a transducer system. The sensing element binds a biological agent of interest to the biosensor platform through highly specific bonding. The bio-recognition elements for biosensors are divided into three groups: biocatalytic, bioaffinity and hybrid receptors. The choice of bio-recognition element depends on selectivity, sensitivity, and longevity among

others. The transducer/platform converts an observed change (physical or chemical) into a measurable signal. Based on the signal transducer, biosensors can be divided into electrochemical, optical, thermal, and mass-sensitive biosensors.

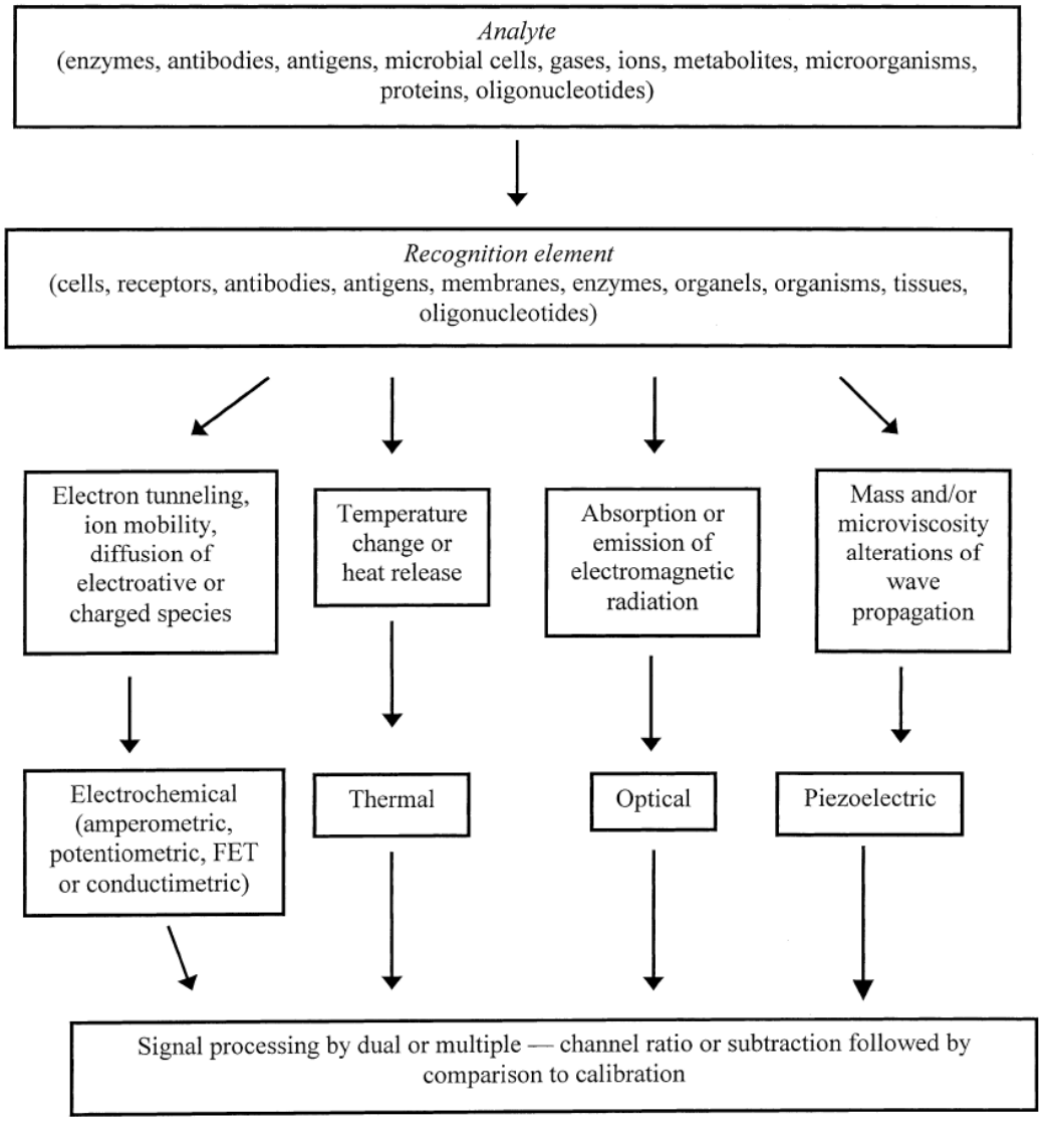

Figure 2.1 Bio-recognition elements and transducers employed in construction of biosensors [11].

2.2.1 Electrochemical biosensors

At present, electrochemical technologies play a very important role in clinical diagnosis, biochemical analysis, and environmental monitoring. The interaction of the target analytic and the recognition elements creates an electrical signal, which represents the analytical information [12]. Biosensors based on the electrochemical transducer have the advantages of being fast and economical. For an electrochemical biosensor, biologically active materials, usually enzymes or antibodies, are immobilized on the surface of the electrode. When microorganisms metabolize uncharged and weakly charged substances, such as carbohydrates, fats or proteins, into highly charged end products, such as organic acids, fatty acids, and amino acids, the electric current changes in this bio-medium. Electrochemical biosensors transmit impedimetric, potentiometric or amperometric signals. Impedimetric biosensors are based on the change of conductivity of the medium when the microorganisms metabolize uncharged substrates. Impedance is usually measured by a bridge circuit. A reference module is necessary to measure nonspecific changes in the test module. Amperometric biosensors measure the current generated by the chemical reaction of an electroactive species under an applied potential, which is proportional to the concentration of the electroactive species in the solution. Compared to other types of electrochemical biosensors with logarithmic concentration dependence, amperometric biosensors that have a linear relationship are more suited for bacterial detection. Potentiometric biosensors measure the potentiometry in relation to a reference electrode. Figure 2.2 shows a schematic of a potentiometric biosensor: a

semiconductor immune biosensor that detects potential changes associated with the formation of an antibody complex [13]. With the controlling of the conductivity of the n-channel region in the p-type semiconductor by the electrical field strength, the application of a voltage between the source and drain electrodes is the measured signal for the potentiometric biosensor [14].

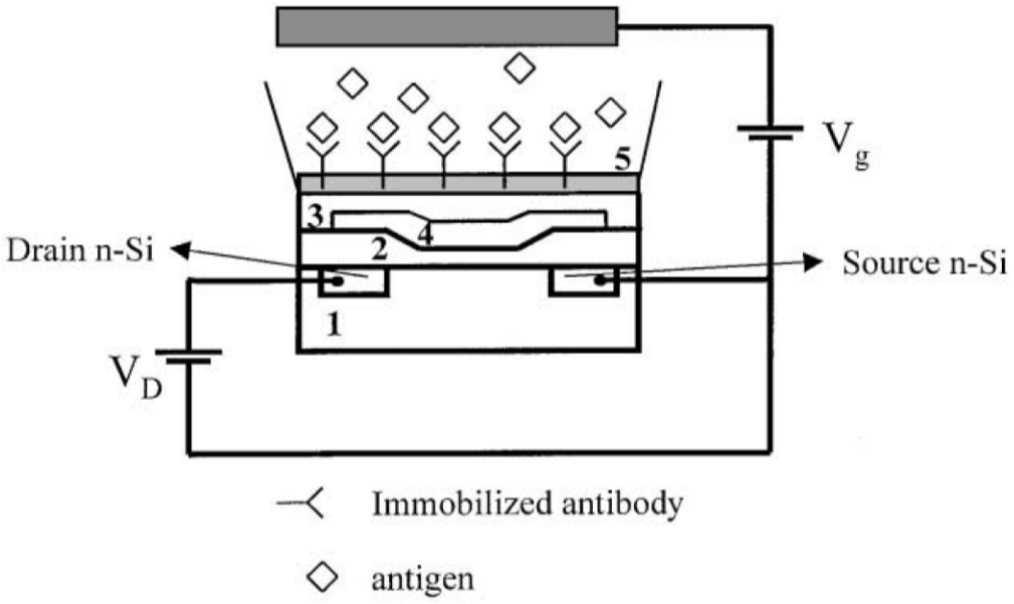

Figure 2.2 Schematic of a potentiometric transducer biosensor [13].

2.2.2 Optical biosensors

Optical biosensors, which detect by absorption or emission of electromagnetic radiation, are very attractive because of their quick and direct ability to detect bacteria. A large variety of optical methods has been used in biosensors: ellipsometry, spectroscopy (e.g., luminescence, phosphorescence, fluorescence, and Raman), interferometry, spectroscopy of guided modes in optical waveguide structures and

surface plasmon resonance. The refractive index, absorbance and fluorescence properties of analytic molecules are the measurement data for optical biosensors [15].

Surface Plasmon Resonance (SPR) detection, which is based on the internal reflection of light, is one kind of the refractive index-based detection techniques [16]. SPR is a quantum optical electrical phenomenon based on the fact that energy carried by photons of light can be transferred to electrons in a metal. This transfer can be observed by measuring the amount of light reflected by the metal surface. As shown in Fig. 2.3, SPR is a charge-density oscillation that may exist at the interface of two media with dielectric constants of opposite signs [17]. A change in the condition of the metal surface, such as antibody-antigen binding, results in a change of the refractive index. SPR biosensors are able to detect tiny changes in refractive index when cells bind to receptors immobilized on the transducer surface. The detection of the SPR change can be accomplished by monitoring the resonant angle [18], resonant wavelength [19], resonant intensity change [20], or the changes in phase and polarization [21-22]. In the past few years, SPR has been applied in molecular biology for detection of proteins or DNA molecules for food safety and bio-security. The detection limit for proteins can be down to nanomolar or even picomolar concentrations with a signal amplification. Although rapid and remote sensing can be achieved with the SPR biosensors, they still have some limitations: easy interference of signals and narrow concentration range for detection [23]

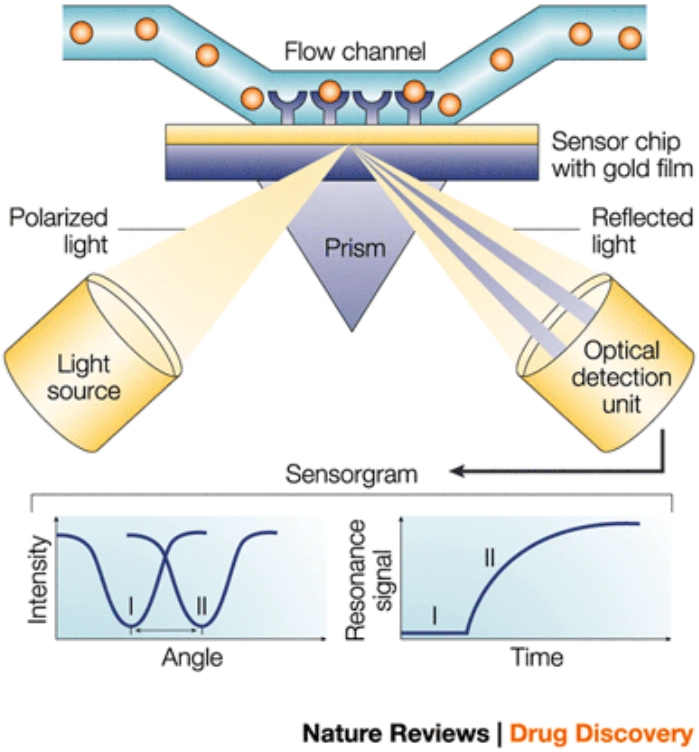

Figure 2.3 The phenomenon of interaction between light waves and biomolecules [17].

Fluorescence-based detection is also a widely used optical method for biosensing [24]. A fluorescence biosensor monitors the frequency change of electromagnetic radiation. In a typical fluorescence measurement, a fluorophore is excited by a specific wavelength of light and emits light at a different wavelength [25]. Because single molecules could be repeatedly excited and detected to produce a bright and measurable signal, the sensitivity of the fluorescence biosensor can reach single-cell level. In general, the fluorescence detection has three types: 1) direct sensing of a target molecule that is fluorescent; 2) indirect sensing of a fluorescent-labeled target molecule; and 3) fluorescence resonance energy transfer (FRET). Unlike the typical

fluorescence measurement, FRET can generate a unique fluorescence signal when two fluorophores are paired. The emission wavelength of one overlaps with the excitation of the other, and the excitation of one of them will stimulate fluorescence of the complementary pairing fluorophore [26].

2.2.3 Thermal biosensors

Thermal biosensors detect a change in temperature within the reaction medium caused by biological reactions (absorption or evolution of heat). Thermal biosensors are based on the principle that the total heat evolution or absorption in a biochemical reaction is proportional to the molar enthalpy change and to the total number of product molecules created in the reaction [27, 28]. In order to improve thermal biosensor's sensitivity, recycling the co-enzyme or the substrate resulting in enzymatic amplification was used to improve the thermometric measurement [29]. A thermistor, which is a very sensitive temperature transducer, was also used for the sensitivity improvement. The thermistor has several resistors with a high negative temperature coefficient of resistance [30]. Figure 2.4 shows a conventional thermal biosensor.

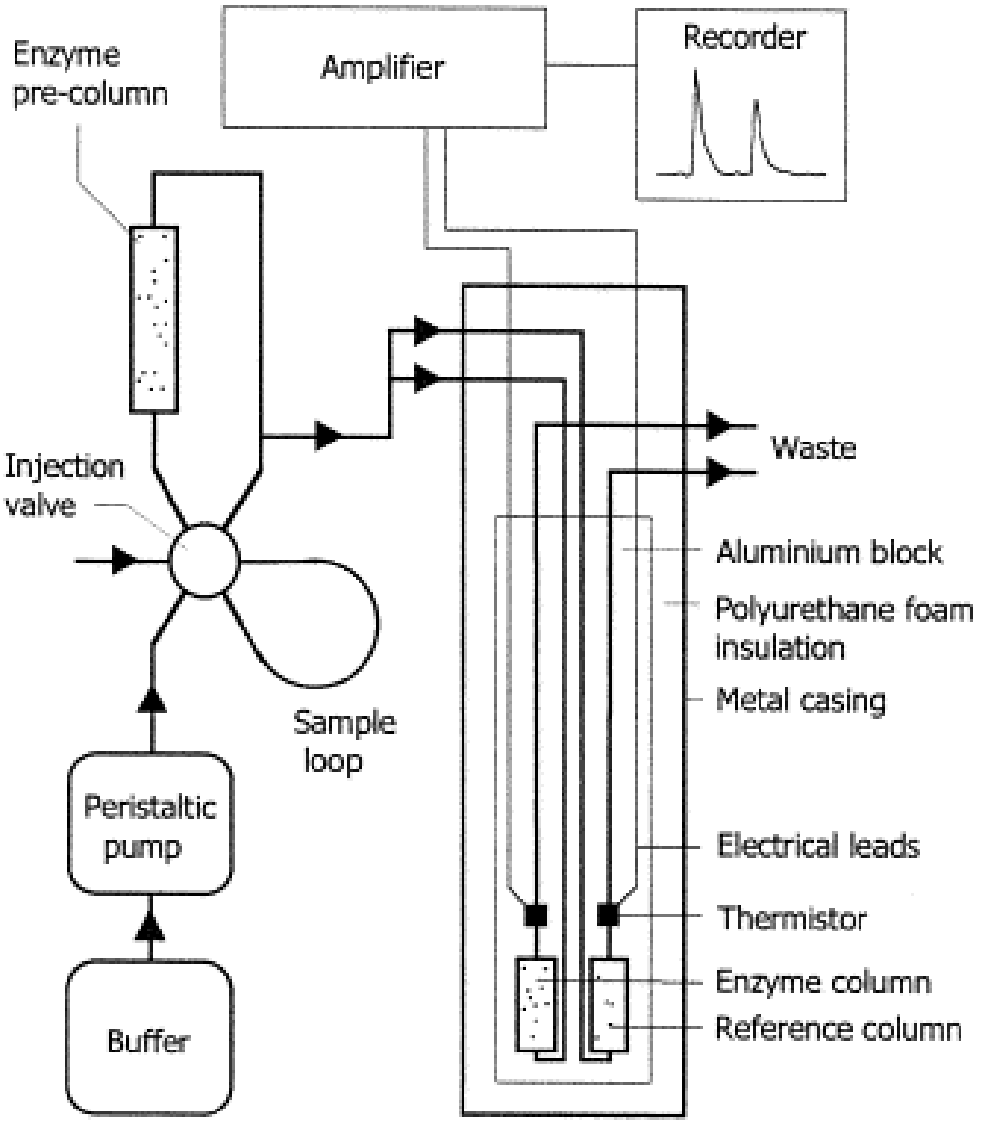

Figure 2.4 The schematic of a conventional thermal biosensor [27].

2.2.4 Acoustic wave biosensors

Acoustic wave (AW) biosensors are a class of the microelectromechanical system which transduces an input electrical signal into a mechanical wave to sense a physical phenomenon. AW transducers can sense the change of pressure, strain, torque, temperature and mass [12]. As our research of the magnetoelastic biosensor is one of

mass-sensitive AW biosensors, the research about AW biosensors will be discussed in chapter 3.

2.2.5 The development of portable biosensors

Recently, rapid pathogen detection with a portable device became one of most popular research topics. The researchers from Lawrence Livermore National Laboratory created a three-inch biodetector for quickly scanning and detecting bacteria and viruses at once (Figure 2.5) [31]. The Lawrence Livermore Microbial Detection Array (LLMDA) device, with a size of one-inch wide and three-inch long, is packed with 388,000 probes to detect multiple viruses and bacteria. The process requires a sample of DNA or RNA labeled with a fluorescent dye, and applied across LLMDA. A scanner analyzes the fluorescent response, measures the peak frequencies and identifies bacterium/virus by comparison with known fluorescent signatures. The detector can identify more than 3,000 different viruses or bacteria in 24 hours [32].

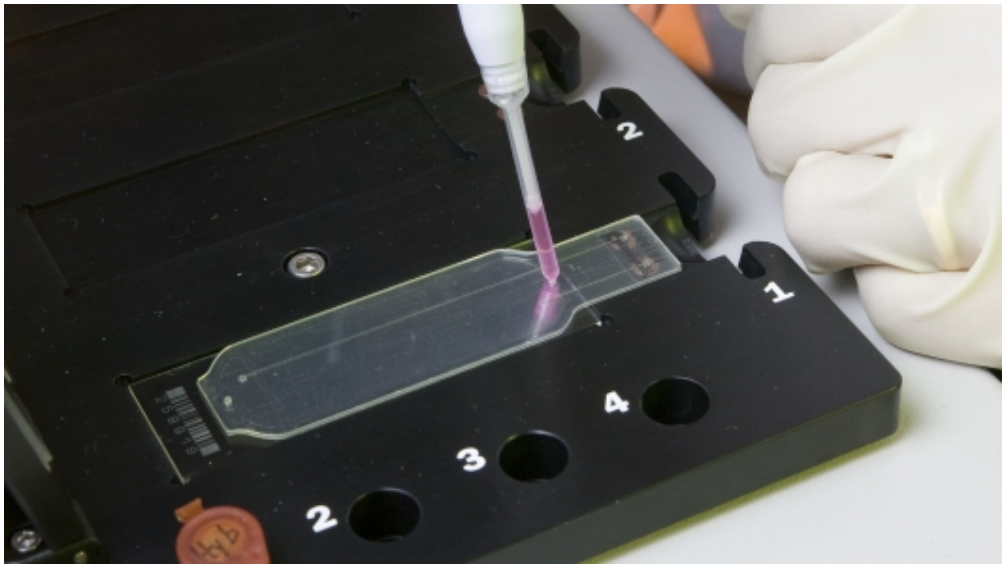

Figure 2.5 The Lawrence Livermore Microbial Detection Array [31].

Meanwhile, researchers at the University of Illinois at Urbana-Champaign have developed an iPhone-based biosensor [33]. This handheld iPhone biosensor uses photonic crystal (PC) for label-free bacterial pathogen detection [34]. The PC biosensor consists of a low refractive index plastic material with a microfabricated periodic surface structure. A thin layer of high refractive dielectric material is coated on the surface. The PC surface resonantly reflects a single wavelength which is modulated by the absorption of biomaterial to the biosensor surface. The resonantly reflected wavelength is shifted by the attachment of biomolecules to the guided mode filter [35]. Small changes in the surface optical density can be quantified without attachment of a label to the detected biomolecule. The portable detection system is shown in Fig. 2.6. A fabricated cradle holds a smartphone's back camera in alignment with the PC and detection optics. Broadband light from an external source is collimated by the combination of an entrance pinhole and a collimating lens. After passing through a linear polarizing filter, light passes through the PC with one narrow band of wavelengths' reflection [36]. This handheld biosensor may be used in several independent locations: home, clinic and remote locations.

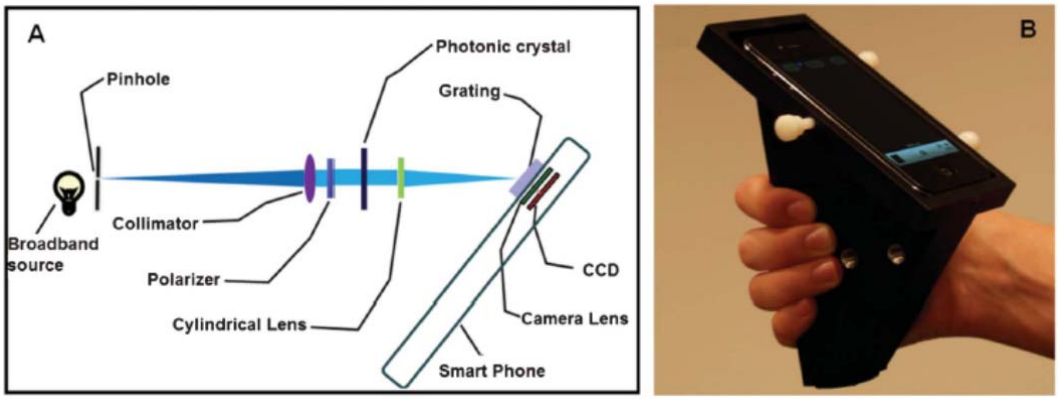

Figure 2.6 Schematic of the optical components with the smartphone cradle [33].

To successfully transfer technologies from the research laboratories to the marketplace, cost, stability, sensitivity, quality assurance and instrumentation design must be considered. The main barriers for most of the previously described devices are methods of biosensor calibration, high cost, reliability, stabilization, longevity, and complex fabrication of the biosensors.

2.3 Target pathogenic bacteria to be detected

Bacteria as well as viruses are the leading causes of contamination of food. *Campylobacter* spp., *Salmonellae, Staphylococcus* spp., *E. coli* O157, *Clostridium* spp. *and Listeria monocytogenes* are, in fact, the major foodborne pathogens in the United States as summarized in Table 2.1 [37]. In the U.S., *Salmonella enterica* is among the most prevalent causes of bacterial foodborne disease, with more than estimated one million cases annually [38]. *Salmonella enterica*, which is related to 31% of food-related deaths, is one of the most common intestinal infections and the second

most common foodborne bacterial pathogen in the U.S. The CDC has tracked annually the prevalence of *Salmonella enterica* in the USA, and has reported less than a 10% reduction in human cases between 1996–98 and 2007 [39]. With fresh produce being increasingly responsible for outbreaks of foodborne illnesses, more effective food safety interventions are needed throughout the production, processing and distribution of fresh vegetables and fruits. Fresh vegetables and fruits have come to the forefront as important vehicles of foodborne illnesses, accounting for 13% (713/5416) of reported outbreaks between 1990 and 2005 with an identified food source [40]. Salad greens, lettuce, sprouts and melons were the leading vehicles of illness. The target pathogenic bacterium in this research is *Salmonella enterica* subspecies *enterica* serovar Typhimurium. Therefore, we pursued rapid, real-time, *in situ Salmonella* Typhimurium detection on fresh food surfaces (tomatoes, egg shells, watermelon, spinach leaves, etc.) [40, 41].

Table 2.1 Major bacterial pathogens causing food-borne infections in the U.S. [37]

Bacteria	Est. Annual Cases	Est. Annual Hospitalizations	Est. Annual Deaths	Infectious Dose(CFUs)
Campylobacter spp.	1,963,141	10,539	99	400 to 10^6
Salmonella enterica	1,342,532	16,102	556	10^4 to 10^7
Staphylococcus spp.	185,060	1,753	2	$>10^6$
E. coli	173,107	2,785	78	10^1 to 10^2
Clostridium perfringens	248,520	41	7	$>10^8$
Listeria monocytogenes	2,493	2,298	499	400 to 10^3
Source: Economic Research Service, USDA				

Figure 2.7 shows an image of *Salmonella* Typhimurium cells. *Salmonella* Typhimurium is gram-negative bacterium with a cylindrical rod shape and size of 0.5 microns diameter by 2 microns long. Symptoms of Salmonellosis include diarrhea, fever, abdominal pain, headache, vomiting, etc. The incubation period ranges from several hours to two days. *S. enterica* can cause more serious illness in older adults, infants, and persons with chronic diseases. *S. enterica* serovar Typhimurium causes typhoid fever, a sometimes deadly disease that is more common in developing countries [40, 42].

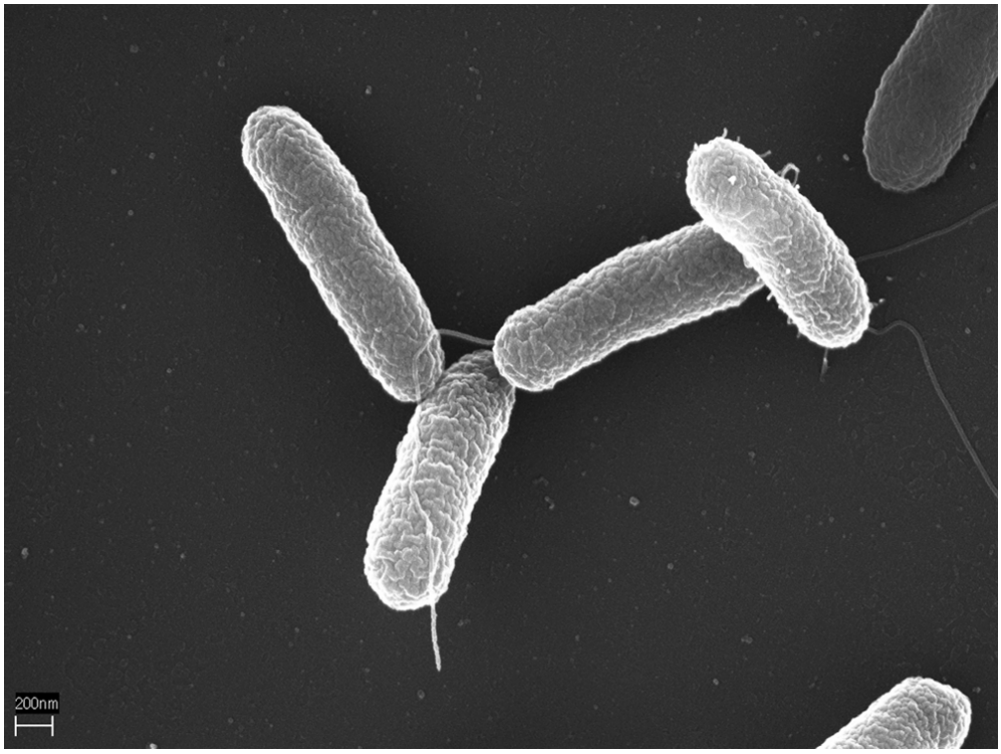

Figure 2.7 Scanning electron micrograph of *Salmonella* Typhimurium [43].

Bibliography

1. J.J., Gooding, Biosensor technology for detecting biological warfare agents: Recent progress and future trends, *Analytica Chimica Acta* 559(2): 137-151, 2006.
2. T.W., Alexander, T., Reuter, E., Okine, R., Sharma, and T.A., McAllister. Conventional and real-time polymerase chain reaction assessment of the fate of transgenic DNA in sheep fed Roundup Ready (R) rapeseed meal, *British Journal of Nutrition* 96(6): 997-1005, 2006.
3. K., Lind, A., Stahiberg, N., Zoric, and M., Kubista. Combining sequence-specific probes and DNA binding dyes in real-time PCR for specific nucleic acid quantification and melting curve analysis, *Biotechniques*, 40(3): 315-319, 2006.
4. B., Vogelstein, and K.W., Kinzler. Digital PCR, *Proceedings of the National Academy of Sciences of the United States of America* 96(16): 9236-9241, 1999.
5. J., Liu, M., Enzelberger, and S., Quake. A nanoliter rotary device for polymerase chain reaction, *Electrophoresis* 23(10): 1531-1536, 2002.
6. K.D., King, J.M., Vanniere, J.L., LeBlanc, K.E., Bullock, and G.P., Anderson. Automated fiber optic biosensor for multiplexed immunoassays, *Environmental Science and Technology* 34(13): 2845-2850, 2000.

7. F.S., Ligler, G.P., Anderson, P.T., Davidson, R.J., Foch, J.T., Ives, K.D., King, G.,Page, D.A., Stenger, and J.P., Whelan. Remote sensing using an airborne biosensor, *Environmental Science & Technology* 32(16): 2461-2466, 1998.
8. K., Tsuchiya, and C.C., dUrsel. Development of a sensitive ELISA using three monoclonal antibodies against lipopolysaccharides to detec *Xanthomonas campestris* pv. *Vesicatoria*, the causal agent of bacterial spot of tomato and pepper, *Journal of General Plant Pathology* 70: 21-26, 2004.
9. R.M., Lequin. Enzyme Immunoassay (EIA)/Enzyme-Linked Immunosorbent Assay (ELISA), *Clinical Chemistry* 51(12): 2415-2418, 2005.
10. E.C., Alocilja, and S.M., Radke. Market analysis of biosensors for food safety, *Biosensors & Bioelectronics* 18(5-6): 841-846, 2003.
11. R.V., Tauxe, M.P., Doyle, T., Kuchenmuller, J., Schlundt, C.E., Stein. Evolving public health approaches to the global challenge of foodborne infections, *International Journal of Food Microbiology* 139: S16-S28, 2010.
12. L.D., Mello, and L.T., Kubota. Review of the use of biosensors as analytical tools in the food and drink industries Biosensors for detection of pathogenic bacteria, *Food Chemistry* 77(2): 237-256, 2002.
13. S. S., Deshpande, and R. M., Rocco. Biosensors and their potential use in food quality control, *Food Technology*, 48(6): 146–150, 1994.
14. U.B., Trivedi, D., I.L., Lakshminarayana, N.G., Kothari, K.K., Patel, Makhija, P.B., Patel, and C.J., Panchal. Potentiometric biosensor for urea determination in milk, *Sensors and Actuators B: Chemical*, 140 (1) 260-266, 2009.

15. E., Brynda, M., Houska, A., Brandenburg, and A., Wikerstal. Optical biosensors for real-time measurement of analytes in blood plasma, *Biosensors & Bioelectronics* 17(8): 665-675, 2002.

16. A.K., Sharma, R., Jha, and B.D., Gupta. Fiber-optic sensors based on surface plasmon resonance: A comprehensive review, *IEEE Sensors Journal*, 7(7): 1118-1129, 2007.

17. M. A., Cooper. Optical biosensors in drug discovery, *Nature Reviews* 1: 515, 2002.

18. M. Manuel, B., Vidal, R., Lopez, S., Alegre, J., Alonso-Chamarro, I., Garces, J., Mateo. Determination of probable alcohol yield in musts by means of an SPR optical sensor, *Sensors and Actuators B*: *Chemical* 11: 455-459, 1993.

19. J., Dostalek, J., Ctyroky, J., Homola, E., Brynda, M., Skalsky, P., Nekvindova, J., Spirkova, J., Skvor, J. Schrofel. Surface plasmon resonance biosensor based on integrated optical waveguide, *Sensors and Actuators B: Chemical* 76: 8-12, 2001.

20. C., Movet, R.D., Harris, C., Maciag, B.J., Luff, J.S., Wilkinson, J., Piehler, A., Brecht, G., Gauglitz, R., Abuknesha, G., Ismail. Determination of simazine in water samples by waveguide surface plasmon resonance, *Analytical Chimica Acta* 338: 109-117, 1997.

21. H.P., Ho, W.C., Law, S.Y., Wu, C., Lin, S.K., Kong. Real-time optical biosensor based on differential phase measurement of surface plasmon resonance, *Biosensors and bioelectronics* 20: 2177-2180, 2005.

22. A.A., Kruchinin, Y.G., Vlasov. Surface plasmon resonance monitoring by means of polarization state measurement in reflected light as the basis of a DNA-probe biosensor, *Sensors and Actuators B: Chemical* 30(1): 77-80, 1996.
23. C., Situ, M.H., Mooney, C.T., Elliott, and J., Buijs. Advances in surface plasmon resonance biosensor technology towards high-throughput, food-safety analysis, *Trac-Trends in Analytical Chemistry* 29(11): 1305-1315. 2010.
24. X., Fan, I.M., White, S.I., Shopova, H., Zhu. Sensitive optical biosensors for unlabeled targets: A review, *Analytical chemical acta* 620: 8-26, 2008.
25. W.E., Moermer. New directions in single-molecule imaging and ayalysis, *PNAS* 104(31): 12596-12602, 2007.
26. W.G., Cox, and V.L., Singer. Fluorescent DNA hybridization probe preparation using amine modification and reactive dye coupling, *BioTechniques* 36: 114-122, 2004.
27. K., Ramanathan, and B., Danielsson. Principles and applications of thermal biosensors, *Biosensors and Bioelectronics* 16(6): 417-423, 2001.
28. K., Ramanathan, B.R., Jonsson, B., Danielsson, *Analysis in non-aqueous milieu using thermistors. In: Methods and Tools in Biosciences and Medicine*. Birkhauser Verlag, Basel, Switzerland, 174-194, 2000.
29. F., Scheller, N., Siegbahn, B., Danielsson, K., Mosbach. High sensitivity enzyme thermistor determination of L-lactate by substrate recycling, *Annual Chemistry* 57: 1740-1743, 1985.

30. L., Flygare, B., Danielsson, Advantages of organic solvents in thermometric and optoacoustic enzyme analysis, *Ann. NY. Acad. Sci*. 542: 263-268, 1988.

31. http://inhabitat.com/three-inch-device-detects-3000-types-of-viruses-and-bacteria/llmda/

32. S.N., Gardner, C.J., Jaing, K. S., McLoughlin, and T.R., Slezak. A microbial detection array (MDA) for viral and bacterial detection, *BMC Genomics* 11: 668, 2010.

33. http://www.cdc.gov/salmonella/outbreaks.html

34. P.Y., Li, B., Lin, J., Gerstenmaier, B.T., Cunningham. A new method for label-free imagning of biomolecular interactions, *Sensors and Actuators B: Chemical* 99(1): 6-13, 2004.

35. D., Gallegos, K.D., Long, H., Yu, P.P., Clark, Y., Lin, S., George, P., Nath, and B.T., Cunningham. Label-free biodetection using a smartphone, *Lab on a Chip* 13: 2124, 2013.

36. C.J. Choi, and B.T., Cunningham. Single-step fabrication and characterization of photonic crystal biosensors with polymer microfludic channels, *Lab on a Chip* 6: 1373-1380, 2006

37. http://www.ers.usda.gov/Briefing/FoodSafety/

38. R., Mead, R. N. Curnow, and A. M. Hasted. 2003. *Statistical methods in agriculture and experimental biology*, Chapman & Hall/CRC press, Boca Raton

39. http://www.foodsafety.gov/poisoning/causes/bacteriaviruses/salmonella/

40. http://www.cdc.gov/healthypets/

41. http://www.cdc.gov/salmonella/outbreaks.html

42. http://www.cdc.gov/salmonella/

43. V. Brinkmann. A Novel Data-Mining Approach Systematically Links Genes to Traits. *PLoS Biol* 3(5): e166, 2005.

Chapter 3

Phage-Based ME Biosensors

The biosensor introduced in this research consists of a transducer (ME resonator) that is coated with a bio-molecular recognition element for the specific capture and binding of a pathogenic target bacterium. In this chapter, the background of mass-sensitive biosensors, principle of magnetostriction, and fundamentals of landscape phage will be described in depth.

3.1 Acoustic wave biosensors

Acoustic wave (AW) transducers sense by producing a change in the characteristics of the path over which the acoustic wave travels [1]. When the acoustic wave produced propagates through or on the surface of the substrate, the velocity or amplitude of the wave will change if the characteristics of the propagation path change [2]. The frequency or phase characteristic of the sensor is measured to monitor such changes, which can then be correlated to the corresponding physical quantity. With the advantages of fast detection, simplicity of use, and cost-effectiveness, AW sensor has been commonly used for chemical and biological applications [3]. Some of more common types of acoustic wave biosensors are: the surface acoustic wave (SAW) biosensor, the quartz crystal microbalance (QCM) biosensor, the thin-membrane

flexural-plate-wave biosensor and the cantilever biosensor.

3.1.1 Surface acoustic wave biosensors

SAW devices based on horizontally polarized surface shear waves enable label-free and sensitive detection of biomolecules [4]. A SAW device typically consists of a piezoelectric substrate with interdigital transducers (IDT) as a planar electrode structure. The oscillation with a specific resonant frequency is mainly defined by the surface wave velocity of the device substrate. Usually, the substrate material used for SAW biosensors has to feature both a high dielectric constant and a low temperature coefficient. The basic SAW biosensor setup is shown in Fig. 3.1: the biosensor and antibodies are immersed in a flowing solution containing the target bacterium; the arrows at the top of the container indicate the flow of the liquid sample; the IDT is on the piezoelectric crystal substrate; the driving electronics operate the SAW biosensor and generate changes in the output signal [4]. The SAW biosensor has been applied for bacterial pathogens [5], small molecules [3], and DNA [6] detection. However, when the SAW biosensor is placed in a liquid medium, the waves will be strongly dampened. Therefore, SAW biosensors are unsuitable for liquid sensing.

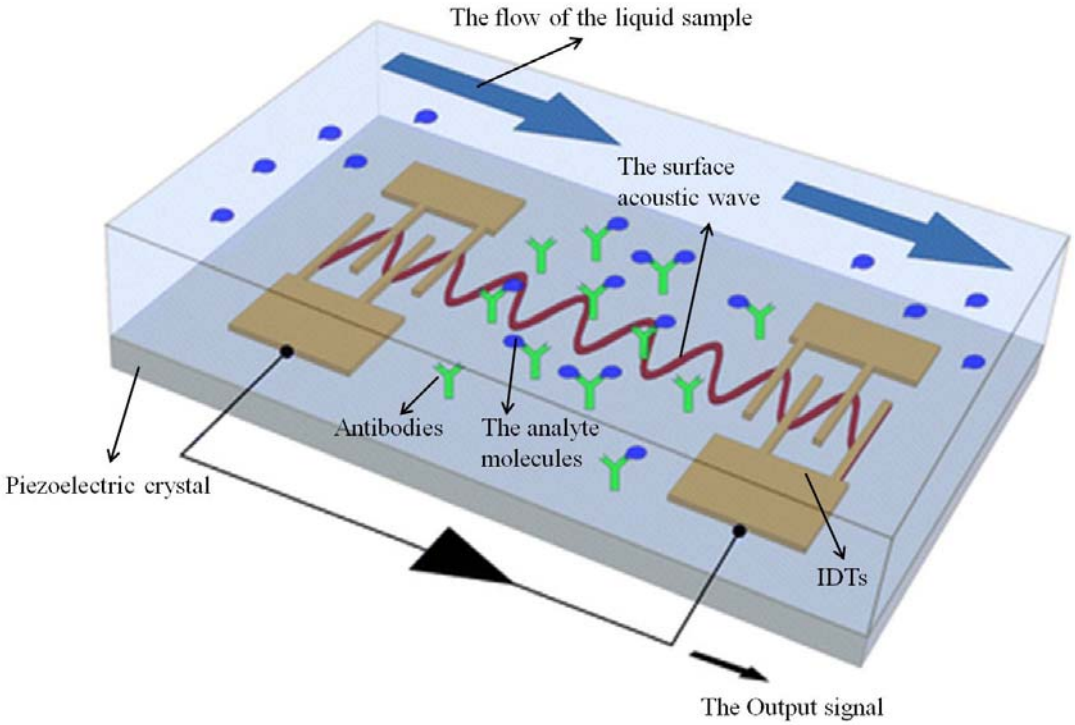

Figure 3.1 Basic SAW biosensor setup [4].

3.1.2 Quartz-crystal microbalance biosensors

A quartz-crystal microbalance (QCM), which is a thickness-shear mode, bulk acoustic wave transducer, is one of the most widely used acoustic wave sensor platforms in both research and commercial applications for biological detection. As the QCM is piezoelectric, an oscillating electric field applied across the device induces an acoustic wave that propagates through the crystal and meets minimum impedance when the thickness of the device is a multiple of a half wavelength of the wave [7]. Research on QCM for biosensor has grown steadily by the increasing needs from health care and food security [8]. Recently, a multiple QCM array system, which is commonly referred as a monolithic multichannel quartz-crystal microbalance (MQCM), has been developed. Figure 3.2 shows arrayed microbalances coated with

different sensing layers on a single quartz substrate [7]. The MQCM is able to bind with different receptors and select individual components in the target mixture. In this way, each resonant frequency shift with the specific receptor can be used to directly identify the presence of each component and determine its concentration.

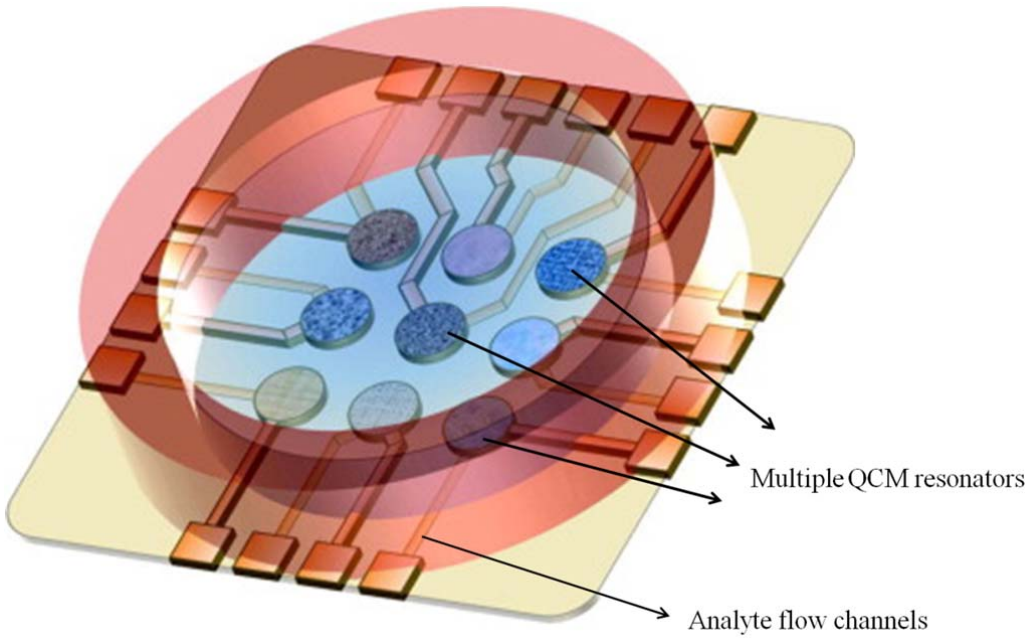

Figure 3.2 MQCM platform: a static multichannel detector [7].

3.1.3 Cantilever biosensors

A microcantilever acts as a mass-sensitive device, producing a frequency shift when there is a mass loading on the device. These cantilever-based sensor techniques are derived from the atomic force microscopy (AFM) [9] technique, which utilizes a sharp tip to scan a surface topography controlled by keeping the force between the tip and surface constant. Due to the microcantilever's high sensitivity and simple MEMS-based structure, a large number of papers have reported on the potential of

microcantilevers for physical, chemical, and biological sensing. Recently, a nano-cantilever device with extremely high sensitivity has successfully detected a single bacterial cell [10].

A fundamental cantilever is constructed from a long and thin micro-beam with one end fixed by a support. The most common read-out schemes are optical read-out [10] and piezo-resistive read-out [11]. For the optical read-out technique, the displacement of the free end of the cantilever is measured using the optical deflection of an incident laser beam on a position-sensitive photodetector (shown in figure 3.3 (A)) [12]. In this way, the absolute value of the cantilever displacement can be calculated. However, the main disadvantages of this read-out technique are that it requires external devices for deflection measurements, and the alignment and calibration are time consuming [10]. The piezo-resistive read-out is based on a resistivity change of the cantilever as a consequence of a surface-stress change. The surface-stress change is caused by the specific binding of molecules. To measure the change of the resistance, a dc-biased Wheatstone bridge needs to be included for silicon cantilevers (Figure 3.3 (B)). The main disadvantage of the piezo-resistive read-out technique is that the intrinsic noise directly affects the cantilever's resolution and sensitivity.

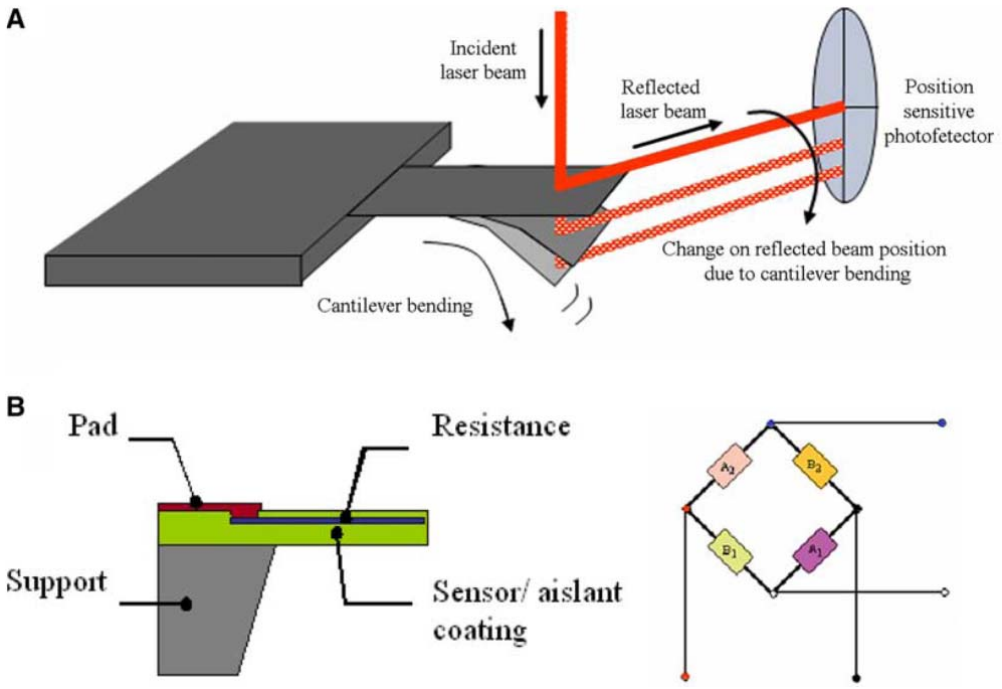

Figure 3.3 (A) The optical read-out method for a cantilever bending evaluation; (B) the piezo-resistive read-out and the Wheatstone bridge configuration [11].

Depending on the material of the transducers, cantilevers can be divided into different types: single beam cantilevers (e.g., silicon-based cantilevers), composite-beam cantilevers (e.g. piezoelectric cantilevers), magnetoelastic cantilevers and among others [13]. As the flexibility of a cantilever determines its sensitivity to the surface-stress, cantilevers fabricated from polymers with better sensitivity have been commonly discussed [11]. An epoxy-based polymer SU-8, which is 40 times softer than silicon, was fabricated to cantilevers. Figure 3.4 shows an image of SU-8 cantilevers with integrated gold resistors in a microfluidic channel.

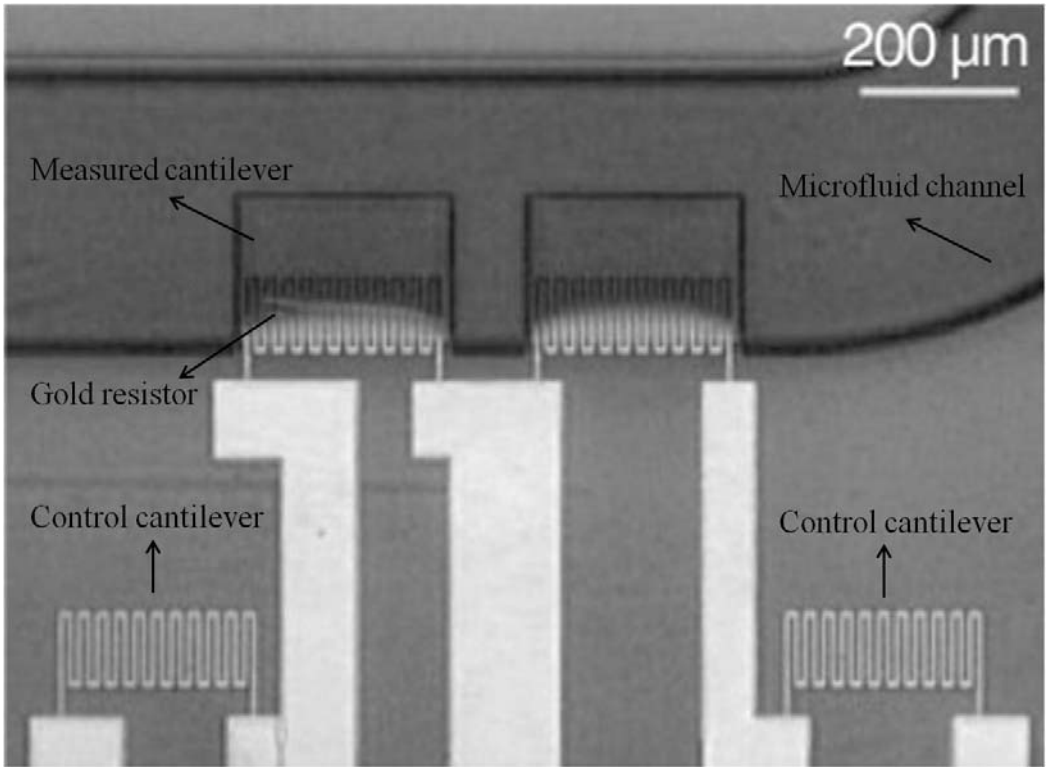

Figure 3.4 The polymer cantilevers with integrated gold resistors [11].

3.2 ME transducer

3.2.1 Magnetoelasticity

Magnetic materials exhibit ME behavior: the dimensions and elastic properties are dependent upon their magnetic states and the magnetic properties are influenced by applied mechanical stresses. In this research, amorophous ferromagnets of Metglas Alloy 2826 MB were used for the construction of ME signal transducers. The ME biosensor consists of ME resonators that work on the principle of Joule magnetostriction, where the resonator experiences a change in its dimensions in the presence of a magnetic field [1, 14]. When demagnetized at temperatures lower than its Curie temperature, a ferromagnetic material is divided into a number of magnetic

domains to minimize the material's internal energy [15]. During the magnetization process, the material is strained due to the ME coupling since the distribution of the elementary magnetic moments becomes anisotropic. As a result, spontaneous Joule magnetostriction is induced. An ideal material for the construction of ME signal transducers is a magnetically soft material that possesses a high saturation Joule magnetostriction, λ_s, and a high magnetomechanical coupling factor, κ, which can be defined as [15]:

$$\kappa = \frac{E_{me}}{\sqrt{E_e E_m}} \tag{3.1}$$

where E_{me}, E_e, and E_m are the mutual elastic and magnetic energy density, elastic self-energy density, and magnetic self-energy density, respectively.

3.2.2 The frequency signal of ME transducer

When subjected to a time-varying magnetic field in the direction of the resonator's length, the ME resonator longitudinally vibrates with a characteristic resonant frequency [16]. In order to derive the resonant frequency of a freestanding, strip-shaped ME sensor, a wave equation that describes the vibration of the sensor needs to be established. For thicknesses much smaller than the length and width, the fundamental resonant frequency under longitudinal vibration is expressed as [17]:

$$f = \frac{1}{2L}\sqrt{\frac{E}{\rho(1-\nu)}} \tag{3.2}$$

where E, ρ, and ν are the elastic modulus, density, and Poisson's ratio of the material, respectively.

To form the biosensor, the resonator is coated with a bio-molecular recognition element that is specific to the bacterium being detected. When the ME biosensor comes into contact with the specific target bacterium, the organisms are captured and bound to the biosensor's surface by the bio-molecular recognition element. This binding causes an increase in the mass of the biosensor that results in a decrease in resonant frequency. This decrease in resonant frequency is proportional to the number of bacterial cells bound to the ME biosensor surface [18]. An electromagnetic coil is used to generate the oscillating magnetic field and measure the biosensor's resonant frequency. Since oscillation and measurement are all controlled through changes in the magnetic field, the ME biosensor is a wireless device and the ME biosensors require no on-board power. A detailed explanation and schematic of the theory of operation can be found in the following references [14, 18-19]. Mass-sensitive biosensors measure the change in the mass load from the resonant frequency shift. Mass sensitive platforms have the advantages of rapid detection, simplicity of use and cost effectiveness. The ME biosensors are one type of mass-sensitive biosensors. The ME resonator can elongate or contract under an applied time-varying magnetic field [16]. During this process, the resonator converts the magnetic energy into mechanical oscillation. The resonant frequency of the resonator is related to its shape, dimensions, and materials properties. If the attached mass (Δm) is much smaller than the mass of the sensor (M), there will be a corresponding decrease in the sensor's resonant frequency (Δf). The change in resonant frequency, Δf, can be approximated by [17]:

$$\Delta f \approx -\frac{f}{2}\frac{\Delta m}{M} \tag{3.3}$$

The frequency change depends on the additional mass attached to the sensor surface, which is equivalently the number of bacterial cells bound to the ME sensor surface. The mass sensitivity (S_m) of the ME sensor is inversely proportional to the initial mass (M) and proportional to the initial resonant frequency (f). When Δm << M, it is given as [18]:

$$S_m = \frac{\Delta f}{\Delta m} \approx -\frac{f}{2M} = -\frac{1}{4L^2WT}\sqrt{\frac{E}{\rho^3(1-\nu)}} \tag{3.4}$$

Different size ME biosensors may be used with different bio-molecular recognition elements to identify different pathogenic bacteria simultaneously [20]. ME biosensors are wireless devices and require no on board power. Hence they have been fabricated using standard microelectronic fabrication procedures and are very inexpensive. The ME transducers were used in this research with a size of 1mm × 200μm × 30μm.

3.3 Landscape phages

For biological detection, antibodies and phages can be employed as the probe to capture target biological agents. For the past decades, antibodies have been the most commonly used biomolecular recognition elements [21]. Compared with antibodies, phages are highly robust, easy to store and inexpensive [21]. Purified phage can be stored indefinitely at moderate temperatures without losing infectivity and probe-binding activity. Thermal stability studies of phage have shown that

recombinant phage are resistant to heat up to 80˚C. In addition, landscape phage can be resistant to heat, organic solvent, acid, alkali and other chemicals.

Ff class of filamentous phages which includes f1, fd and M13 are the predominant phage used for phage-display technology [22]. The wild-type Ff virion is 900nm long and 6 nm in diameter, which consists of arrayed coat proteins on the exterior of DNA. The length of the virion is dictated by the length of the viral DNA that it contains. Foreign peptides and proteins can be fused genetically to the coat proteins and thereby displayed on the virion's outer surface. E2 phage, which is used as the bio-reorganization element in this research, is a landscape fd phage of recombinant gene VIII with peptide coding sequence and recombinant pVIII with displayed peptide. Thus, most of the surface area of phage displays selected peptides that provide the active binding sites. The landscape fd phage (shown in figure 3.5) becomes longer, because the length of the virion increases in proportion when the viral DNA is artificially lengthened by adding segments. Meanwhile, the three-dimensional recognition surface with multiple binding sites provides strong multivalent interactions with the target pathogens [23].

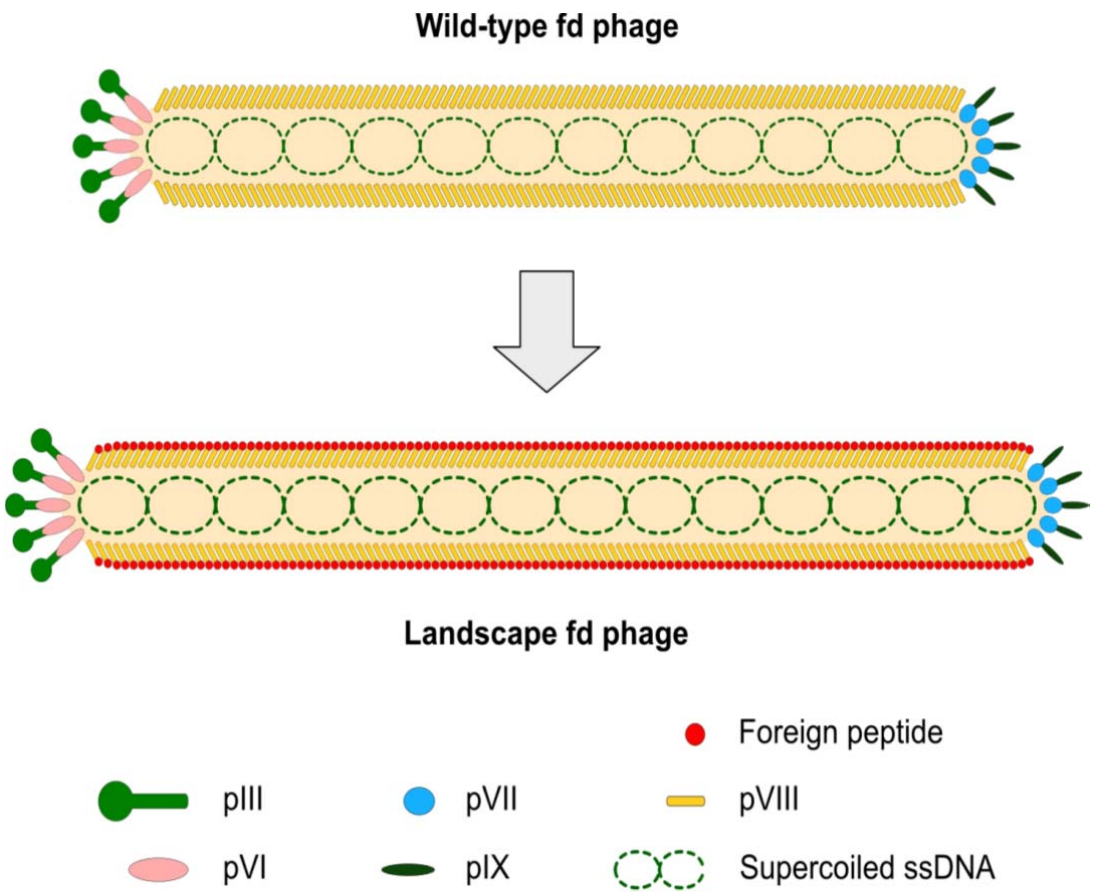

Figure 3.5 Schematic illustration of the wild-type fd phage and its genetically engineered form, displaying a foreign peptide on the major coat protein pVIII.

Phage display technique is used to select recombinant antibodies against various antigens. In this research, the whole landscape phage particles were directly used as bioprobes in biosensors [24]. During the affinity selection procedure, the target antigen is added and spread on a Petri dish. The f8/8 landscape phage library is then added to the target antigen-coated Petri dish and is incubated for 1h at room temperature. The unbound phage from the Petri dish was washed with a mixture of TBS and Tween. An elution buffer is then used to elute the phage bound to the target antigen attached to the Petri dish. The phage recovered from the eluate was used in

the subsequent cycles of the selection process. The whole procedure of selection is repeated several times to provide the clones highly specific to the target antigen.

The filamentous E2 phage with highly specific and selective properties towards *S.* Typhimurium derived from a landscape f8/8 phage library was used in this study. The E2 phage has been shown to possess 10- to 1,000-fold greater binding affinity for *S.* Typhimurium versus other bacteria [22].

Bibliography

1. D.S. Ballantine, R.M. White, S.J. Martin, A.J. Ricco, E.T. Zellers, G.C. Frye, and H. Wohltjen, *Acoustic Wave Sensors: Theory, Design and Physico-Chemical Applications* (Academic, New York, 1997).
2. G.N., Ferreira, AC., Silva, and B. Tome. Acoustic wave biosensors: physical models and biological applications of quartz crystal microbalance, *Trends in Biotechnology* 27(12): 690-697, 2009.
3. F.J., Gruhl, B.E., Rapp, M., Rapp, and K., Lange. Surface acoustic wave (SAM) biosensor chip system-a promising alternative for biomedical applications, *IFMBE proceedings* 25(8): 73-76, 2010.
4. K., Lange, B.E., Rapp, and M., Rapp. Surface acoustic wave biosensors: a review, *Anal Bioanal Chemistry* 391: 1509-1519, 2008.
5. F., Liu, F., Li, A.N., Nordin, and I., Voiculescu, A novel cell-based hybrid acoustic wave biosensor with impedimetric sensing capabilities, *Sensors* 13(3): 3039-3055, 2013.
6. Q., Xu, K., Chang, W., Lu, W. Chen, Y., Ding, S., Jia, K., Zhang, F., Li, J., Shi, L., Cao, S., Deng, and M., Chen. Detection of single-nucleotide polymorphisms with novel leaky surface acoustic wave biosensors, DNA ligation and enzymatic signal amplification, *Biosensors and Bioelectronics* 33(1): 274-278, 2012.
7. A., Tuantranont, A., Wisitsora-at, P., Sritongkham, and K., Jaruwongrungsee. A

review of monolithic multichannel quartz crystal microbalance: A review, *Analytica Chimica Acta* 687: 114-128, 2011.

8. C.K., O'Sullivan, and G.G., Guilbault. Commercial quartz crystal microbalances-theory and applications, *Biosensors and Bioelectronics* 14: 663-670, 1999.
9. R., Raiteri, M., Grattarola, H-J., Butt, and P., Skladal. Micromechanical cantilever-based biosensors, *Sensors and Actuators B* 79: 115-126, 2001.
10. K.M., Hansen, H-F., Ji, G., Wu, R., Datar, R., Cote, A. Majumdar, and T. Thundat, Cantilever-based optical deflection assay for discrimination of DNA single-nucleotide mismatches, *Anal. Chem.* 73: 1567-1571, 2001.
11. A., Boisen, and T., Thundat. Design and fabrication of cantilever array biosensors, *Materialstoday* 12(9): 32-38, 2009.
12. L.G., Carrascosa, M., Moreno, M., Alvarez, and L.M., Lechuga. Nanomechanical biosensors: a new sensing tool, *Trends in Analytical Chemistry* 25(3): 196-206, 2006.
13. A., Noy, A.B., Artyukhin, and N., Misra. Bionanoelectronics with 1D materials, *Materialstoday* 12(9): 22-31, 2009.
14. P. Kabos and V.S. Stalmachov, *Magnetostatic Waves and Their Application* (Chapman & Hall, London, 1994) p.163.
15. E.T., Lacheisserie, *Magnetostriction Theory and Applications of Magnetoelasticity* (CRC Press, London, 1993).
16. S. Li, S. Horikawa, M. Park, Y. Chai, V.J. Vodyanoy, and B.A. Chin. Amorphous

metallic glass biosensors, *Intermetallics* 30, 80-85, 2012.

17. C. Liang, S. Morshed, and B.C. Prorok. Correction for longitudinal mode vibration in thin slender beams, *Applied Physics Letters* 90, 221912, 2007.
18. P.G., Stoyanov, and C.A. Grimes. A remote query magnetostrictive viscosity sensor, *Sensors and Actuators A: Physical* 80(1): 8-14, 2000.
19. S. Li, and Z. Cheng. Nonuniform mass detection using magnetostrictive biosensors operating under multiple harmonic resonant modes, *Journal of Applied Physics* 107: 114514, 2010.
20. S. Huang, H. Yang, R.S. Lakshmanan, M.L. Johnson, J. Wan, I.-H. Chen, H.C. Wikle, V.A. Petrenko, J.M. Barbaree and B.A. Chin. Sequential detection of *Salmonella* Typhimurium and *Bacillus anthracis* spores using magnetoelastic biosensors, *Biosensors and Bioelectronics* 24: 1730-1736, 2009.
21. R.S. Lakshmanan, R. Guntupalli, J. Hu, D.-J. Kim, V.A. Petrenko, J. M. Barbaree, and B.A. Chin. Phage immobilized magnetoelastic sensor for the detection of Salmonella typhimurium, *Journal of Microbiological Methods* 71(1): 55-60, 2007.
22. V.A. Petrenko, G.P. Smith, X. Gong, and T. Quinn, A library of organic landscapes on filamentous phage, *Protein Engneering* 9: 797-801, 1996.
23. G.P. Smith and V.A. Petrenko, Phage display, *Chemical Reviews* 97: 391-410, 1997.
24. V.A. Petrenko, and S.P. George, *Phage nanobiotechnology* (RSC Nanoscience & Nanotechnology, Cambridge UK) p.110.

Chapter 4

The Possibility of *Salmonella* Typhimurium Detection on Fresh Food Surfaces

4.1 Introduction

Frequent outbreaks of foodborne illness are significant public health concerns. In order to pursue the vision of direct bacteria detection on food surfaces, proof in principle of *in situ* bacteria detection is necessary. As *Salmonella* Typhimurium can be a surrogate of *Salmonella* Enteritidis, *Salmonella* Typhimurium was detected on egg shell surfaces in this research. The recent *Salmonella* Enteritidis outbreak in eggs gained the attention of mainstream America in July 2010. The outbreak led to the recall of 380 million eggs nationwide after the Centers for Disease Control and Prevention received a 300% increase in reported *Salmonella* Enteritidis cases [1]. One of the possible sources of the *Salmonella* is the external contamination of shell eggs. *Salmonella* contamination through shell eggs accounts for approximately 50% of foodborne *Salmonella* outbreaks in the United States [2]. Raw eggs are believed to be a potentially hazardous food and refrigeration during storage and transport is required by the Food and Drug Administration. Although the transmission mechanism for *Salmonella* contamination of shell eggs is not fully understood, feces contamination and contact of the shell eggs with contaminated surfaces are possible sources leading to *Salmonella* contamination of the external surfaces of the shell eggs [3]. The current

microbiological detection techniques usually require sample preparation prior to the testing (i.e., capturing, purification and concentration), which is time-consuming. In order to achieve rapid and low-cost *Salmonella* detection, the direct testing of shell egg surfaces eliminates the preceding procedures and simplifies the testing methodology. This chapter focuses on the possibility of this direct detection. The curvature of food surfaces, binding specificity between the bacterium and ME biosensors, and the bacterial cells' distribution on food surfaces were considered and discussed in this chapter.

4.2 Material and methods

4.2.1 Sensor fabrication and metal deposition.

METGLAS 2826MB alloy, obtained from Honeywell International, was used to fabricate the ME resonator platforms for the biosensors. The ribbon was taped to 4 inch Silicon wafer and then diced into strip-shaped platforms of 1 mm × 0.2 mm × 0.028 mm by an automatic dicing saw (DAD 3220, Disco Corp, Tokyo, Japan). A diamond dicing blade with the thickness of 0.127 mm was utilized. The dicing speed was 3.00 mm per second, and the spindle speed was 25,000 revolutions per minute. Two layers of plastic tape were used to fix the metallic glass samples to Silicon wafer. The thickness of the tape was 0.105 mm. Once diced, the platforms were cleaned with acetone, then ethanol and annealed at 220°C in vacuum (10^{-3} Torr) for 2 h. Annealing removes residual stresses generated by the dicing process. Two metal layers (Cr and

Au) were then sputter-deposited onto all the platform surfaces. The layer of Cr acts as an adhesive interface between the platform and the Au layer. The Au layer provides corrosion resistance and a ready surface for bio-probe immobilization [4, 5].

4.2.2 E2 phage immobilization.

The filamentous E2 phage, with highly specific and selective properties towards *S.* Typhimurium, was derived from a landscape f8/8 phage library [6]. Dr. James M. Barbaree's lab in the Department of Biological Sciences at Auburn University prepared and provided the E2 phage for this research. The concentration of E2 phage solution was 5×10^{11} vir/ml in a tris-buffered saline (TBS) solution. The resonator platforms were immersed in the phage solution for 1 h. The immobilization of the E2 phage on the platform surface is based on physical adsorption. For the bare gold surface, the filamentous phage coverage is about 50% [7]. After the phage immobilization, the biosensors were washed with deionized water twice in order to remove unbound phage and salt originating from the TBS. In order to compensate for the environmental effects and non-specific binding, control sensors were prepared following the same steps but without the E2 phage immobilization.

4.2.3 Bovine serum albumin (BSA) blocking.

Both measurement (with phage) and control (without phage) biosensors were blocked with BSA to reduce non-specific binding. The biosensors were immersed in a 1 mg/ml BSA solution for 40 min and washed with deionized water twice.

4.2.4 *Salmonella* detection on egg shell surfaces.

S. Typhimurium culture with a concentration of 5×10^8 CFU/ml was provided by Dr. James M. Barbaree's laboratory. The culture solution was stored in a refrigerator at 4°C and equilibrated to room temperature before the test. In this research, the original *S.* Typhimurium solution was diluted to lower concentrations (ranging from 5×10^7 CFU/ml to 5×10^1 CFU/ml) with deionized water. The eggs were purchased from a local supermarket, and the shell egg surfaces were cleaned with deionized water. The *S.* Typhimurium solutions of eight different concentrations (5×10^8 CFU/ml to 5×10^1 CFU/ml) with the same volume (2.5×10^{-2} ml) were inoculated on the shell surface. The contamination area was a 1 cm-diameter circle. This corresponds to the surface bacterial concentration from 1.6×10^7 CFU/cm^2 to 1.6 CFU/cm^2. After the solutions dried for 20 min, both measurement and control biosensors were placed on the contaminated shell surface. The egg shells with the biosensors were then placed in a humidity-controlled chamber (95% RH) for 20 min to allow binding of the bacteria to the biosensors to occur. Seven measurement biosensors and three control biosensors were used for each concentration. The resonant frequency for each biosensor was measured with a network analyzer (model 8751A, HP, Santa Clara, CA, USA) before and after biosensors' exposure to the contaminated shell eggs. The eggs were bought from grocery and egg surfaces were cleaned before the target bacteria contamination. Figure 4.1 depicts the experimental procedure.

The network analyzer, responsible for the generation of a time-varying external

magnetic field and signal detection, was connected to a solenoid coil wound around a glass tube. In order to amplify the frequency signal (output), a static magnetic bias was provided with a bar magnet which was fixed outside of the tube. The test biosensor was placed inside of the coil. The attachment of *S.* Typhimurium cells can be detected by the biosensor's resonant frequency change. After the frequency measurements, all biosensors and shell eggs were exposed to osmium tetroxide (O_SO_4) vapor for 45 min in preparation for scanning electron microscope (SEM) analysis.

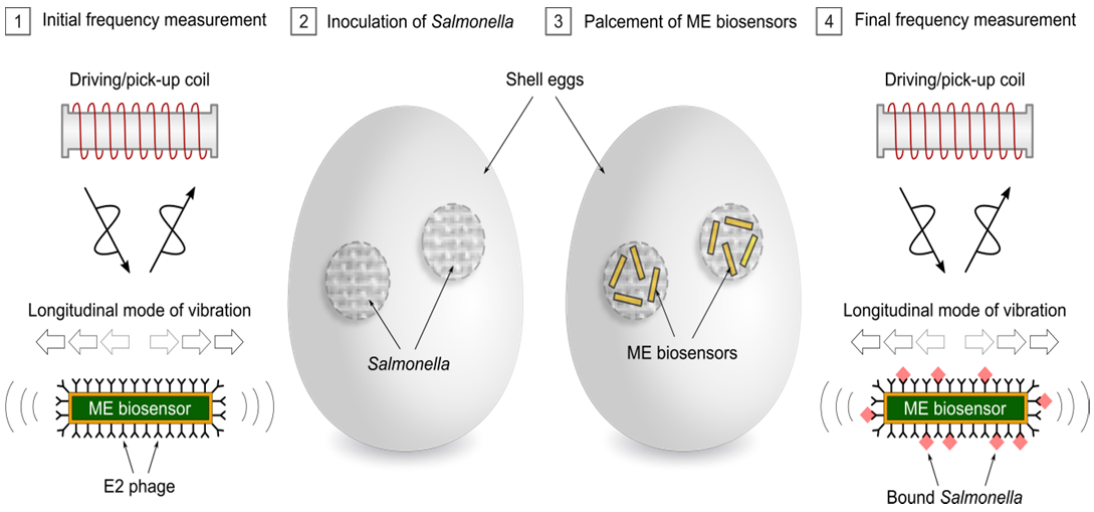

Figure 4.1 Schematic of the process used for the detection on shell egg surface using ME biosensors

4.2.5 Scanning electron microscopy.

The osmium-treated biosensors were mounted onto an aluminum platform using a conductive tape for SEM observation using a (JSM-7000F, JEOL, Tokyo, Japan). SEM observation was performed to confirm *S.* Typhimurium cells were bound to the biosensor surface and responsible for the observed frequency changes.

4.3 Specific binding between E2 phage based ME biosensors and *Salmonella* Typhimurium on food surfaces.

The specificity of E2 phage-based ME biosensor binding to *S.* Typhimurium has been reported previously [12, 13]. Furthermore, Figure. 4.2 shows the cross-reactivity of E2 phage-based ME biosensors with different bacteria on food surfaces (*S.* Typhimurium, *Bacillus anthracis* spores, *Escherichia coli* and *Listeria monocytogenes*). In addition, ME biosensors were also tested on bare surface as a reference. There are ten samples for each group and the standard deviation is shown as the error bar. Hence, the results of resonant frequency changes in Fig. 4.2 shows E2 phage-based ME biosensors have highly specific binding with *S.* Typhimurium.

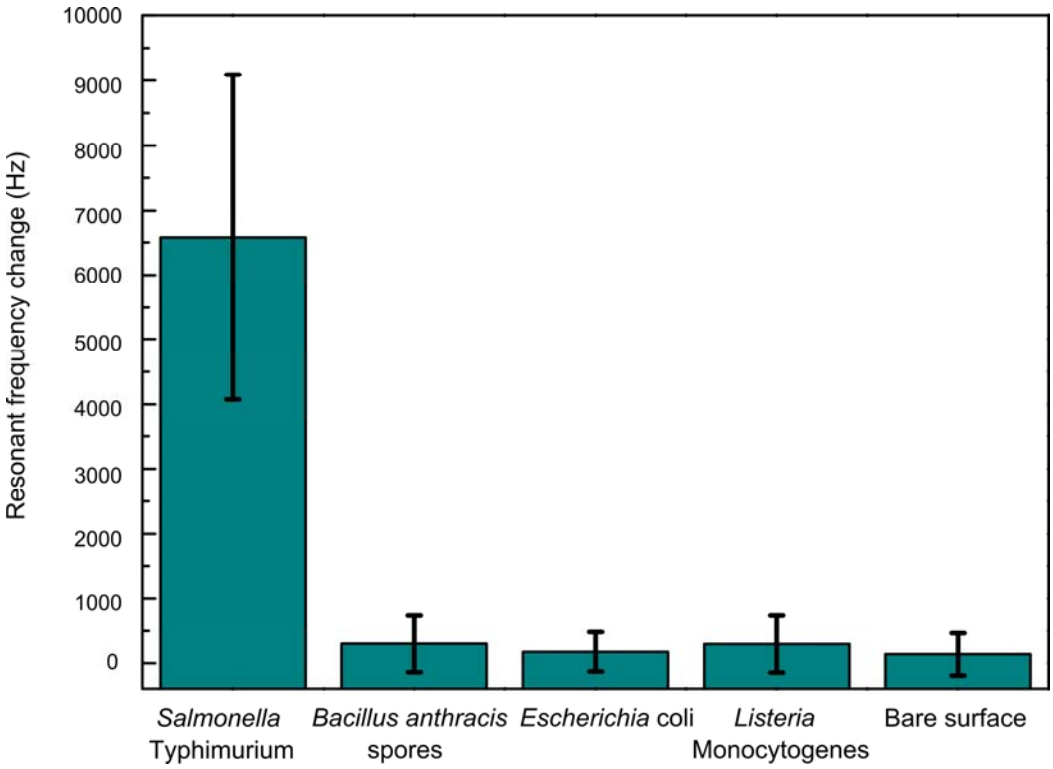

Figure 4.2 Cross-reactivity of E2 phage-based ME biosensors with different bacteria

(The reference is a bare surface without bacteria).

4.4 The effect of food surface curvature on the contact between the biosensors and *S.* Typhimurium.

Figure 4.3 shows a representative image of the egg's outline which has non-uniform curvatures. Hence, the surface curvature needs to be evaluated to estimate the contact between a 1 mm-long biosensor and *S.* Typhimurium on egg shell. Assuming the egg is axisymmetric around the axis OP, only the top half of the egg outline (i.e.,$\overset{\frown}{OEP}$) is considered. The curvature of $\overset{\frown}{OEP}$ decreases from point O, which has the largest curvature, to point E and increases from point E to point P. In real situation, the *S.* Typhimurium cells move and assemble with flagella or fimbriae, creating a dynamic varying layer on the egg shell surface. Based on the curvature calculations with the estimated *S.* Typhimurium layer thickness of larger than 2 μm [14], 100% contact between the biosensor and bacterium can be achieved on $\overset{\frown}{MEP}$, where point M is located between points O and E. The left of Figure 1 shows 100% contact at point M, while less than 100% contact at point O. As the area with larger curvatures ($\overset{\frown}{MON}$) is less than 5% of the whole surface, 1 mm-long biosensors are able to detect the contamination on over 95% of the egg shell surface.

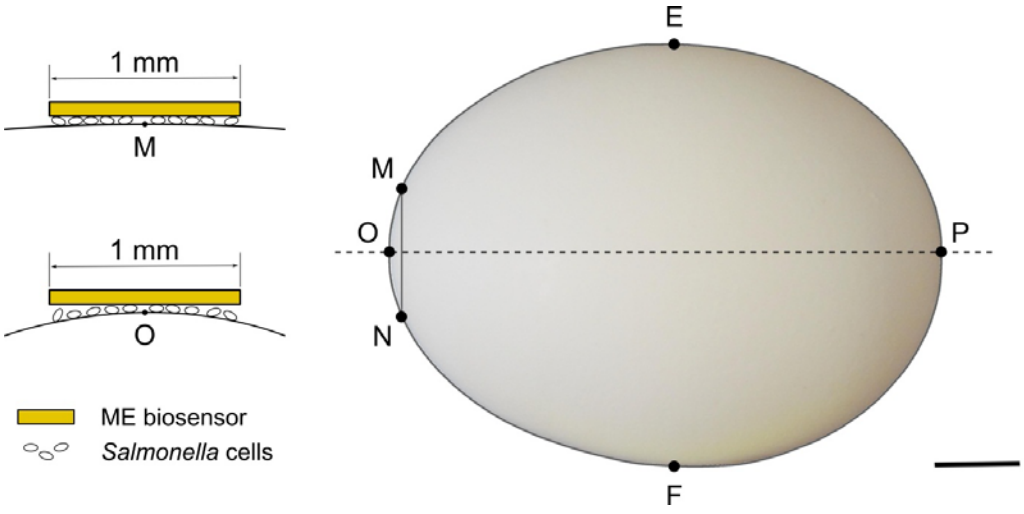

Figure 4.3 The effect of egg's surface curvature on the contact area (Scale bar: 1cm). The figures on the left show the contact area around points M and O (not to scale)

4.5 The detection of *S.* Typhimurium of various concentrations on shell eggs.

The resonant frequency changes for measurement and control biosensors are shown in Fig. 4.4. In the figure, the dashed line shows the initial frequency curve of the biosensors, whereas the solid line shows the final frequency curve after the placement of the biosensors on *S.* Typhimurium-spiked surfaces. Resonant frequency changes for typical measurement biosensors exposed to three different concentrations of *S.* Typhimurium (1.6×10^5 CFU/cm^2 to 1.6×10^7 CFU/cm^2) are shown in Fig.4.4a to Fig.4.4c, respectively. These figures display a decrease of the biosensor's initial resonant frequency after binding of *S.* Typhimurium to the biosensors. The resonant frequency changes were found to be smaller as the biosensors were exposed to lower concentrations. In other words, the resonant frequency changes were in accordance

with the level of bacterial contamination of the shell eggs. By contrast, the frequency changes for control biosensors were negligible compared with the measurement biosensors.

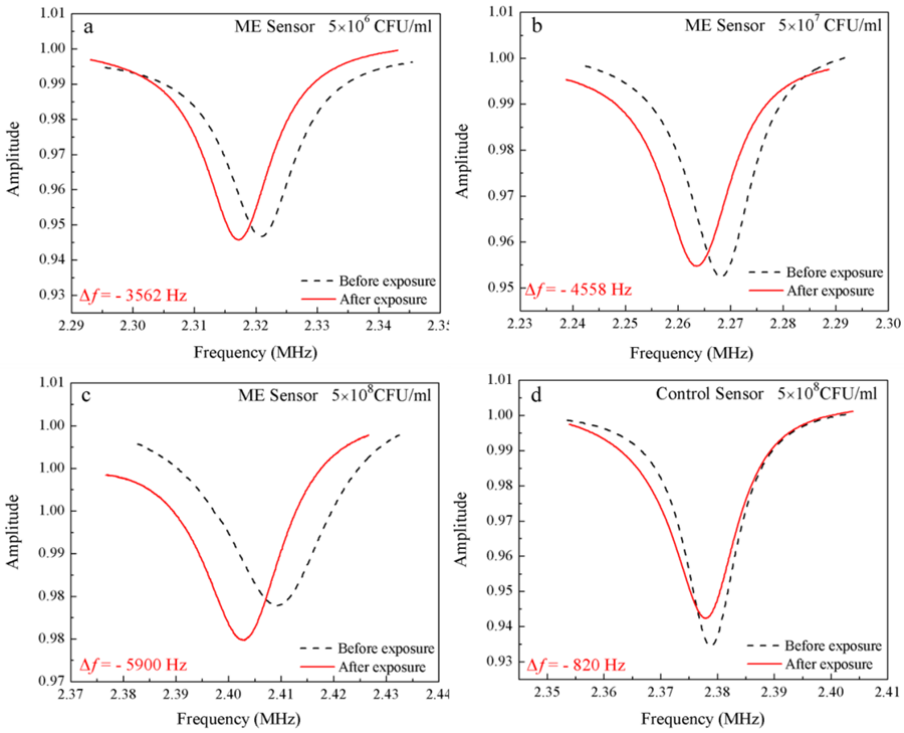

Figure 4.4. The frequency curves before (dashed line) and after (solid line) exposure to spiked shell eggs for ME measurement and control biosensors: (a) measurement biosensor exposed to 1.6×10^7 CFU/cm^2; (b) measurement biosensor exposed to 1.6×10^6 CFU/cm^2; (c) measurement biosensor exposed to 1.6×10^5 CFU/cm^2; (d) control biosensor exposed to 1.6×10^7 CFU/cm^2.

Figure 4.5 shows representative SEM micrographs for ME biosensors placed on shell eggs inoculated with different concentrations of *S.* Typhimurium. The number of *S.* Typhimurium cells on the biosensor surfaces was smaller as the concentration of

the bacterial cells in solutions was decreased. In addition, as shown in Fig. 4.5d, the control biosensor surface is much cleaner without bacteria binding. Hence, these SEM micrographs verified that specific binding between the E2 phage and *S.* Typhimurium occurred, resulting in the corresponding large resonant frequency changes of the measurement biosensors.

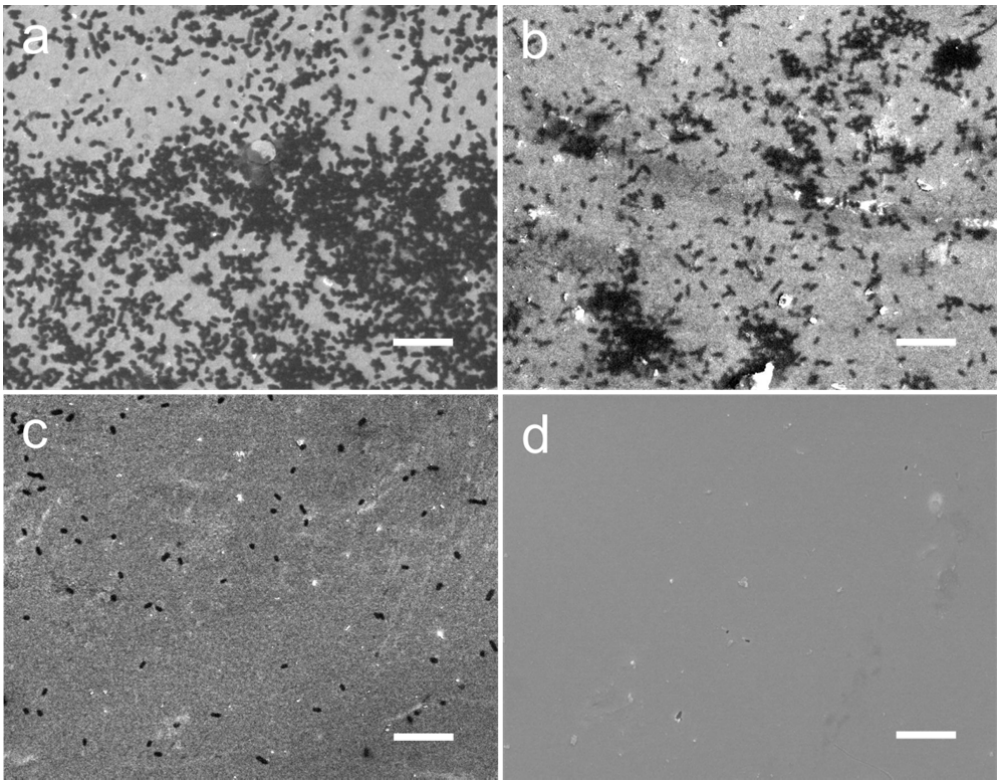

Figure 4.5 SEM micrographs of biosensor surfaces placed on shell eggs spiked with different ***S.*** Typhimurium concentrations: (a) 1.6×10^7 CFU/cm^2; (b) 1.6×10^6 CFU/cm^2; (c) 1.6×10^5 CFU/cm^2; d) control biosensor exposed to 1.6×10^7 CFU/cm^2. (Scale bar: 10 μm)

4.6 Use of multiple biosensors and the determination of the detection limit.

Figure 4.6 displays SEM micrographs of the egg shell surfaces inoculated with different concentrations of *S.* Typhimurium. Figures 4.6a to 4.6c correspond to the bacterial concentrations of 1.6×10^7 CFU/cm^2 to 1.6×10^5 CFU/cm^2, respectively. Figure 4.6d is the as-purchased egg surface without *S.* Typhimurium spiking. The SEM microphotographs show the bacterial cells on the surface are not uniformly distributed, especially when the bacterial concentration is low. This is because the cells can migrate and move freely on the humid surface, searching for regions and pores with nutrients and water. Based on this situation, the response of ME biosensors largely depends on where the biosensors fall on the egg shell surface. In other words, a single biosensor is unlikely to be able to provide contamination information of the whole egg shell when the bacterial cells are non-uniformly distributed on the shell surface. The lower the bacterial concentration, the more non-uniform the cell distribution is on the surface. Therefore, multiple biosensors need to be employed to improve the probability of detection. Multiple biosensors were placed on different areas of the egg surface. Figure 4.7 plots measured frequency changes for both measurement (triangles) and control (circles) biosensors. The resonant frequency changes for measurement biosensors largely depend on the concentration of the *Salmonella* solution. The average frequency changes decreased with decreasing *S.* Typhimurium concentration as anticipated. Furthermore, the resonant frequency changes for the control biosensors were much smaller and not sensitive to the bacterial solution concentration.

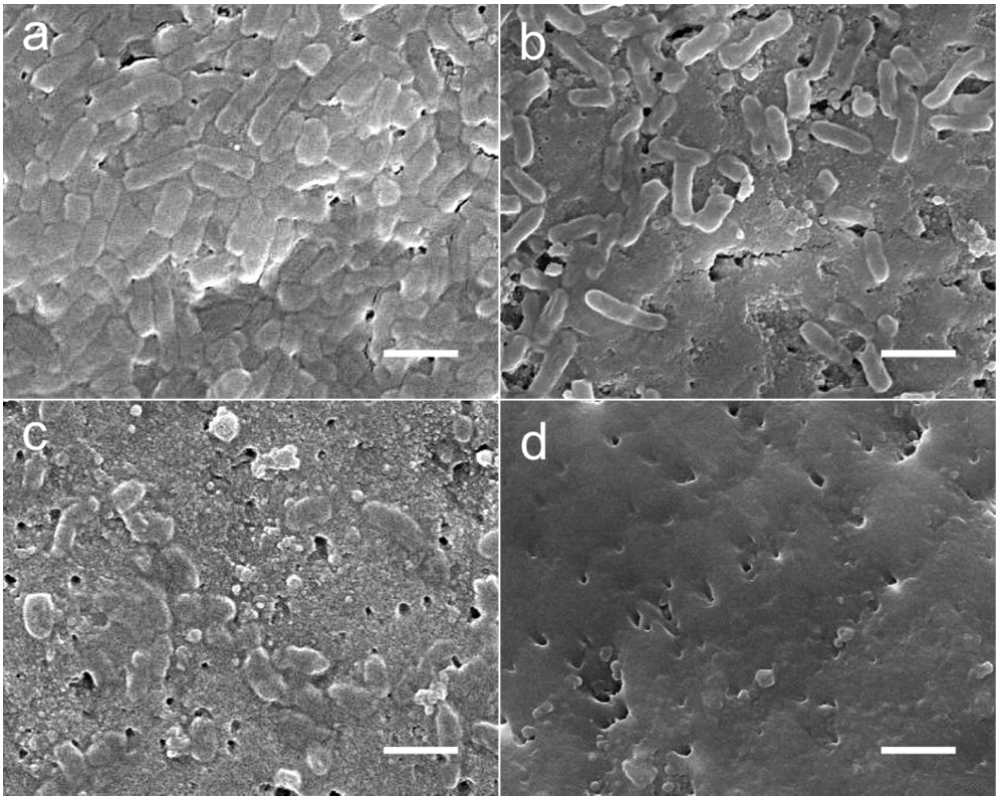

Figure 4.6 SEM micrographs of shell egg surfaces spiked with different *S.* Typhimurium concentrations: (a) 1.6×10^7 CFU/cm^2; (b) 1.6×10^6 CFU/cm^2; (c) 1.6×10^5 CFU/cm^2; (d) as-received shell egg, no bacterial spiking. (Scale bar: 2μm)

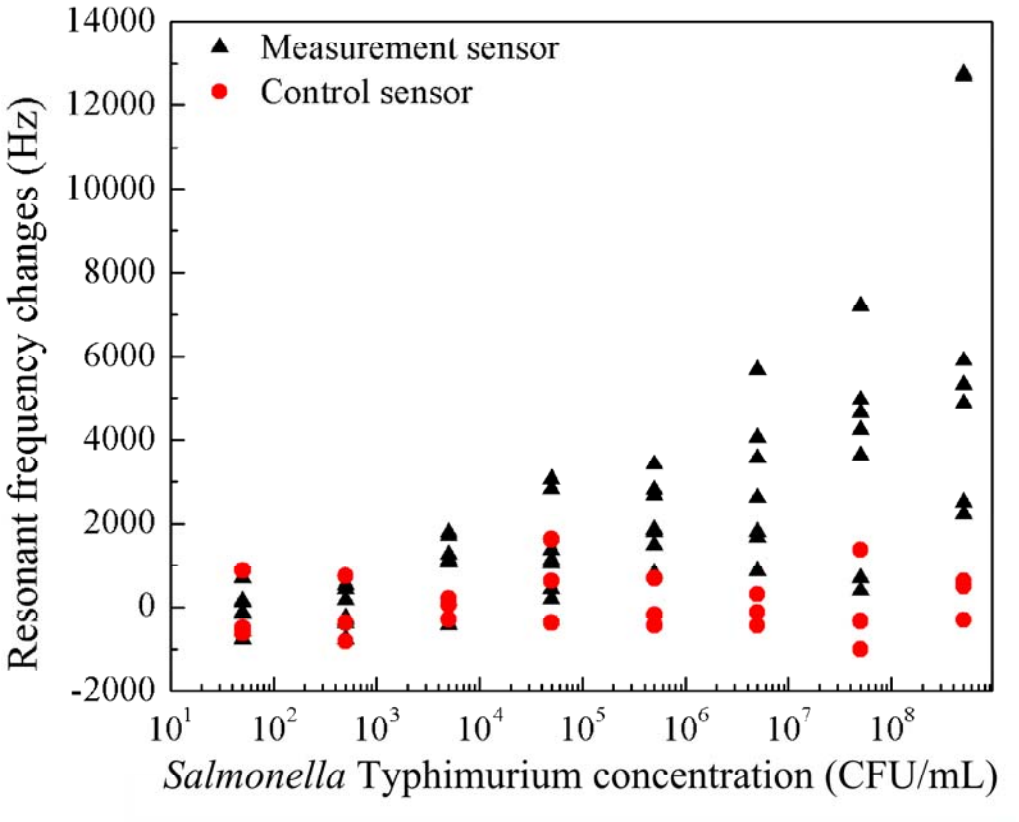

Figure 4.7 The resonant frequency changes for measurement and control biosensors exposed to shell eggs spiked with different concentrations of ***S.*** Typhimurium.

Finally, a statistical analysis based on the one-tail-unpaired student's t-test [15, 16] was performed to determine the limit of detection. Table 4.1 summarizes the results of the frequency measurements. As anticipated, there is a variance in the resonant frequency changes of measurement biosensors even for the highest spiked concentration. This is due to the fact that the *S.* Typhimurium on the egg shell was not uniformly distributed and, hence, the measurement depends on where the biosensor falls. From the statistical analysis, the detection limit was determined to be 160 CFU/cm^2 for 1 mm long biosensors on egg shell surface.

Table 4.1. Statistical analysis of resonant frequency changes for measurement and control biosensors placed on egg surface.

S. Typhimurium Concentration (CFU/ml)	Type of biosensors	Mean (Hz)	Standard deviation (Hz)	Probability of t-test	Confidence level of difference (%)
1.6×10^7	Measurement biosensor	6619.64	4389.71	0.004176	99.58
	Control biosensor	271.00	508.75		
1.6×10^6	Measurement biosensor	3688.90	2413.65	0.007178	99.28
	Control biosensor	12.67	1225.50		
1.6×10^5	Measurement biosensor	2902.14	1652.24	0.00127	99.87
	Control biosensor	-83.33	376.73		
1.6×10^4	Measurement biosensor	2130.14	886.58	0.002354	99.76
	Control biosensor	20.83	590.73		
1.6×10^3	Measurement biosensor	1444.87	1105.22	0.155241	84.48
	Control biosensor	625.00	1000.00		
1.6×10^2	Measurement biosensor	963.43	809.44	0.025457	97.45
	Control biosensor	-13.67	255.52		
1.6×10^1	Measurement biosensor	-75.96	473.86	0.414938	58.51
	Control biosensor	-145.83	806.06		
1.6×10^0	Measurement biosensor	-88.21	487.98	0.496555	50.34
	Control biosensor	-83.33	832.29		

4.7 Conclusions

Unlike previous studies on the detection in bacteria in solutions [13, 17-19], the methodology in this work employs direct placement of the biosensors on the contaminated food surface and eliminates any preceding sampling procedures facilitated by the wireless nature of detection. In addition, the results demonstrated

that the bacterial binding and detection can be realized in a high humid environment (95% RH) within 30 min.

Bibliography

1. U.S. Food and Drug Administration. Egg Safety Final Rule. http://www.fda.gov/Food/FoodSafety/Product-SpecificInformation/EggSafety/EggSafetyActionPlan/ucm170615.htm.
2. W.L. Messens, K. Duboccage, Grijspeerdt, M. Heyndrickx and L. Herman. Growth of *Samonella* serovars in hens' egg albumen as affected by storage prior to inoculation, *Food Microbiology* 21 (1): 25-32, 2004.
3. http://www.fda.gov/Food/FoodSafety/Product-SpecificInformation/EggSafety/ucm241588.htm.
4. S. Huang, J. Hu, J. Wan, M. L. Johnson, H. Shu and B.A. Chin. The effect of annealing and gold deposition on the performance of magnetoelastic biosensors, *Materials Science and Engineering* C 28: 380-386, 2007.
5. S. Li, Y. Li, H. Chen, S. Horikawa, W. Shen, A. Simonian and B.A. Chin. Direct detection of *Salmonella* Typhimurium on fresh produce using phage-based magnetoelastic biosensors, *Biosensor and Bioelectronic* 26 (4): 1313-1319, 2010.
6. V.A. Petrenko and I.B. Sorokulova. Detection of biological threats. A challenge for directed molecular evolution, *Journal of Microbiological Methods* 58 (2): 147–168, 2004.
7. S. Horikawa, D. Bedi, S. Li, W. Shen, S. Huang, I. Chen, Y. Chai, M.L. Auad,

M.J. Bozack, J.M. Barbaree, V.A. Petrenko and B.A. Chin. Effects of surface functionalization on the surface phage coverage and the subsequent performance of phage-immobilized magnetoelastic biosensors, *Biosensors and Bioelectronics* 26: 2361-2367, 2011.

8. R.S. Lakshmanan, R. Guntupalli, J. Hu, D. Kim, V.A. Petrenko, J.M. Barbaree and B.A. Chin. Phage immobilized magnetoelastic sensor for the detection of *Salmonella* Typhimurium, *Journal of Microbiological Methods* 71: 55-60, 2007.
9. V.A. Petrenko and V.J. Vodyanoy. Phage display for detection of biological threat agents, *Journal of Microbiological Methods* 53 (2), 253-262, 2003.
10. V.A. Petrenko, G.P. Smith, X. Gong and T. Quinn. A library of organic landscapes on filamentous phage, *Protein Engineering* 9 (9): 797-801, 1996.
11. I.B. Sorokulova, E.V. Olsen, I. Chen, B. Fieber, J.M. Barbaree, V.J. Vodyanoy, B.A. Chin and V.A. Petrenko. Landscape phage probes for *Salmonella typhimurium*, *Journal of Microbiological Methods* 63 (1): 55-72, 2005.
12. R.S. Lakshmanan. Phage-Based Magnetoelastic Sensor for the Detection of *Salmonella* Typhimurium, PhD Dissertation, Auburn University. 2008.
13. S. Huang, H. Yang, R.S. Lakshmanan, M.L. Johnson, J. Wan, I.-H. Chen, H.C. Wikle, V.A. Petrenko, J.M. Barbaree and B.A. Chin. Sequential detection of *Salmonella* Typhimurium and *Bacillus anthracis* spores using magnetoelastic biosensors, *Biosensors and Bioelectronics* 24: 1730-1736, 2009.
14. Paul Arnold. Molecular Biology, *Salmonella* Bacteria FAQ.

http://www.brighthub.com/science/genetics/articles/50010.aspx.

15. D.M. Prescott. *Methods in cell biology*, Academic press, New York. 1977.
16. R. Mead, R.N. Curnow and A.M. Hasted. *Statistical methods in agriculture and experimental biology*, Chapman & Hall/CRC press, Boca Raton, 2003.
17. R. Guntupalli, J. Hu, R.S. Lakshmanan, T.S. Huang, J.M. Barbaree and B.A. Chin. A magnetoelastic resonance biosensor immobilized with polyclonal antibody for the detection of *Salmonella* Typhimurium, *Biosensors and Bioelectronics* 22: 1474-1479, 2007.
18. M.L. Johnson, J. Wan, S. Huang, Z. Cheng, V.A. Petreko, D. Kim, I. Chen, J.M. Barbaree, J. W. Hong, and B. A. Chin. A wireless biosensor using microfacbricated phage-interface magnetioelastic particles, *Sensor and Actuators A: Physical* 144: 38-47, 2008.
19. W. Shen, R.S. Lakshmanan, L.C. Mathison, V.A. Petrenko and B.A. Chin. Phage coated magnetoelastic micro-biosensors for real-time detection of *Bacillus anthracis* spores, *Sensors and actuators B: Chemical* 137 (2): 501-506, 2009.

Chapter 5

Detection Technique for ME biosensors

5.1 Introduction

A rapid, low-cost biosensor is needed for the routine monitoring of pathogenic bacteria on fresh food items (tomatoes, lettuce, spinach, etc.) and preparation surfaces to ensure the safety and quality of our food supply [1-2]. Here, we describe a new extracoil method for *in situ* bacteria detection that eliminates labor-intensive and time-consuming procedures currently required to extract and prepare test samples. ME biosensors measured with a surface-scanning coil detector were used to detect bacteria directly upon fresh food surfaces. ME biosensors coated with a bacterium-specific, bio-recognition layer (phage) were distributed over the surface of a food item [3-5]. The coil detector was scanned across the food surface to interrogate the ME biosensors and determine whether the food surface was contaminated with a bacterial pathogen. This chapter presents an examination of the coil design and determination of factors that affect the performance and optimization of the ME biosensor measurement.

The ME biosensor used in this work is based on a low-cost, wireless acoustic wave sensor platform (i.e., ME resonator) [6-9]. A common way of using the ME biosensor for bacterial detection is shown in Fig. 5.1a [3-5, 9]. An ME biosensor is

placed within the confines of a solenoid coil, and a sample solution potentially containing target bacterial cells is flowed across the biosensor surface. During this process, the biomolecular-recognition element coated on the ME resonator's surface captures the bacterial cells from the solution. As bacteria capture occurs, the biosensor's mass increases, and its resonant frequency decreases [8, 10]. The need for preparation of sample solutions, however, limits the speed and usability of the intracoil test method. In the new extracoil test method, developed to bypass preparation of fluid samples, the presence of bacteria on the surface of fresh foods can be measured directly using a newly designed surface-scanning coil (Fig. 5.1b).

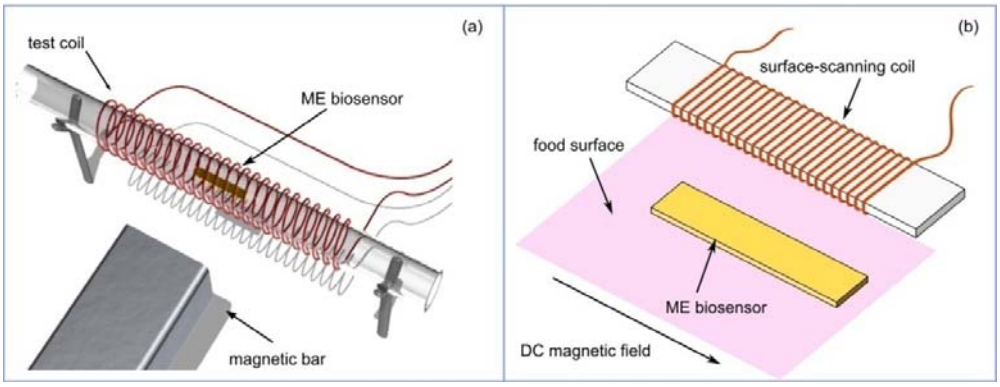

Figure 5.1 Comparison between (a) the intracoil and (b) the extracoil detection methods.

The main challenge of this new surface-scanning detection method is the small measurement signal [11]. Figure 5.2 compares signal amplitudes of a typical 1 mm × 200 μm × 30 μm sensor measured outside (red dashed line) and inside (black solid line) a coil. Outside the coil, the amplitude is much smaller than inside the coil; hence,

enhancement of the signal amplitude is necessary. This research focuses on the electric coil design to increase the sensitivity of the detection method. Simulation of the excitation magnetic field generated by the coil and the calculation of the magnetic flux change due to a vibrating sensor were used to demonstrate that measured signal amplitude is sensitive to the geometry of the coil.

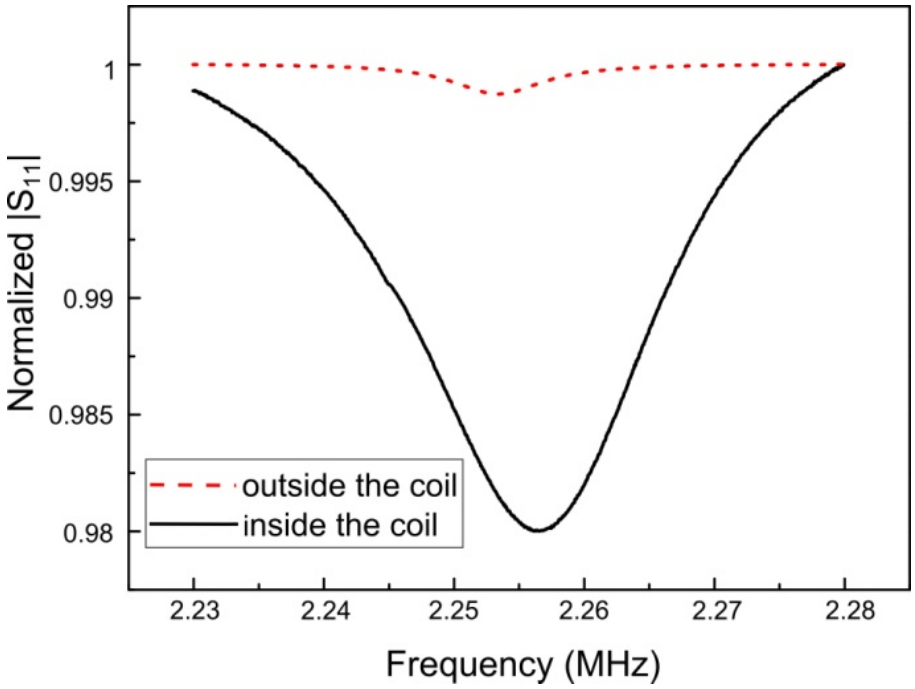

Figure 5.2 Comparison between sensor signals measured outside and inside a solenoid coil.

5.2 Theory

5.2.1 Circuit impedance change caused by a vibrating ME sensor

The ME sensor works on the principle of Joule magnetostriction, where the sensor changes its dimensions as a result of the rotation and alignment of magnetic

moments within the material's magnetic domains (magnetization) in response to an external magnetic field [12, 13]. Upon application of a magnetic field, the randomly oriented magnetic domains in the material tend to align in the direction of the applied field. When subjected to an oscillating external magnetic field, a sensor will mechanically vibrate, due to the oscillating internal material magnetization. The mechanical resonant characteristics of the ME sensor may be detected by the mutual inductive coupling of the material's internal magnetization with an electromagnetic coil. In other words, the coil is used to generate an oscillating magnetic field and measure characteristics of the sensor's resonance. Figure 3 depicts an equivalent circuit of a network analyzer, an electromagnetic coil, and the ME sensor. In loop I, V and Z_s respectively denote the network analyzer's source signal and impedance. Loop II comprises the electromagnetic coil. This coil is inductively coupled with the ME sensor, shown in loop III. To simplify the analysis, the motional, core, and leakage impedances of the ME sensor are lumped together in the form of a series *RLC* circuit [14, 15]

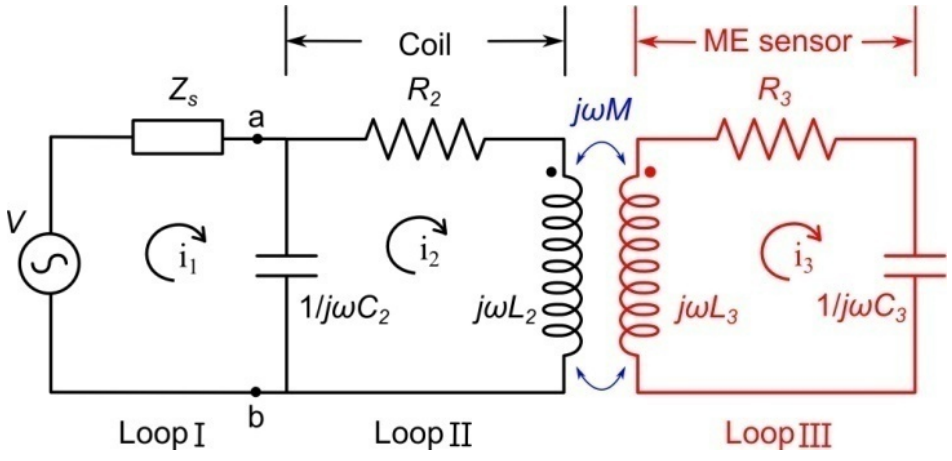

Figure 5.3. Equivalent electric circuit for an ME sensor inductively coupled with an

electromagnetic coil.

Now let Z_i to be the impedance of loop i. Hence, $Z_{\mathrm{II}} = Z_{R_2} + Z_{L_2} + Z_{C_2} = R_2 + j\omega L_2 + \frac{1}{j\omega C_2}$and $Z_{\mathrm{III}} = Z_{R_3} + Z_{L_3} + Z_{C_3} = R_3 + j\omega L_3 + \frac{1}{j\omega C_3}$, where j is the unit imaginary number, and ω is the angular frequency. Neglecting the ME resonator and the mutual inductance, the load impedance of only the coil is given by:

$$Z_{ab_0} = \frac{Z_{C_2}\left(Z_{R_2} + Z_{L_2}\right)}{Z_{\mathrm{II}}} \tag{5.1}$$

When the ME sensor is in the vicinity of the solenoid coil and coupled magnetically with the coil, the load impedance becomes:

$$Z_{ab} = \frac{Z_{C_2}\left[\left(Z_{R_2} + Z_{L_2}\right)Z_{\mathrm{III}} + \omega^2 M^2\right]}{Z_{\mathrm{II}}Z_{\mathrm{III}} + \omega^2 M^2} \tag{5.2}$$

It is obvious that if the mutual inductance M = 0, Eq. 5.2 simplifies to Eq. 5.1. The impedance difference, due to the presence of the ME sensor, is:

$$\Delta Z_{ab} = Z_{ab} - Z_{ab_0} = \frac{\omega^2 M^2 Z_{C_2}^2}{Z_{\mathrm{II}}(Z_{\mathrm{II}}Z_{\mathrm{III}} + \omega^2 M^2)} \tag{5.3}$$

Eq. 5.3 shows the load impedance difference increases with increasing mutual inductance as a result of the vibration of the ME sensor. Since the test signal mainly depends on the load impedance difference, increasing the mutual inductance is a key to improving signal amplitude.

5.2.2 The relationship between signal amplitude and mutual inductance

Resonance characteristics of the ME sensors are measured with the detection coil

that is connected to a network analyzer used for signal excitation and analysis. The network analyzer is responsible for generating an oscillating electric current. When this time-varying current is driven through the coil, an oscillating external magnetic field is created, which then excites the sensor to vibrate. This mechanical vibration consequently causes a change in the sensor's magnetic flux, which goes through the coil and induces an impedance change of the measurement circuit. This impedance change was measured over a proper range of frequencies as the input reflection coefficient, S_{11}, of the circuit using the network analyzer. As the internal impedance of the network analyzer is Z_s, the equation for the relationship between the load impedance, Z_{ab}, and S_{11} signal is as follows [15]:

$$S_{11} = \frac{Z_{ab} - Z_s}{Z_{ab} + Z_s} \tag{5.4}$$

S_{11} and Z_{ab} show dramatic changes at the sensor's resonant frequency, the degree to which is caused by the strength of the mutual inductance. The absolute value of S_{11} ($|S_{11}|$) was used to quantify the sensor's signal amplitude (Fig. 5.4). The test data were recorded as a normalized value of $|S_{11}|$, which was used to eliminate the background effects of the coil. The signal amplitude at the resonant frequency, $\Delta|S_{11}|$, shown as the peak amplitude in Fig. 5.4, is used to compare the various coil designs.

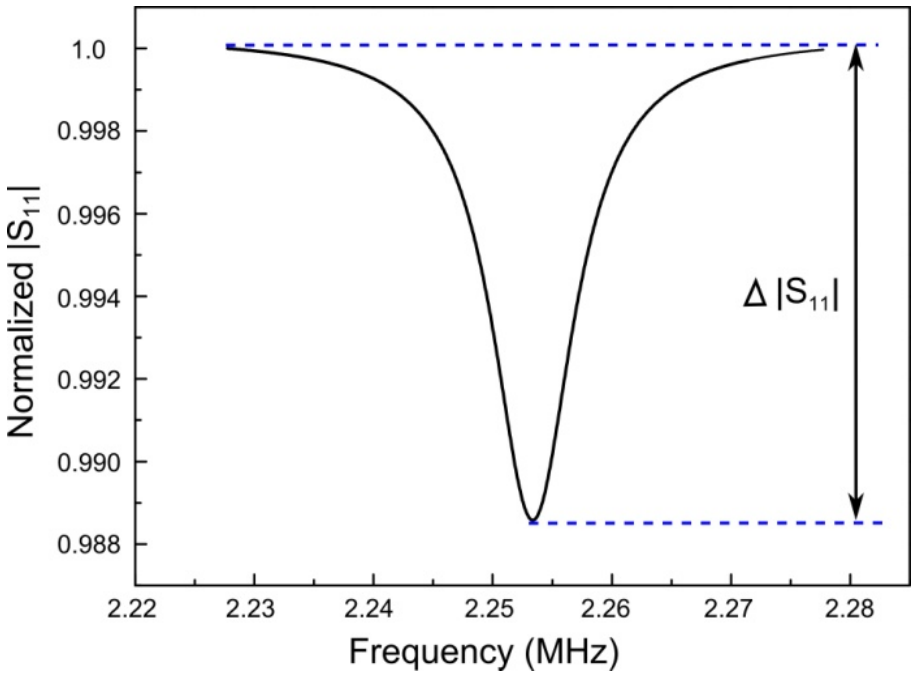

Figure 5.4. Definition of signal amplitude, $\Delta|S_{11}|$.

Figure 5.4 shows that normalized $|S_{11}|$ dramatically decreases at the sensor's resonant frequency. Compared with the intracoil measurement method, the signal amplitude in the extracoil measurement method is much smaller as previously shown in Fig. 5.2 because the mutual inductive coupling between the ME sensor and the coil is much weaker. Therefore, this mutual coupling needs to be enhanced to generate a larger $\Delta|S_{11}|$. In general, the mutual inductance monotonically increases with magnetic flux change caused by a sensor and the number of turns of the coil. In order to calculate the magnetic flux change, the model that describes the interaction between a vibrating sensor and coil will be discussed.

5.3 Design and modeling

5.3.1 Magnetic field distribution around the coil

The ME sensor's vibration is actuated by the time-varying magnetic field that is created by the coil. A strong magnetic field results in large vibration amplitude [8, 12]. Meanwhile, the magnetic field distribution is based on the geometry of the coil, the number of coil turns, and the electrical characteristics of the coil (resistance, inductance and capacitance) [17-18]. Therefore, the magnetic field distribution for various coil designs was first simulated. Figure 5.5 shows an example of field distribution for a specific coil geometry (the working length of the coil, L, is 1 mm, the width, W, is 1 mm, and the thickness, T, is 0.5 mm). Figure 5.5a shows an illustration of the coil's geometry and axes of orientation for the modeling. The Y and Z axes lie along the directions of the sensor length and thickness, respectively. Figure 5.5b illustrates normalized magnetic field distribution inside and outside of the coil, where the origin is located at the center of the coil. The Biot-Savart law was used for magnetic field calculation [19]. The color bar on the right shows the normalized values of the magnetic field. The magnetic field outside of the coil is weaker than that inside of the coil. This result, combined with the displacement of sensor's vibration, will be used for signal amplitude calculations.

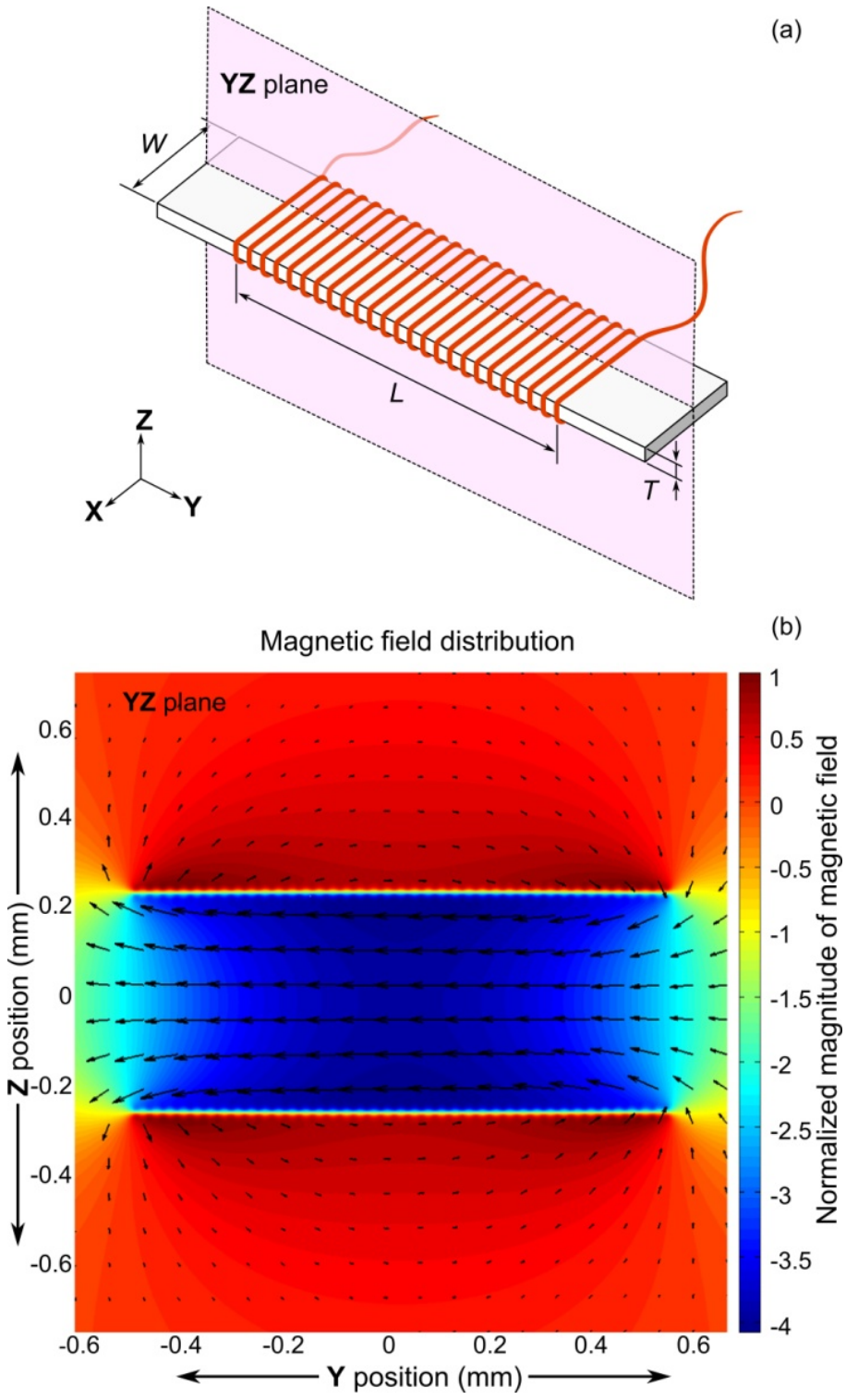

Figure 5.5 (a) Illustration of the coil's geometry and axes of orientation for the modeling; and (b) normalized magnitude of magnetic field on the YZ plane at X = 0.

5.3.2 Calculations of magnetic flux changes

The ME sensor was placed under the coil with the freestanding longitudinal vibration along the direction of the applied time-varying magnetic field (Fig. 5.6a). The magnetic flux change, which is due to the sensor's vibration, was calculated in this section. During the vibration, the displacement of points along the length of the sensor can be expressed as a function of position, *y*, and time, *t* [12]. When the ME sensor undergoes fundamental longitudinal vibration, the point displacement is of the form [8, 12]:

$$u_n(y,t) = \gamma B_{ac} \cos\left(\frac{\pi}{l_0}\, y - \frac{\pi}{2}\right) \mathrm{e}^{j\omega t} \tag{5.5}$$

for $-\frac{l_0}{2} \leq y \leq \frac{l_0}{2}$, where *j* is the unit imaginary number; ω is the angular fundamental resonant frequency of the sensor; l_0 is the initial length of the sensor; γ is a constant determined by magnetoelastic coefficients of the material [8, 12-13]; B_{ac} is the magnetic induction that depends on H_{ac}, the time-varying magnetic field shown in Fig. 5.5b. In this way, the maximum displacement amplitude, a_0, is $a_0 = \gamma B_{ac}$.

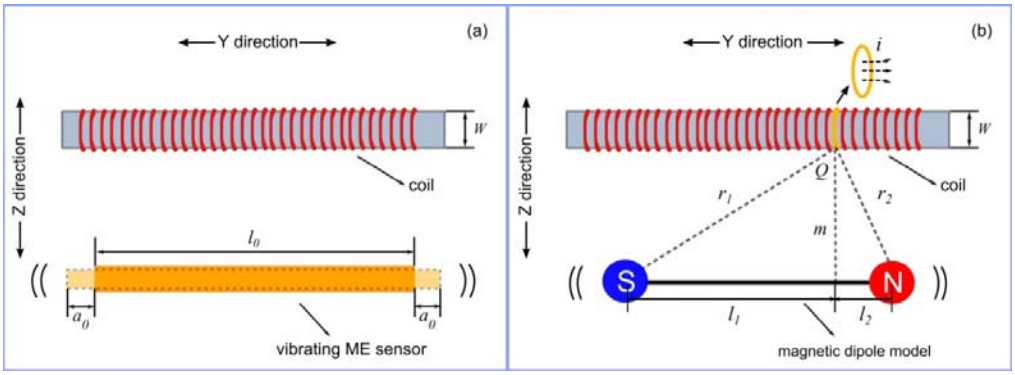

Figure 5.6 Calculation model for the magnetic flux change: (a) ME sensor subjected to the time-varying magnetic field; and (b) the sensor modeled as a magnetic dipole.

Since the ME sensor vibrates longitudinally, and Poisson effect is expected to be small, the displacement along the Y axis is much larger than those along the X and Z axes [5]. Hence, the ME sensor was modeled as a one-dimensional magnetic dipole, and the sensor's vibration was treated as periodic changes in the distance between the south and north poles (Fig. 5.6b). In this way, the magnetic flux change due to the sensor's vibration can be calculated from the vibrating magnetic dipole. For this dipole model, the effective magnetic flux along the Y axis passes perpendicularly through the loop area of the coil (XZ plane). Hence, the magnetic induction along the Y axis (B_y) equals $B_{sy} + B_{ny}$, where B_{sy} and B_{ny} are the component magnetic induction of B_y due to the south and north poles of the magnetic dipole. Based on the Biot-Savart law, the magnetic induction at an arbitrary point Q around the magnetic dipole is [19]:

$$B_y = \left(\frac{\mu_0 P}{4\pi\, r_1^2} \times \frac{l_1}{r_1}\right) + \left(\frac{\mu_0 P}{4\pi\, r_2^2} \times \frac{l_2}{r_2}\right) \tag{5.6}$$

where, l_1, l_2, r_1 and r_2 are distances shown in Fig. 5.6b, μ_0 is the permeability of free space, and *P* is the strength of the magnetic poles. For the dipole model of the sensor, *P* can be expressed as [19]:

$$P = \mu_r H A_s \tag{5.7}$$

where μ_r is the relative permeability, A_s is the cross-sectional area of the sensor, and *H* is the magnetic field around the sensor. In this experiment, a uniform, constant bias magnetic field, H_{dc}, in the direction along the sensor's length was applied with magnets to amplify the signal. As H_{dc} is much larger than H_{ac} (the time-varying magnetic field created by the coil), it is assumed the strength of the magnetic dipole is dependent on H_{dc} (i.e., $H \approx H_{dc}$).

As the magnetic field is not uniform along the X and Z axes, the magnetic flux due to the ME sensor that goes through the loop *i* of the coil (Fig. 5.6b) is:

$$\Phi_i = B_{yi} A_c = \int_{-W/2}^{W/2} \int_{m+T}^{m} B_{yi}\, dz\, dx \tag{5.8}$$

where A_c, *W* and *T* are the cross-sectional area, width and thickness of the coil, respectively, and *m* is the perpendicular distance from the dipole to point Q. As the magnetic field is also not uniform along the Y axis, the total magnetic flux is calculated by accumulating the magnetic flux of each turn of the coil:

$$\Phi_{total} = \sum_{i=1}^{N_c} \Phi_i = \sum_{i=1}^{Nc} (B_{yi} A_c) \tag{5.9}$$

where *Nc* is the number of turns of the coil. As Eq. 5.6 shows, the magnetic induction,

B_{yi}, is a function of l_1 and l_2, where $l_1 + l_2$ is equal to the sensor's length, and thus the magnetic flux is also a function of the sensor's length. When the sensor vibrates, the length of the sensor changes between the minimum of $l_{min} = l - 2a_0$ and the maximum of $l_{max} = l + 2a_0$. Hence, $\Delta\Phi_{\max}$, the maximum change of magnetic flux because of the change of the sensor's length, can be expressed as:

$$\Delta\Phi_{\max} = \Phi_{\text{total}}(l_{max}) - \Phi_{\text{total}}(l_{min}) \tag{5.10}$$

Therefore, the relationships among S_{11} parameter, load impendence, mutual inductance, and magnetic flux due to the sensor's vibration are summarized in Fig. 5.7. The amplitude of $|S_{11}|$ signal is a result of $\Delta\Phi_{\max}$. The measured $|S_{11}|$ and calculation result of $\Delta\Phi_{\max}$ will be discussed in the next section.

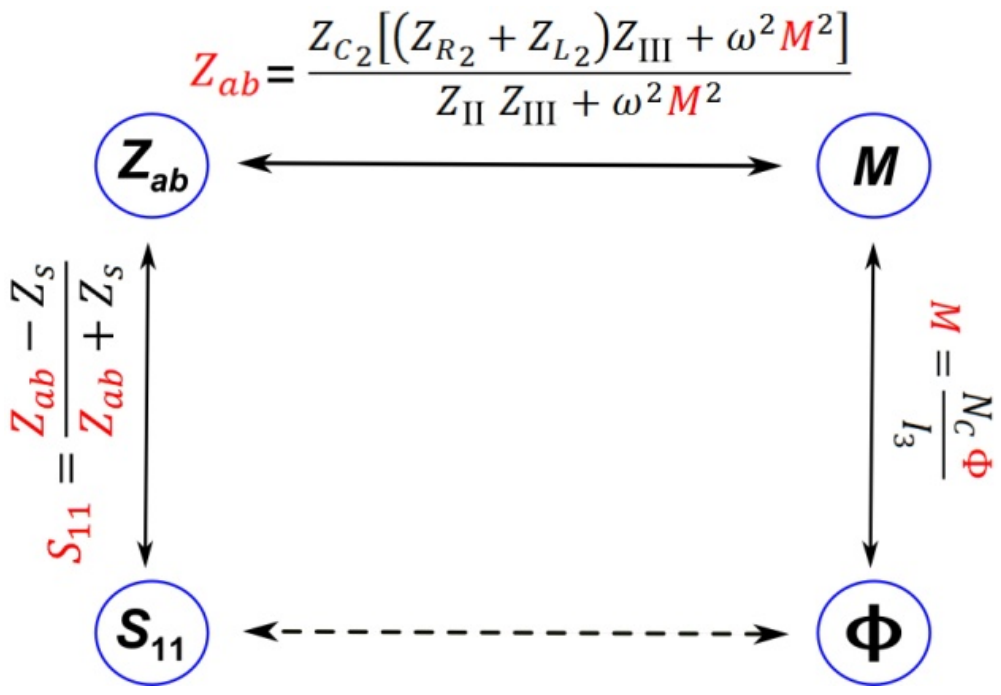

Figure 5.7 Summary of the relationships among S_{11} parameter, load impendence,

mutual inductance, and magnetic flux.

5.4 Experimental results and discussion.

There is a large body of research on the signal-to-noise ratio (SNR) for coils, most of which focus on the coil's self-resonance [17, 18]. However, the specific functions of the coil for ME sensor detection in this research are the excitation of the sensor's vibration and detection of the associated resonant frequency. Hence, the design of the coil can significantly alter the amplitude of $|S_{11}|$ signal due to the coupled mutual inductance. Furthermore, from Eq. 5.5, the two ends of the sensor have the largest vibrating displacements, which are responsible for the largest effect on the magnetic flux changes [13]. Therefore, to efficiently detect the sensor's vibration, the measured signal amplitude is especially sensitive to the working length of the coil, a significant factor in the coil design.

Figure 5.8 shows typical normalized $|S_{11}|$ signals of a 1 mm-long ME sensor measured with coils of different working length. The number of turns (40 turns), the resistance (50 Ω), the width (1 mm) and thickness (0.5 mm) of the coils were kept the same. The working lengths (L) of the coils were 0.8 mm, 1.3 mm and 3.0 mm, respectively. At the resonant frequency, the 1.3 mm-long coil showed the largest peak amplitude, $\Delta|S_{11}|$.

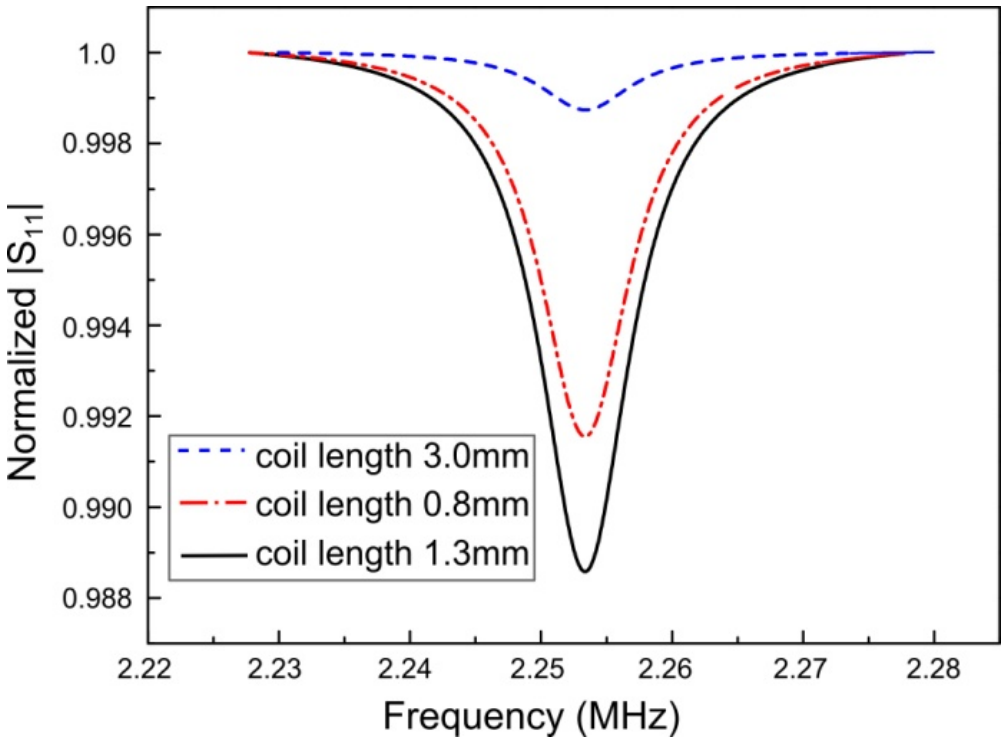

Figure 5.8 Normalized S_{11} signals of a 1 mm-long ME sensor measured with coils of different working length.

Based on the previous discussion, $\Delta|S_{11}|$ monotonically increases with magnetic flux change as a result of the sensor's vibration. Figure 5.9 shows a comparison between normalized measured $\Delta|S_{11}|$ at the resonant frequency (red circle points) and the simulation result of normalized magnetic flux change calculated using Matlab (the black curve). Five samples of 1 mm-long sensors were tested by using coils with different working lengths: 0.8, 1.0, 1.3, 2.0, and 3.0 mm. The experimental data showed $\Delta|S_{11}|$ is maximum when the working length is 1.3 mm; while the simulation results, which show the same trend, predict the magnetic flux change is maximum with a working length of 1.35 mm. In addition, the experimental data with the 3 mm-long coil was much lower than the simulation result, which is due to the magnetic

flux leakage caused by the larger space between each turn of the coil.

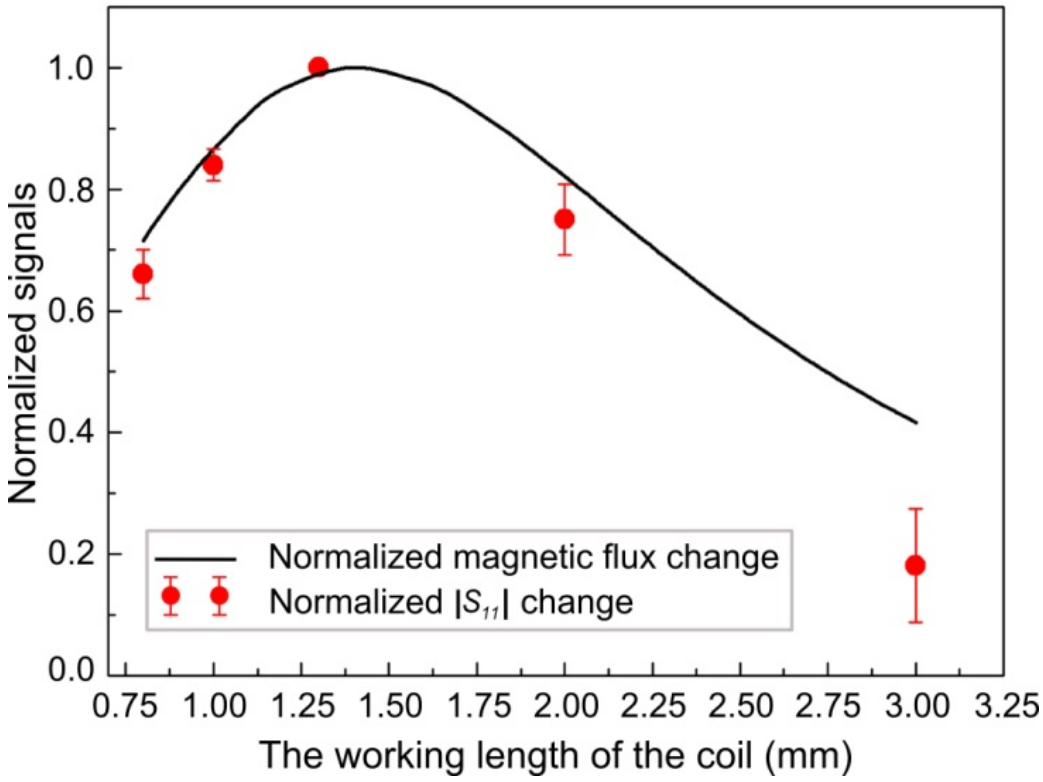

Figure 5.9 Comparison between normalized $\Delta|S_{11}|$ experimental data and the calculated result of normalized magnetic flux change.

5.5 Conclusions

A newly designed surface-scanning coil detector was introduced for bacteria detection with ME biosensors. The interaction between the coil and the sensor is due to mutual inductance caused by the sensor's vibration. A model of sensor's longitudinal vibration and an equivalent electric circuit of the detection system were constructed to theoretically evaluate the new design. The model predicted that the working length of the coil significantly affects the signal amplitude. Agreement

between the model and experiment was found to be excellent. For a 1 mm-long sensor, the coil with a working length of 1.3 mm showed the best signal amplitude. Proof in principle has been established for the direct detection of pathogenic bacteria on fresh fruits and vegetable surfaces by this new technique. This new technique eliminates time-consuming and costly sample selection and preparation steps previously required.

Bibliography

1. CDC, Estimates of Foodborne Illness in the United States, 2011.
2. FDA, Survey of Domestic Fresh Produce-Domestic Produce Assignment (DFP # 05-20). Attachment D: Tomato Soak Method for *Salmonella* analysis, 2005.
3. Y. Chai, S. Li, S. Horikawa, M. Park, V. Vodyanoy, and B.A. Chin. Rapid and sensitive detection of *Salmonella* Typhimurium on eggshells by using wireless biosensors, *Journal of Food Protection* 6: 631-636, 2012.
4. S. Horikawa, D. Bedi, S. Li, W. Shen, S. Huang, I. Chen, Y. Chai, M.L. Auad, M.J. Bozack, J.M. Barbaree, V.A. Petrenko and B.A. Chin. Effects of surface functionalization on the surface phage coverage and the subsequent performance of phage-immobilized magnetoelastic biosensors, *Biosensors and Bioelectronics* 26: 2361-2367, 2011.
5. S. Li, Y. Li, H. Chen, S. Horikawa, W. Shen, A. Simonian, and B.A. Chin. Direct detection of *Salmonella* typhimurium on fresh produce using phage-based magnetoelastic biosensors, *Biosensors and Bioelectronics* 26(4): 1313-1319, 2010.
6. M. Park, H.C. Wikle, Y. Chai, S. Horikawa, W. Shen, and B.A. Chin. The effect of incubation time for *Salmonella* Typhimurium binding to phage-based magnetoelastic biosensors, *Food Control* 26(2): 539-545, 2012.
7. C.A. Grimes, P.G. Stoyanov, D. Kouzoudis, and K.G. Ong. Remote query

pressure measurement using magnetoelastic sensors, *Review of Scientific Instruments* 70(12): 4711-4714, 1999.

8. P. Kabos and V.S. Stalmachov, *Magnetostatic Waves and Their Application* (Chapman & Hall, London, 1994) p.163.
9. S. Li, S. Horikawa, M. Park, Y. Chai, V.J. Vodyanoy, and B.A. Chin. Amorphous metallic glass biosensors, *Intermetallics* 30, 80-85, 2012.
10. W. Shen, L.C. Mathison, V.A. Petrenko, and B.A. Chin. A pulse system for spectrum analysis of magnetoelastic biosensors, *Journal of Applied Physics* 96: 163502, 2010.
11. C. Liang, S. Morshed, and B. C. Prorok. Correction for longitudinal mode vibration in thin slender beams, *Applied Physics Letters* 90, 221912, 2007.
12. Y. Chai, S. Horikawa, S. Li, H.C. Wikle, and B.A. Chin. A surface-scanning coil detector for real-time, *in-situ* detection of bacteria on fresh food surfaces, *Biosensors and Bioelectronics* 50(15): 311-317, 2013.
13. D.S. Ballantine, R.M. White, S.J. Martin, A.J. Ricco, E.T. Zellers, G.C. Frye, and H. Wohltjen, *Acoustic Wave Sensors: Theory, Design and Physico-Chemical Applications* (Academic, New York, 1997).
14. S. Li, and Z. Cheng. Nonuniform mass detection using magnetostrictive biosensors operating under multiple harmonic resonance modes, *Journal of Applied Physics* 107: 114514, 2010.
15. S. Butterworth and F.D. Smith. The equivalent circuit of the magnetostriction oscillator, *Proceedings of the Physical Society* 43: 166, 1931.

16. C. Xue, X. Li, and C. Yang. Modeling and design of magnetoelastic micro-resonator system for ultrasensitive mass sensing applications, *IEEE transactions on magnetics* 48(11): 4092-4095, 2012.
17. W.V. Moer, and Y. Rolain. A large-signal network analyzer: why is it needed? *Microwave Magazine, IEEE* 7(6): 46-62, 2006.
18. B. Fateh. Master thesis, University of Rostock, Germany, 2006.
19. K. Surendra. Master thesis, Virginia Polytechnic Institute and State University, 2011.
20. J.D. Jackson, *Classical Electrodynamics* (John Wiley & Sons, Danvers, 1998) p.175.
21. S. Li, L. Orona, Z. Li, and Z. Cheng. Biosensor based on magnetostrictive microcantilever, *Applied Physics Letters* 88: 073507, 2006.

Chapter 6

Surface-Scanning Magnetic Coil Design and Microfabrication

6.1 Introduction

The real-time *in situ* detection of bacteria using ME biosensors was introduced in previous research [1]. The ME biosensor is an acoustic wave device whose resonant frequency is monitored to detect and quantify biochemical reactions that occur on the resonator platform [2-3]. With the surface scanning technique, bacteria may be directly detected on a food surface without removing the ME biosensors prior to performing the frequency measurements, and thus real-time *in situ* detection is possible [4-6]. A major challenge of this surface scanning technique is the weak mutual inductive coupling between the ME biosensor and the measurement circuit. A planar spiral coil was designed and microfabricated to increase the mutual inductance. There is a large body of research on the signal-to-noise ratio (SNR) for coils, most of which focus on the coil's self-resonance. However, the specific functions of the coil for ME sensor detection in this research are the excitation of the sensor's vibration and detection of the associated resonant frequency [7-9]. In addition, this planar coil can largely improve the detector's standoff detection distance, which enables bacterial detection on fruits and vegetables with surfaces of large curvature and roughness.

6.2 Model calculation

ME resonators work on the principle of Joule magnetostriction, where the material undergoes dimensional changes in the presence of a magnetic field [10-11]. As it was discussed in Chapter 5, the ME materials can efficiently convert the applied magnetic energy into mechanical vibration when a time-varying magnetic field is applied. The resonant frequency of the ME sensor is inversely proportional to the resonator's mass [12]. When the ME biosensor comes into contact and binds with the specific target bacteria, the binding causes an increase in the mass of the sensor, which results in a decrease in resonant frequency [13-14]. This decrease in resonant frequency is also proportional to the number of bacterial cells bound to the biosensor surface [15].

The oscillating magnetic field that excites the sensor's vibration is generated by an electromagnetic coil. The coil and the sensor are mutually inductively coupled, so that the mechanical vibration results in a varying magnetic flux that affects the impedance of the measurement circuit [16-17]. The amplitude of the sensor's vibration reaches its maximum at the sensor's resonant frequency, causing the largest impedance change of the measurement circuit. Increasing the mutual inductance will increase the magnitude of the impedance change at resonance [16-18].

Figure 6.1 shows two types of surface-scanning coils used to monitor the vibration of ME biosensors for the detection of bacteria on fresh food surfaces. After the ME biosensors are placed on the food surface, the detection coil is brought close to the biosensors to measure their resonant frequencies. Figure 6.1a shows a

rectangular-cross-section solenoid coil; while Fig. 6.1b shows a planar spiral coil. The magnetic field along the Y axis is used to excite the sensor's longitudinal vibration. The mutual inductance monotonically increases with the number of turns of the coil and the magnetic flux change due to the sensor's vibration. In order to focus on the effect of different coil structures on the detection signal, these two coils with the same number of turns (40 turns) were designed with similar electric resistances (49.83 Ω for the solenoid coil and 49.37 Ω for the planar spiral coil) and comparable reactances (1.96 μH for the solenoid coil and 2.08 μH for the planar coil).

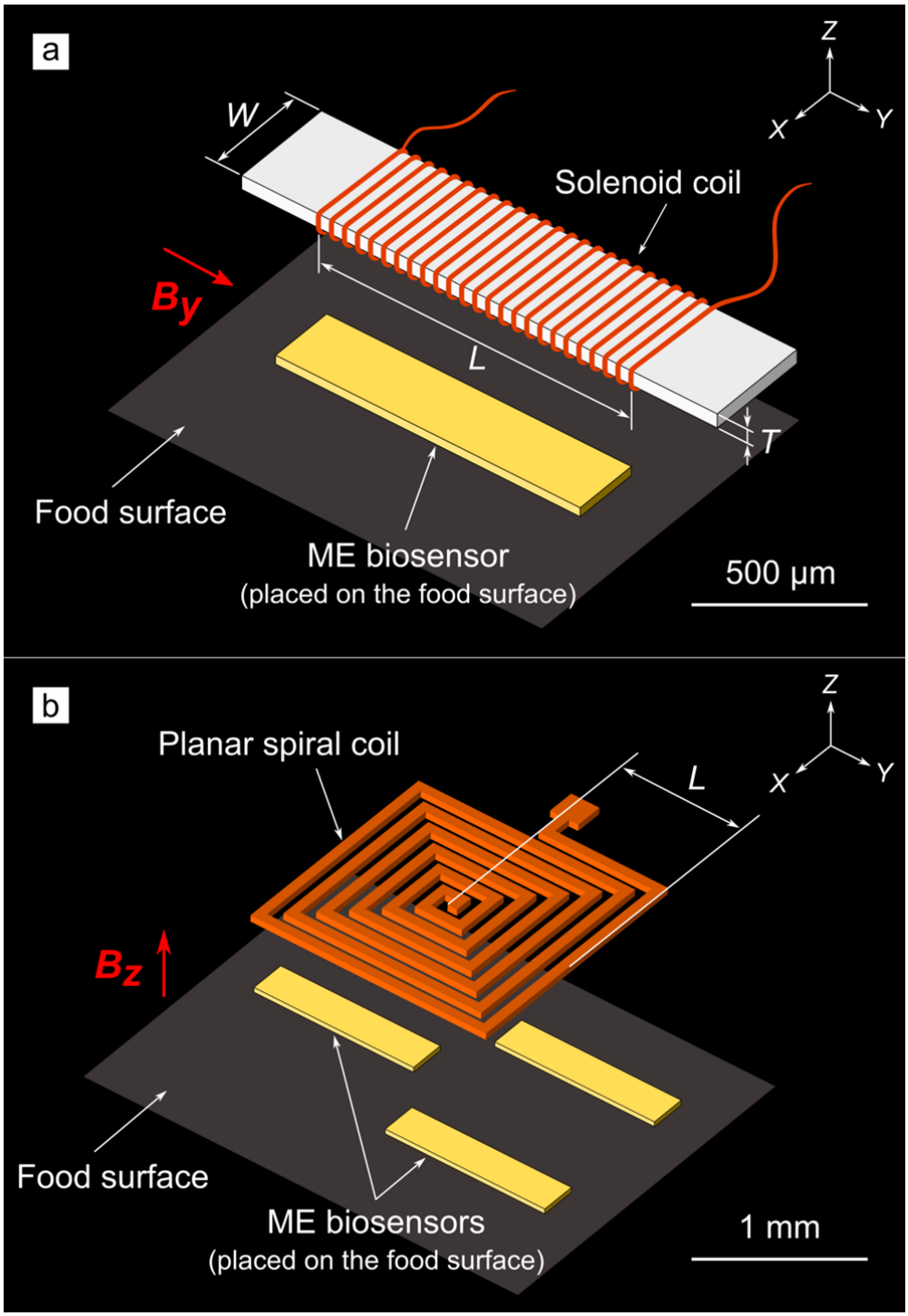

Figure 6.1 Comparison of two types of coil detectors: (a) a solenoid coil and (b) a planar spiral coil.

The magnetic flux from the sensor's vibration is calculated as:

$$\Phi_{total} = \sum_{i=1}^{N} \Phi_i = \sum_{i=1}^{N} (B_i A_i) \tag{6.1}$$

where B_i and A_i are the magnetic flux density created by the ME sensor and the cross-sectional area at each turn of the coils. The flux, Φ_i, passing through an area A_i is the integral of the magnetic flux density B_i over that area. As the flux density and the cross-sectional areas are not uniform, the total magnetic flux, Φ_{total}, is calculated by accumulating the magnetic flux at each turn of the coils (N is the total number of turns) [17, 19]. For the solenoid and planar coils, the directions of the magnetic flux that passes through the coil's cross-sectional areas are different. As shown in Fig. 6.1, the cross-sectional areas are in the X-Z plane for the solenoid coil and X-Y plane for the planar coil. Hence, the magnetic flux densities B_y (perpendicular to the X-Z plane) and B_z (perpendicular to the X-Y plane) are mutual inductively coupled with the solenoid and planar coils, respectively.

With the same assumptions in Chapter 5, the ME sensor was modeled as a one-dimensional magnetic dipole, and the sensor's vibration was treated as periodic changes in the distance between the south and north poles (Fig. 5.6b). Letting B_s and B_n be the component magnetic inductances due to the south and north poles of magnetic dipole, the magnetic flux density created by the ME sensor can be calculated as $\vec{B} = \overrightarrow{B_s} + \overrightarrow{B_n}$. Based on Biot-Savart law [20, 21], B_y was calculated by Eq. 5.6 and B_z at an arbitrary point (Q) around the magnetic dipole is:

$$B_z = \left(\frac{\mu_0 P}{4\pi\, r_1^2} \times \frac{d}{r_1}\right) + \left(\frac{\mu_0 P}{4\pi\, r_2^2} \times \frac{d}{r_2}\right) \tag{6.2}$$

where μ_0 is the permeability of free space; l_1, l_2, r_1, r_2 and d are distances shown in Fig. 5.6b (i.e., $l_1 + l_2$ is equal to the ME sensor's length, and d is the detection distance between the sensor and coil); and P is the strength of the magnetic poles, determined by the relative permeability of the ME material, the cross-sectional area of the sensor, and the excitation magnetic field around the sensor. As the magnetic flux density, B, is a function of sensor length, the longitudinally vibrating sensor changes its length and creates a magnetic flux change. The displacement of points during this vibration was calculated by Eq. 5.5 and the maximum change of magnetic flux, $\Delta\Phi_{max}$, due to the change of sensor length was calculated by Eq. 5.10. Depending on the relationship between S_{11} parameter and magnetic flux (shown in Fig. 5.7), the experiment data and simulation results were compared and discussed.

6.3 The spiral planar coil's fabrication process

The spiral planar coil detector was microfabricated on a transparent silicon glass wafer with the electrodeposition method. The fabrication masks were designed with AutoCAD. The whole fabrication process was completed in Electrical Engineering of Auburn University. The geometry of the coil was calculated and adjusted to control the coil's self-resistance, self-inductance and self-capacitance. The top surface of the coil was covered by SU-8 photoresist to resist Cu surface oxidization and physical damage. The process details are shown in Fig. 6.2.

Cleaning of a substrate

Ar plasma cleaning 10mins

E-beam of Ti/Cu

Ion mill 2 mins
Ti 1000 Å (10nm)
Cu 4000 Å (400nm)

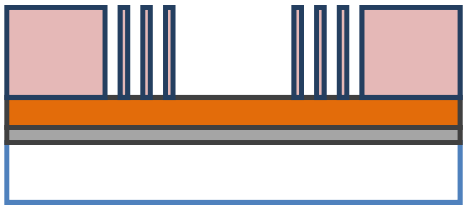

Wafer patterning with AZ resist

Dry surface:
(Ultra clean) 120˚C 20min (cool down 5min)
AZ 9245 (7.9-um thick)
Spin-coated @ 900rpm (500rpm/s) for 5 sec
1000rpm (1000rpm/s) for 30 sec
Soft bake: 105 ˚C 60 sec
UV exposure for 30 sec
Develop AZ400K (1:2 water), 2min+30sec

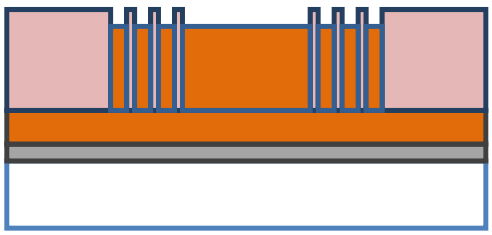

Cu electroplating

7 um/15 um thick
Electric current density: 3.12 mA/cm^2
Area to be deposited: 1.7/3.7cm^2
HCl 1% solution to clean Cu surface (3 sec)
Plating process:
2.35mA/cm^2 30mins + 3.12mA/cm^2

Removal of the AZ resist

Immersed in acetone
no sonicated

Etching of the Ti/Cu

Wet etching of Cu at 30 ˚C, about 8min (just check it by microscope) (etch solution: 49-1)
BOE water for Ti layer
O_2: 8sccm & SF_6: 40 sccm, 700W RF

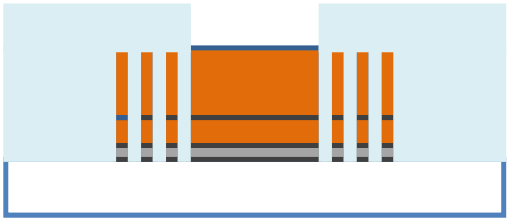

Wafer patterning with SU-8 resist

SU-8 3005 (cover 7um/ 13um structure on glass)
Spin-coated @500 rpm (100 rpm/s) for10 sec
1500/900 rpm (200 rpm/s) for 30 sec
Delay several time (2-3 min)
Soft bake: 95 ˚C,3 min/7 min
Exposure: 14sec/15 sec
Post exposure bake: 65˚C 1min; 95 ˚C 2min
Developer (no dilution) 3min/5min
Hard bake: 150 ˚C 15min

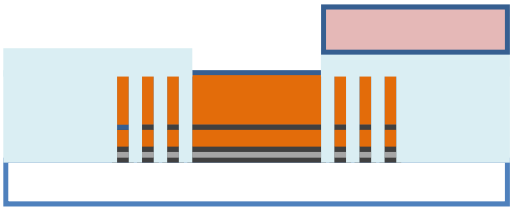

Wafer patterning with AZ resist

AZ 5214Z (2.2-2.3 um thick)
Spin-coated @ 300rpm (100rpm/s) for 5 sec
1000rpm (500rpm/s) for 30 sec
Soft bake: 110 ˚C 60 sec
UV exposure for 15 sec
Development: 1:3 water 1.5 min

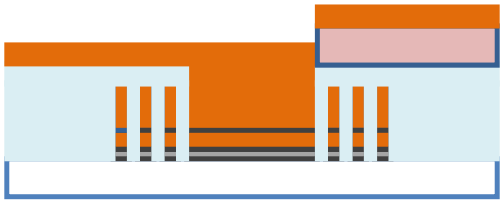

Sputtering of Cu

Cu 250 W DC for 1200 sec (1um)
Ar: 25 sccm
Substrate holder rotation: 50%

Removal of the AZ

Immersed in acetone
Rotated sonicated

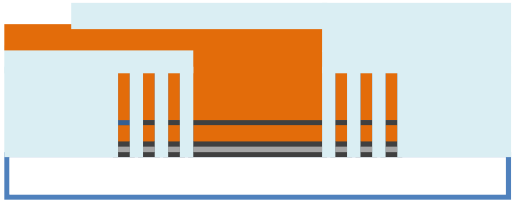

Wafer patterning with SU-8 resist

SU-8 3005 (As thin as possible)
Spin-coated @500 rpm (100 rpm/s) for10 sec
6000rpm (200 rpm/s) for 45 sec
Delay several time
Soft bake: 95 ˚C, 2.5min
Exposure: 13sec
Post exposure bake: 65 ˚C 1min; 95 ˚C 1.5min
Developer (no dilution) 2min
Hard bake: 150 ˚C 15min

Figure 6.2 Microfabrication process for spiral planar coil detector.

6.4 Results and discussion

6.4.1 Comparison of theoretical simulations result and experiment data

This magnetic flux change causes an impedance change in the measurement circuit through mutual inductive coupling. The impedance change was determined using a network analyzer configured to measure the input reflection coefficient (S_{11} parameter) at around the sensor's resonant frequency. The S_{11} parameter is related to the impedance of the measurement circuit and internal impedance of the network analyzer [20]. Figure 6.3 compares the normalized absolute value of S_{11}, $|S_{11}|$, for two types of the coil detectors in the presence of a 1 mm-long sensor. Using the same ME sensor, the $|S_{11}|$ peak amplitude ($\Delta|S_{11}|$) for the planar coil is almost triple that for the solenoid coil. Therefore, the coil structure affects the coil's ability to sense the magnetic flux change and $|S_{11}|$ signal amplitude.

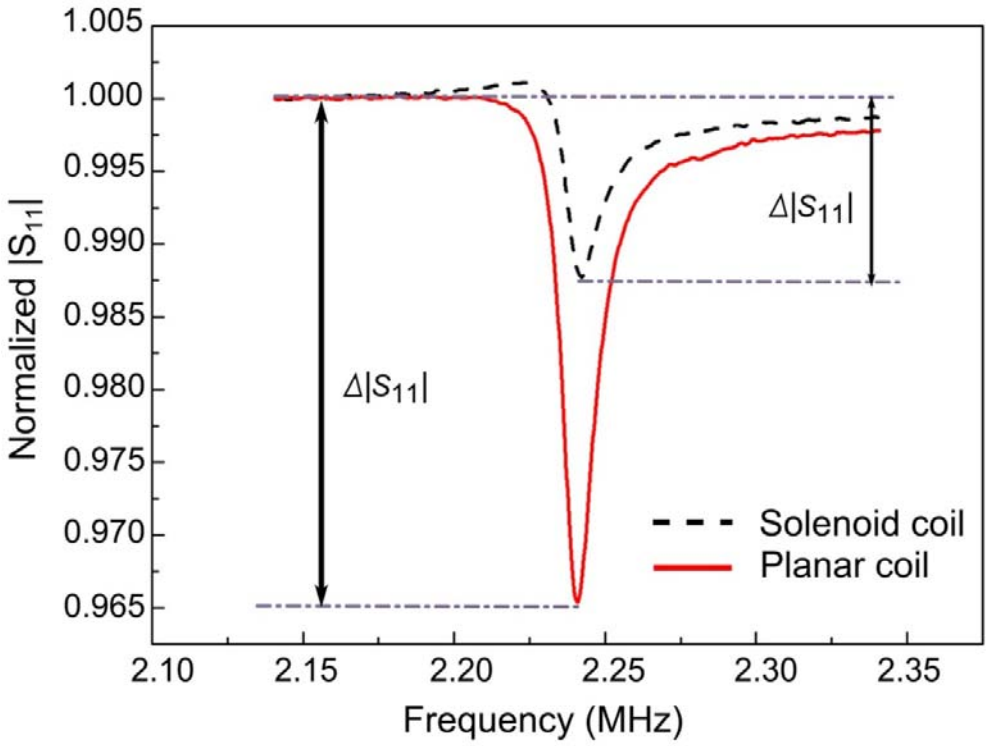

Figure. 6.3 Comparison of normalized $|S_{11}|$ for the solenoid and planar coil detectors in the presence of a 1 mm-long sensor.

As the $|S_{11}|$ peak appears due to the coupled magnetic flux changes, Fig. 6.4 compares theoretical simulations (normalized magnetic flux changes) and experimental measurements (normalized $|S_{11}|$ peak amplitude) as a function of detection distance, d, for the two types of coils. In this experiment, the sensor was placed on surface of a tomato, and the coils were brought close to the sensor to read its characteristic resonant frequency (the process is shown in Fig. 6.1). The scattered points in Fig. 6.4 represent the normalized $|S_{11}|$ peak amplitude (triangles and stars represent the measurements using the planar and solenoid coils, respectively), whereas the smooth lines are the normalized magnetic flux changes (solid and dashed

lines represent planar and solenoid coil calculations, respectively). The signal amplitude decreases as detection distance increases, which is due to the decreasing mutual inductance. In order to pursue rapid *in situ* bacteria detection via surface-scanning, a longer detection distance is desired, especially for the detection on surfaces with large curvature or roughness. Both the theoretical simulation results and the experimental data show that for the same normalized signal, the detection distance of the planar coil is much larger than that of the solenoid coil. This is because the magnetic flux change perpendicular to the sensor's longitudinal vibration direction (B_z) is larger than that parallel to the sensor's vibration (B_y). If the standoff distance (the longest distance in which the ME biosensor signal may be distinguished) is defined as the distance where $\Delta|S_{11}| > \overline{\Delta|S_{11}|}' \pm 3\sigma$ ($\Delta|S_{11}|$ is the signal amplitude, $\overline{\Delta|S_{11}|}'$ is the arithmetic mean of the peak-to-peak noise amplitude, and σ is the standard deviation of the noise amplitude) [21], the standoff distances for the solenoid coil and planar coil were 0.4 mm and 1.25 mm, respectively (Fig. 6.4).

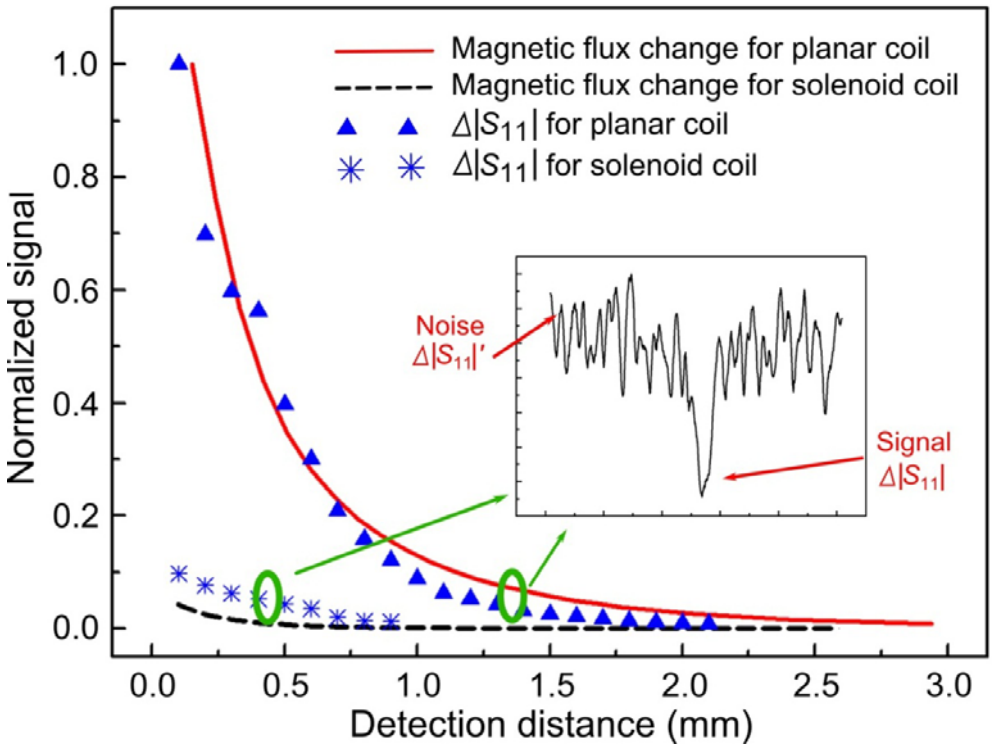

Figure. 6.4 Comparison of the experimental measurements and theoretical simulation results with detection distances for solenoid and planar coils.

Meanwhile, the theoretical simulations agree with experimental measurements in Fig. 6.4, though the experimental measurements of the solenoid coil by normalization are closer to the planar coil's data. It is because the experimentally measured signal amplitude, $\Delta|S_{11}|$, and theoretically calculated magnetic flux change, $\Delta\Phi$, cannot be directly compared by normalization. Table 6.1 shows the selected data of the experiment test and simulation result，which were normalized by the largest value of $\Delta|S_{11}|$ and $\Delta\Phi_{max}$, respectively. In order to compare the signal from different coils, "Ratio" shows the ratio of solenoid and planar coils' signal at each distance position. In Table 6.1, $\Delta|S_{11}|$ and $\Delta\Phi_{max}$ keep the same trend and the planar coil detector has

much larger signal amplitude. However, comparing with the $\Delta|S_{11}|$ signal, the ratio of $\Delta\Phi_{max}$ is much smaller. Furthermore, the ratio of $\Delta|S_{11}|$ signal maintains at a certain range, while the ratio of $\Delta\Phi_{max}$ decreases in an exponential curve (shown in Fig. 6.5). Hence, the relationship between S_{11} signal and magnetic flux change needs to be discussed.

Table 6.1 Comparison of experimental data and theoretical results.

Experimental data ($\Delta\|S_{11}\|$)				Theoretical results ($\Delta\Phi_{max}$)			
Distance (mm)	Solenoid Coil	Planar Coil	Ratio (100%)	Distance (mm)	Solenoid Coil	Planar Coil	Ratio (100%)
0.1	0.09776	1	9.776	0.15	0.03010	1	3.101
0.2	0.07591	0.69838	10.8694	0.24	0.01941	0.76284	2.5444
0.3	0.06256	0.59651	10.4877	0.33	0.01445	0.56782	2.5448
0.4	0.05165	0.56273	9.17847	0.42	0.00954	0.43739	2.1811
0.5	0.04289	0.39710	10.8008	0.51	0.00650	0.34689	1.8737
0.6	0.03511	0.29967	11.7162	0.60	0.00454	0.28117	1.6147
0.7	0.02018	0.20833	9.68655	0.69	0.00362	0.23165	1.5627
0.8	0.01330	0.15816	8.40921	0.78	0.00261	0.19323	1.3507
0.9	0.01190	0.12020	9.90017	0.87	0.00192	0.16273	1.1799
1.0	0.00949	0.08830	10.7475	0.96	0.00143	0.13811	1.0354

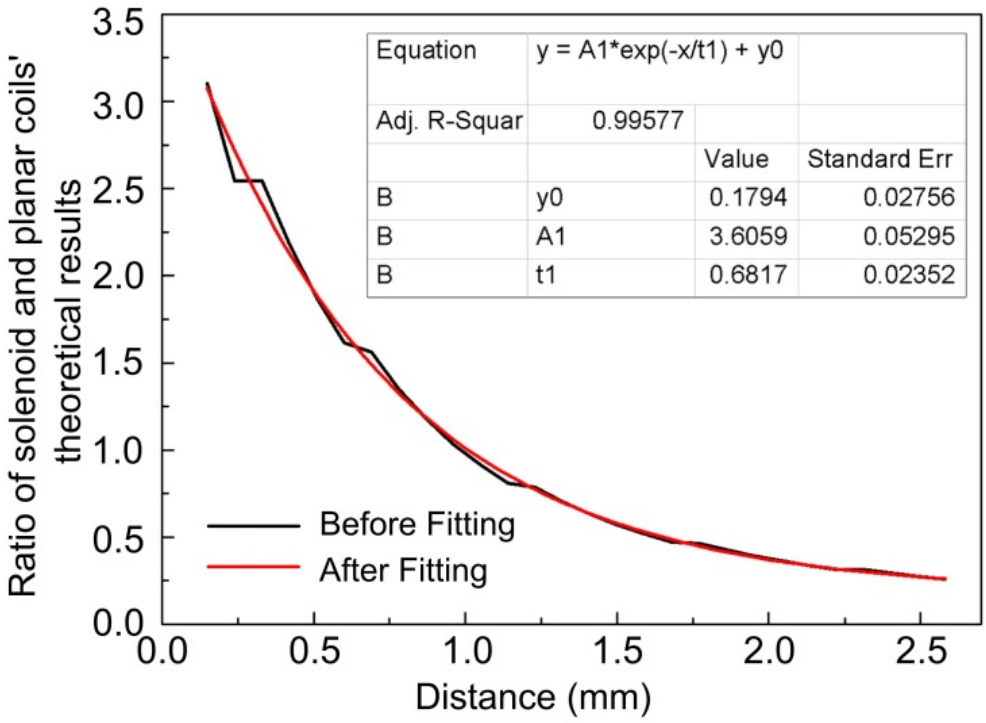

Figure 6.5 The ratio of the theoretical results with detection distance.

The magnetic flux change from sensor's vibration is mutually coupled with the coil detector and change the impedance of the measurement circuit. The impedance change was determined using a network analyzer configured to measure the input reflection coefficient (S_{11} parameter). Fig. 5.3 shows the equivalent circuit of a network analyzer, an electromagnetic coil, and the ME sensor. The relationship between $|S_{11}|$ and Φ_{max} was summarized in Fig. 5.7. Based on the previous discussion in Chapter 5, the load impedance difference increases with increasing mutual inductance as a result of the vibration of the ME sensor; the test signal mainly depends on the load impedance difference, increasing the mutual inductance is a key to improving signal amplitude. Therefore, the signal of $\Delta|S_{11}|$ mainly depends the magnetic flux change, but they are not linear related.

6.4.2 The multiple ME biosensors detection with the spiral planar coil

The longer detection distance and open detection space surrounding the planar coil detector also provides the opportunity for simultaneous measurement of multiple biosensors on food surfaces. As shown in Fig. 6.5a, three ME sensors are placed in the large working space of the planar coil. The lengths of these sensors were slightly different so that they would have different and distinguishable resonant frequencies. Hence, the multiple peaks appear in Fig. 6.5b. Previous research has shown that the multiple biosensors are necessary since bacterial cells may not be uniformly distributed across the food surfaces [1, 4]. As the solenoid coil can only detect over a shorter distance and has little working space, only one biosensor at a time can be detected using the solenoid coil. The simultaneous measurement of multiple biosensors with the newly designed planar coil promises to greatly shorten the analysis time for bacterial detection.

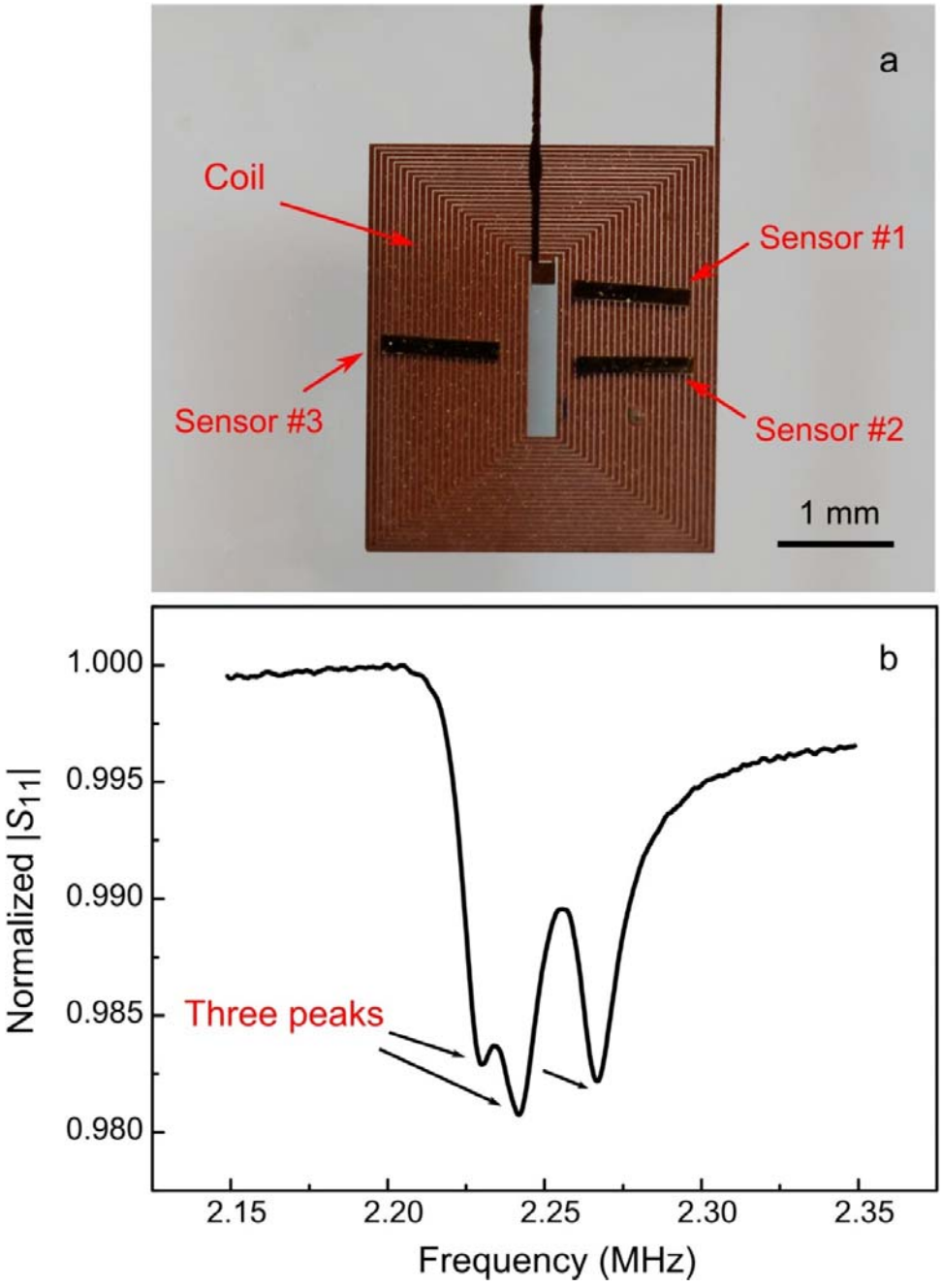

Figure 6.5 Multiple sensors measured with the planar coil: (a) three ME sensors were in the working space of the coil, and (b) three peaks were shown for normalized $|S_{11}|$ signal.

6.5 Conclusions

In this chapter, we have demonstrated that a planar spiral coil can be used as a surface-scanning detector for ME biosensor detection on surfaces. Compared with previous usage of a solenoid coil, the planar coil detector gives a much larger signal amplitude at resonance. In order to explain the reason for the different signal amplitudes, a theory of mutual inductive coupling between a vibrating sensor and the coil detectors was proposed. Based on the sensor's longitudinal vibration and the structure of the coils, the planar spiral coil detector was found to be more sensitive at detecting the coupled magnetic flux changes. In addition, both numerical simulation data and experimental results demonstrate that the planar coil detector has dramatically improved the detection distance, which is significant for surface scanning especially with large curvature or rough surfaces. Furthermore, the ability to simultaneously detect multiple sensors on surfaces has been demonstrated.

Bibliography

1. Y. Chai, S. Horikawa, S. Li, H.C. Wikle, and B.A. Chin. A surface-scanning coil detector for real-time, *in-situ* detection of bacteria on fresh food surfaces, *Biosensors and Bioelectronics*. 50(15): 311-317, 2013.
2. S. Li, L. Orona, Z. Li, and Z. Cheng. Biosensor based on magnetostrictive microcantilever, *Applied Physics Letters* 88: 073507, 2006.
3. W. Shen, L.C. Mathison, V.A. Petrenko, and B.A. Chin. A pulse system for spectrum analysis of magnetoelastic biosensors, *Applied Physics Letters* 96: 163502, 2010.
4. S. Li, Y. Li, H. Chen, S. Horikawa, W. Shen, A. Simonian, and B.A. Chin. Direct detection of *Salmonella typhimurium* on fresh produce using phage-based magnetoelastic biosensors, *Biosensors and Bioelectronics* 26(4): 1313-1319, 2010.
5. Y. Chai, S. Li, S. Horikawa, M. Park, V. Vodyanoy, and B.A. Chin. Rapid and sensitive detection of *Salmonella* Typhimurium on eggshells by using wireless biosensors, *Journal of Food Protection* 6: 631-636, 2012.
6. M. Park, H.C. Wikle, Y. Chai, S. Horikawa, W. Shen, and B.A. Chin. The effect of incubation time for *Salmonella* Typhimurium binding to phage-based magnetoelastic biosensors, *Food Control* 26(2): 539-545, 2012.
7. D. Niarchos. Magnetic MEMS: key issues and some applications, *Sensors and*

Actuators A: Physical 106: 255-262, 2003.

8. S. Li, S. Horikawa, M. Park, Y. Chai, V.J. Vodyanoy, and B.A. Chin. Amorphous metallic glass biosensors, *Intermetallics* 30, 80-85, 2012.
9. P. Kabos and V.S. Stalmachov, *Magnetostatic Waves and Their Application* (Chapman & Hall, London, 1994) p.163.
10. C. Liang, S. Morshed, and B. C. Prorok. Correction for longitudinal mode vibration in thin slender beams, *Applied Physics Letters* 90, 221912, 2007.
11. S. Horikawa, D. Bedi, S. Li, W. Shen, S. Huang, I. Chen, Y. Chai, M.L. Auad, M.J. Bozack, J.M. Barbaree, V.A. Petrenko and B.A. Chin. Effects of surface functionalization on the surface phage coverage and the subsequent performance of phage-immobilized magnetoelastic biosensors, *Biosensors and Bioelectronics* 26: 2361-2367, 2011.
12. V.A. Petrenko and V.J. Vodyanoy. Phage display for detection of biological threat agents, *Journal of Microbiological Methods* 53 (2), 253-262, 2003.
13. S. Li, and Z. Cheng. Nonuniform mass detection using magnetostrictive biosensors operating under multiple harmonic resonance modes, *Journal of Applied Physics* 107: 114514, 2010.
14. C. Xue, X. Li, and C. Yang. Modeling and design of magnetoelastic micro-resonator system for ultrasensitive mass sensing applications, *IEEE transactions on magnetics* 48(11): 4092-4095, 2012.
15. S. Butterworth and F.D. Smith. The equivalent circuit of the magnetostriction oscillator, *Proceedings of the Physical Society* 43: 166, 1931.

16. B. Fateh, Master thesis, University of Rostock, Germany, 2006.

17. K. Surendra, Master thesis, Virginia Polytechnic Institute and State University, 2011.

18. S. Li, L. Orona, Z. Li, and Z. Cheng. Biosensor based on magnetostrictive microcantilever. *Applied Physics Letters* 88: 073507, 2006.

19. J.D. Jackson, Classical Electrodynamics (John Wiley & Sons, Danvers, 1998) p.175.

20. D.S. Ballantine, R.M. White, S.J. Martin, A.J. Ricco, E.T. Zellers, G.C. Frye, and H. Wohltjen, *Acoustic Wave Sensors: Theory, Design and Physico-Chemical Applications* (Academic, New York, 1997) p.41.

21. W.V. Moer, and Y. Rolain. A large-signal network analyzer: why is it needed? *Microwave Magazine, IEEE* 7(6): 46-62, 2006.

22. V. Thomsen, D. Schatzlein, and D. Mercuro, Limits of detection in spectroscopy, *Spectroscopy* 18: 112-114, 2003.

Chapter 7

Real-time *in situ* bacteria detection on fresh food surfaces with surface-scanning coil and ME biosensors

7.1 Introduction

This paper demonstrates new technology that enables the ME biosensors to be measured at a location outside the boundaries of a solenoid coil. In all research conducted to date, ME biosensors have been placed inside a solenoid coil to measure their resonant frequency [1-2]. This limits the use of ME biosensors to small objects or volumes that will fit within the coil. Hence, by enabling measurement outside the coil, *in-situ* measurements on surfaces of any size become possible. In this work, we demonstrate proof in principle of a surface-scanning coil detector by measuring bacteria concentration on a food surface using ME biosensors. This technique differs from all previous reports using ME biosensors to measure surface contamination, where retrieval and frequency measurement of the biosensors in the coil were required after exposure to bacteria [3-5].

Figure 7.1 compares the differences between the old and new methods of measurement. In both of the methods, a coil is used to create a time-varying magnetic field that excites and detects the biosensor vibration, hence acquiring the biosensor resonant frequency. However, the measurement procedures and signal results are

different with the different coil designs. In previous work, the ME biosensors required placement inside the solenoid coil for the frequency measurement (Fig. 7.1 a1), and then they were moved out of the coil for bacteria exposure on the food surface [3-5]. Hence, the detection was cumbersome and not real-time because the following three separate steps were required: 1) measurement of the initial resonant frequency of the biosensor inside the coil; 2) exposure to bacteria on the food surface outside of the coil; and 3) placement of the biosensor back inside the coil for the final resonant frequency measurement after bacteria exposure. By contrast, the new detection system shown in Fig. 7.1 b1 enables the measurement of the biosensor frequency directly on a food surface. In this new system, a coil with a rectangular cross-section is utilized to scan the food surface and read the biosensor's response. With the old measurement method, only two frequency measurements were made, before and after bacteria exposure (Fig. 7.1 a2), whereas now continuous, real-time measurements of the resonant frequency can be performed during bacteria exposure (Fig. 7.1 b2).

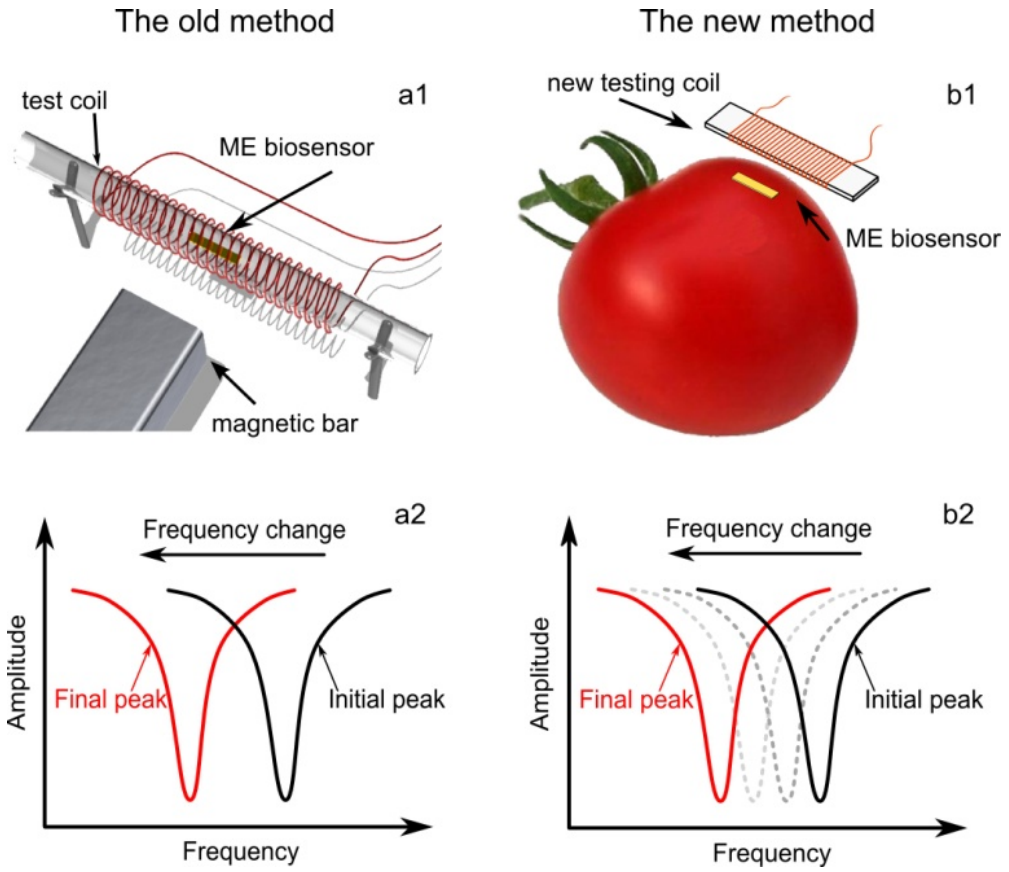

Figure 7.1 Comparison between old and new measurement methods: (a1) ME biosensor's old frequency detection method, (a2) the signal of frequency change for the old method, (b1) ME biosensor's detection in new method, (b2) the continuous measurement of frequency change in new experiment.

7.2 Materials and methods

The ME biosensors' preparation is the same as the previous experiment (E2 phage immobilization and BSA surface blocking). In this research, *Salmonella enterica* serovar Typhimurium culture with a concentration of 5×10^8 CFU/ml was provided by Dr. James M. Barbaree's laboratory. The original *S.* Typhimurium solution was serially diluted to lower concentrations (ranging from 5×10^7 CFU/ml to 5×10^1

CFU/ml) with deionized water. Tomatoes were purchased from a local grocery store and the tomato surfaces were cleaned with deionized water. The *S.* Typhimurium solutions of six different concentrations (5×10^8 CFU/ml to 5×10^3 CFU/ml) with the same volume (2.5×10^{-2} ml) were inoculated onto the tomato surfaces. The contamination area was a circle with a diameter of 3 to 4 mm. The corresponding surface *S.* Typhimurium concentrations ranged from 1.5×10^6 CFU/mm^2 to 1.5×10^0 CFU/mm^2. ME biosensors were then placed on the inoculated regions of the tomato surface and the tomatoes with biosensors placed in a humidity-controlled environment (95 % RH or 50 % RH). The detector coil was then placed above the biosensors during the measurement. Figure 7.2a shows the coil structure and bacteria detection on a tomato surface with ME biosensors. The ME biosensors were located under the coil and on the tomato surface during the entire procedure. An oscillating magnetic field produced outside of the coil actuates longitudinal vibration of the biosensor. The resultant magnetic flux created by the biosensor was then immediately picked up by the same coil, and the resonant frequency was measured (Fig. 7.2b). The sensor's resonant frequency was measured at intervals (3, 8, 15, and 25 min) after the biosensors were exposed to *S.* Typhimurium on the tomato surface. Figure 7.2c and 7.2d illustrate the measurement setup. A constant-bias magnetic field was used to amplify the signal. For this purpose, permanent magnets arrayed upon two parallel sheets of ferromagnetic material were set up on two sides of the coil. The magnets created a strong and uniform magnetic field around the biosensor. The detection coil was connected to a network analyzer (Fig. 7.2d). The network analyzer (HP network

analyzer model 8751A) is responsible for generating the oscillating external magnetic field. The input reflection coefficient of the network circuit, S_{11} (S-parameter), was used to measure the signal.

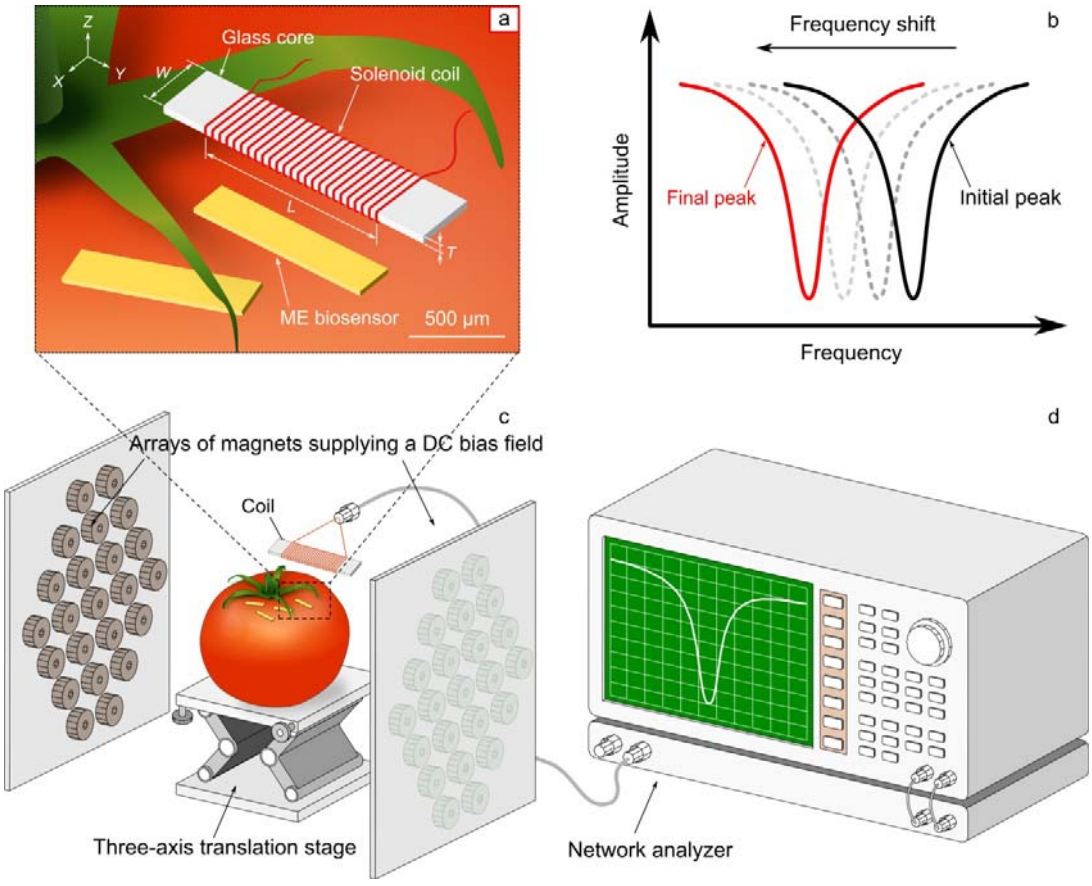

Figure 7.2 New methodology for *S.* Typhimurium detection on tomato surface.

7.3 Results and discussion

7.3.1 Real-time detection and humidity effects

The real-time response of ME biosensors exposed to *S.* Typhimurium on tomato surfaces was examined. Measurement and control biosensors were placed upon a tomato surface for bacteria exposure, and the biosensors' resonant frequency was

measured with time. Figure 7.3 represents the real-time frequency changes during exposure to *S.* Typhimurium at a concentration of 1.5×10^6 CFU/mm^2 in 95 % and 50 % RH environments. In Fig. 7.3, the solid line shows the frequency changes of one sample of measurement biosensor during bacteria exposure, while the dashed line shows a control biosensor. Error bars which represent the measurement error from the environment and resolution of the detection system are shown on each test point. Figure 7.3a shows the biosensor's frequency changes in a high humidity condition (95 % RH). The result showed the frequency from 0 to 10 min had a large change. After 15 min, the frequency reached the upper plateau and remained relatively constant. This result indicates the binding reaction between the E2 phage and *S.* Typhimurium cells is not an instantaneous process; and the detection time should be about 15 min for the ME biosensors.

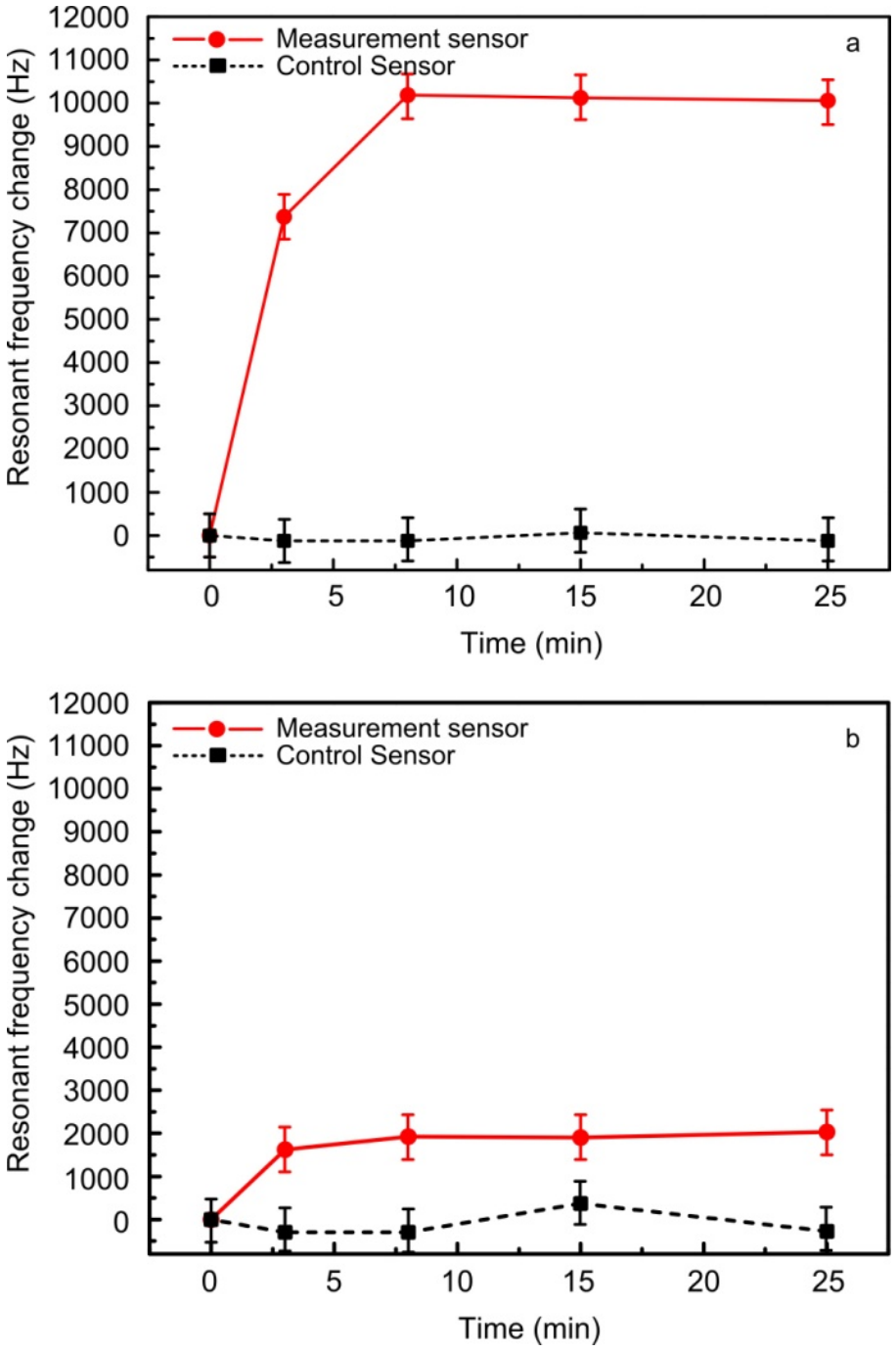

Figure 7.3 Frequency changes with time at different humidity: (a) 95 % RH and (b) 50 % RH (Solid curves show one sample of the measurement biosensor response, while dashed curves show one sample of the control biosensor response).

The environmental humidity has a significant effect on the reaction between E2 phage and *S.* Typhimurium. Figure 7.3a and 7.3b are resonant frequency measurements in humid environments of 95 % RH and 50 % RH, respectively. The control biosensors for both conditions have similar frequency changes. However, the measurement biosensor in 95 % RH environment show much greater frequency changes than that tested in the 50 % RH environment. For the measurement biosensors, the resonant frequency change is approximately 10,000 Hz at 95 % RH and 2,000 Hz at 50 % RH. Hence, the higher humidity led to greater binding between the phage and bacterial cells.

There are two reasons for the effect of humidity on the specific binding reaction. First, water is the medium for the movement of the bacterial cells [6]. With less water available, the phage and bacteria have a lower opportunity to encounter and bind. Second, a high humidity environment helps maintain the three-dimensional structure of the functional protein in the phage [7]. Specifically, the pVIII protein, which is the functional protein of E2 phage for the specific binding with *S.* Typhimurium, may lose the binding affinity with an altered structure in low humidity [8].

7.3.2 Food contamination detection with ME biosensors in different *S.* Typhimurium concentrations.

The effect of *S.* Typhimurium concentration on the biosensor response was studied. Three different bacteria surface concentrations (1.5×10^2, 1.5×10^4 and 1.5×10^6 CFU/mm^2) were inoculated on tomato surfaces, and the biosensors' resonant

frequencies measured. In this experiment, the relative humidity was maintained at 95%. Figure 7.4 displays the frequency changes of the measurement and control biosensors with time for the different bacteria concentrations. As can be seen, the frequency change settled to the final value within 15 min of exposure, with greater frequency changes as bacteria concentration increased. The SEM micrographs (on the right in Fig. 7.4) show the surface of the measurement biosensors with the captured bacterial cells. These micrographs corroborate the frequency change results and demonstrate that the ME biosensors captured more bacterial cells as the bacteria concentrations increased. For the control biosensors, the frequency changes do not show obvious differences for different concentrations. This demonstrates that specific binding to the bacteria occurred on the measurement biosensors. In short, this methodology demonstrates the specific and quantitative real-time detection on fresh food surfaces.

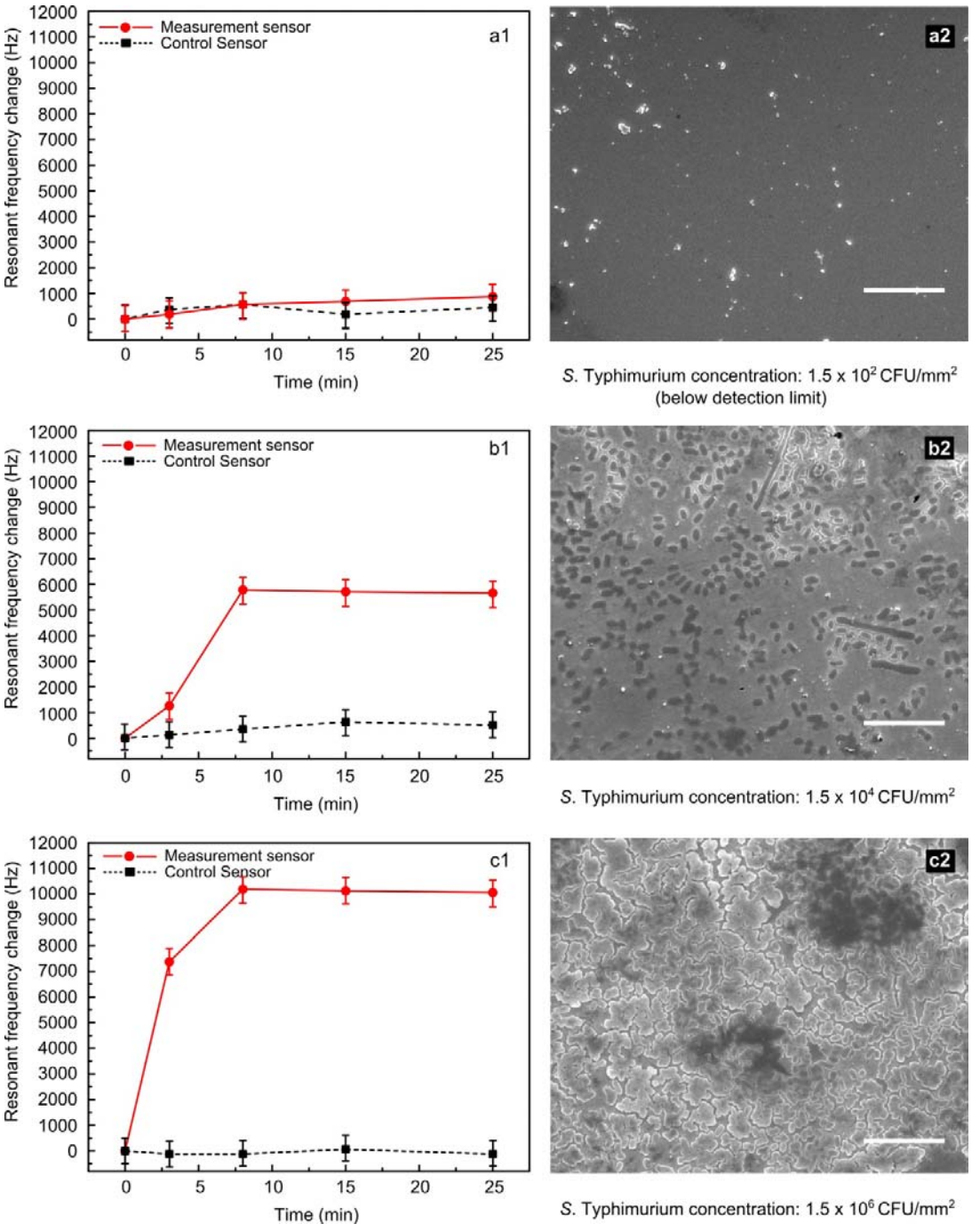

Figure 7.4 Resonant frequency changes with time for different *S*. Typhimurium concentrations: (a) 1.5×10^2 CFU/mm^2, (b) 1.5×10^4 CFU/mm^2 and (c)1.5×10^6 CFU/mm^2 (Measurement bar: 10μm;environmental humidity: 95 % RH).

Previous research has shown that the *S.* typhimurium cells on food surfaces are not uniformly distributed [4]. This is because the *S.* Typhimurium can swim and move freely on moist surfaces. Hence, the response of the ME biosensors largely depends on where the biosensors fall on the tomato surface. Therefore, a single biosensor is unlikely to be able to provide contamination information for the whole tomato. Multiple biosensors, thus, need to be employed to improve the probability of detection. The probability of detection is dependent on several factors, including the number of biosensors, the biosensors' size, and the roughness of food surfaces [9].

In order to study the detection limit of the new detection system, the *in situ* biosensor response of ten measurement biosensors and ten control biosensors were randomly placed on the contaminated surfaces and measured at each bacteria surface concentration (from 1.5×10^1 to 1.5×10^6 CFU/mm^2). A plot of the frequency changes for both the measurement (solid circles) and control (open triangles) biosensors in different bacteria concentrations is shown in Fig. 7.5. The data points are the arithmetic mean value with error bars representing the standard deviation. In addition, a Student's *t*-test calculation was performed to analyze the degree of dissimilarity between the measurement and control biosensors and is shown at each concentration. Figure 7.5 illustrates that the resonant frequency changes of the measurement biosensors were found to be largely dependent on the surface density of *S.* Typhimurium [10]. By contrast, the control biosensors showed much smaller responses, indicating that selective binding of *S.* Typhimurium on the measurement biosensors occurred. Meanwhile, the variance in the resonant frequency changes of

the measurement biosensors is due to the non-uniform distribution of *S.* Typhimurium on the tomato [4]. Increasing the number of biosensors can improve the repeatability of the detection on food surfaces [9]. From the *t*-test analysis, these responses of the measurement and control biosensors were found to be different down to 1.5×10^3 CFU/mm^2 with a confidence level of difference higher than 95 % ($p < 0.05$).

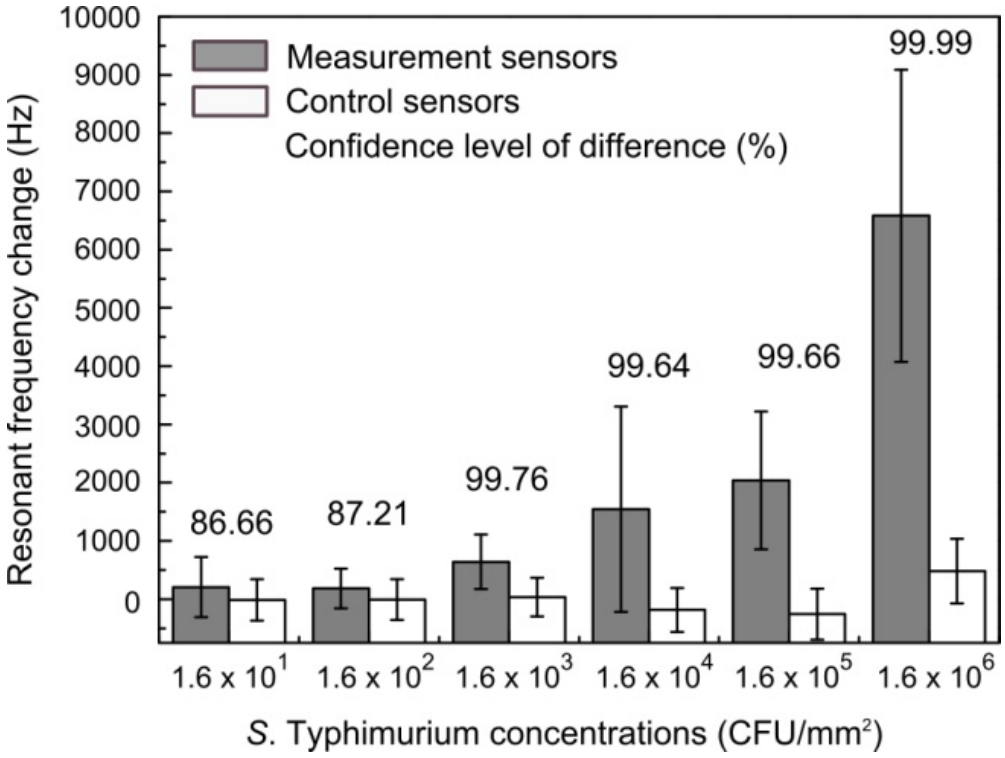

Figure 7.5 Resonant frequency changes for measurement and control biosensors placed on tomato surfaces inoculated with different concentrations of *S.* Typhimurium.

7.3.3 The ME biosensor's detection stability was improved by the new methodology

One of the advantages of this new measurement coil is the reduced variance in the control biosensor resonant frequency measurements, which increases the accuracy of measurements. Control biosensors were prepared following the same procedures as the measurement biosensors except without E2 phage immobilization. The purpose of the control biosensors is to compensate for environmental effects that are encountered and non-specific binding that may occur. Figure 7.6 compares the resonant frequency changes of control biosensors for the new (outside of the coil) and old (inside of the coil) measurement methods. For each concentration, there are ten samples with new and old methods, respectively. The error bars show the standard deviation value. Using the new method, the standard deviation was smaller and more stable than that with the old method in different concentrations. The stable standard deviation of control biosensors means higher reproducibility, which also indicates a lower measurement error of the detection system. A possible reason for this result stems from the differences in the manner of the measurement between the old and new methods. With the old method, the biosensor's resonant frequency needs to be separately measured twice: before and after bacteria exposure. The solenoid coil only exhibits a uniform magnetic field over a very small region, and it is difficult to position the biosensor at exactly the same place twice. Hence, the frequency measurements include a measurement error due to positioning of the biosensor. By contrast, the ME biosensor in the new method can be fixed in the same location within the magnetic field and the resonant frequency measured continuously.

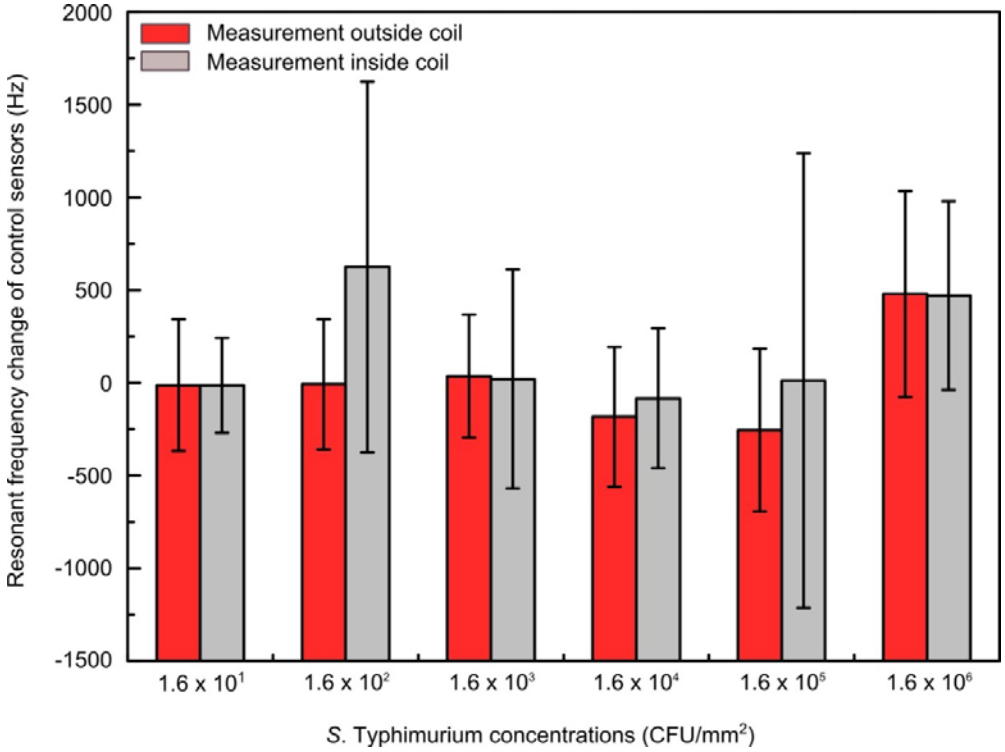

Figure 7.6 Resonant frequency changes of the control biosensors with the new (outside of the coil) and old (inside of the coil) experiments in different bacteria concentrations.

7.3.4 The real-time *in situ* detection on different food surfaces

In order to prove the ME biosensor system works for different food surfaces, this newly designed surface-scanning coil detector with 1mm-long ME biosensors was demonstrated by detecting *S.* Typhimurium on watermelon surfaces. In this biological experiment, the ME biosensors were placed on the surface of a watermelon; the coil was brought close to the biosensors; and the resonant frequency of the biosensors was measured over time. Figure 7.7 shows the absolute value of resonant frequency changes over time for ME biosensors (both measurement and control biosensors) placed on watermelon surfaces contaminated with different bacteria concentrations.

Error bars that represent the measurement error from the environment and resolution of the detection system were shown on each test point. The rectangles, circles and triangles with solid lines indicate the frequency change at bacteria concentrations of 1.5×10^2 CFU/mm^2, 1.5×10^4 CFU/mm^2 and 1.5×10^6 CFU/mm^2, respectively. The ME measurement biosensors have larger frequency changes at higher bacterial concentrations (i.e., More bacteria were bound to the biosensor.). The inversed triangles with a dashed line indicate the frequency change for a control biosensor at the highest bacteria concentration (1.5×10^6 CFU/mm^2), which doesn't show an obvious frequency change. This demonstrates that specific binding to the bacteria occurred on the measurement biosensors. Figure 7.8 presents SEM images of biosensors' surfaces with captured bacteria cells. These images corroborate the frequency change data and demonstrate that the ME biosensors captured more bacteria cells as the bacteria concentrations increased. The control biosensor (Fig. 7.8d) shows no non-specific binding of bacteria. This result represents the time-dependent capture of Salmonella by the ME biosensor. This *S.* Typhimurium detection experiment demonstrates that the real-time, *in situ*, quantitative detection of bacteria on watermelon surfaces has been achieved with this new surface-scanning coil detector.

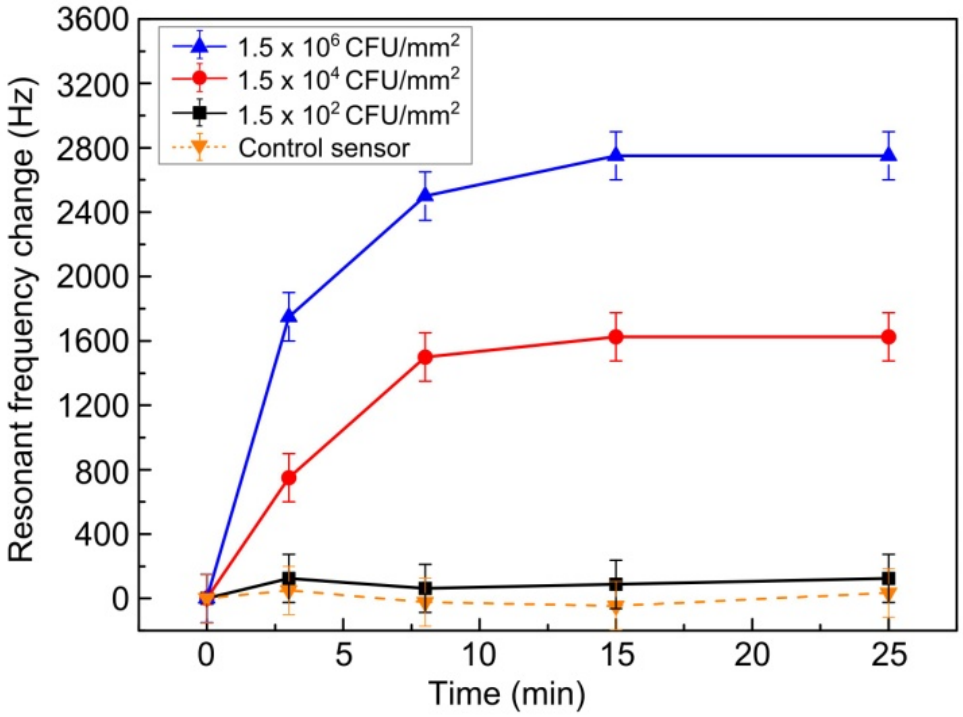

Figure 7.7 Using a surface-scanning coil detector positioned above a watermelon surface, the resonant frequency changes for ME biosensors (measurement and control biosensors) exposed to *S.* Typhimurium at different concentrations were recorded as a function of exposure time.

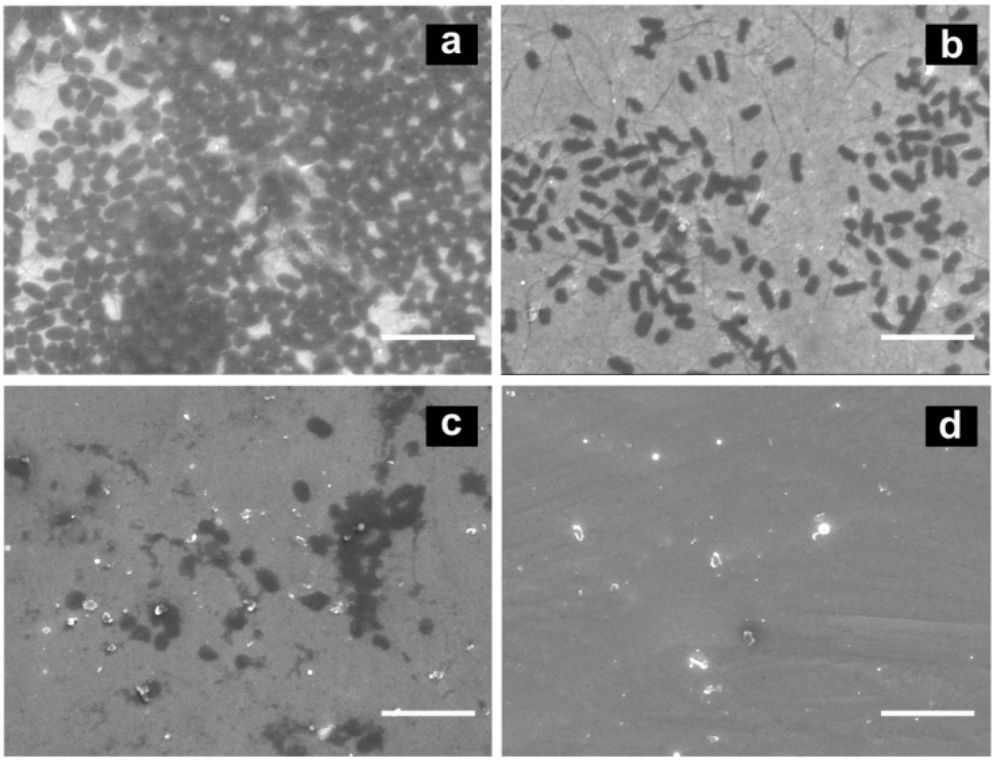

Figure 7.8 SEM images of measurement and control biosensors' surfaces after exposure to different bacteria concentrations: (a) measurement biosensor exposed to 1.5×10^6 CFU/mm^2, (b) measurement biosensor exposed to 1.5×10^4 CFU/mm^2, (c) measurement biosensor exposed to 1.5×10^2 CFU/mm^2 and (d) the control biosensor exposed to 1.5×10^6 CFU/mm^2 (Measurement bar: 5 μm; environmental humidity: 95 % RH).

7.4 Conclusions

Proof in principle of a new coil design was demonstrated. This new coil was used to excite and measure the ME biosensor outside the boundaries of the detection coil, enabling continuous measurements of ME biosensors placed upon surfaces. A gradual change of the resonant frequency was observed over time during the reaction

between an E2 phage-coated ME biosensor and S. Typhimurium on a tomato surface. Real-time, in situ detection was thus achieved with a ME biosensor. The research shows that the bacteria reaction and biosensor detection process depends on environmental humidity. The LOD was statistically determined to be lower than 1.5 × 103 CFU/mm2 with a confidence level of difference higher than 95 % ($p < 0.05$). The LOD can be improved by increasing the number of biosensors and decreasing the biosensor size [9].

Bibliography

1. S. Horikawa, D. Bedi, S. Li, W. Shen, S. Huang, I. Chen, Y. Chai, M.L. Auad, M.J. Bozack, J.M. Barbaree, V.A. Petrenko and B.A. Chin. Effects of surface functionalization on the surface phage coverage and the subsequent performance of phage-immobilized magnetoelastic biosensors, *Biosensors and Bioelectronics* 26: 2361-2367, 2011.
2. C. Liang, S. Morshed, and B. C. Prorok. Correction for longitudinal mode vibration in thin slender beams, *Applied Physics Letters* 90, 221912, 2007.
3. Y. Chai, S. Li, S. Horikawa, M. Park, V. Vodyanoy, and B.A. Chin. Rapid and sensitive detection of *Salmonella* Typhimurium on eggshells by using wireless biosensors, *Journal of Food Protection* 6, 631-636, 2012.
4. S. Li, Y. Li, H. Chen, S. Horikawa, W. Shen, A. Simonian and B.A. Chin. Direct detection of *Salmonella* Typhimurium on fresh produce using phage-based magnetoelastic biosensors, *Biosensor and Bioelectronic* 26 (4): 1313-1319, 2010.
5. M. Park, H.C. Wikle, Y. Chai, S. Horikawa, W. Shen, and B.A. Chin. The effect of incubation time for *Salmonella* Typhimurium binding to phage-based magnetoelastic biosensors, *Food Control* 26(2): 539-545, 2012.

6. I.B. Sorokulova, E.V. Olsen, I. Chen, B. Fieber, J.M. Barbaree, V.J. Vodyanoy, B.A. Chin and V.A. Petrenko. Landscape phage probes for *Salmonella typhimurium*, *Journal of Microbiological Methods* 63 (1), 55-72, 2005.
7. P. Kast and D. Hilvert. 3D structural information as a guide to protein engineering using genetic selection, *Current Opinion in Structural Biology* 7 (4): 470-479, 1997.
8. G.A. Kuzmicheva, P.K. Jayanna, A.M. Eroshkin, M.A. Grishina, E.S. Pereyaslavskaya, V.A. Potemkin, V.A. Petrenko. Mutations in fd phage major coat protein modulate affinity of the displayed peptide, *Protein Engineering, Design & Selection* 22 (10): 631-639. 2009.
9. S., Horikawa. PhD Dissertation, Auburn University. 2013.
10. R. Mead, R.N. Curnow and A.M. Hasted. *Statistical methods in agriculture and experimental biology*, Chapman & Hall/CRC press, Boca Raton, 2003.

Chapter 8

Conclusions

This work uses wireless ME biosensors for the rapid, direct and quantitative detection of *Salmonella enterica* subspecies *enterica* serovar Typhimurium on fresh food surfaces. The ME biosensor consists of an ME resonator as the sensor platform and E2 phage as the bio-recognition element. The specify test has proved E2 phage can specially bind with *S.* Typhimurium on food surfaces.

Proof in principle of a new surface-scanning coil design was demonstrated. This new coil was used to excite and measure the ME biosensor outside the boundaries of the detection coil, enabling continuous measurements of ME biosensors placed upon surfaces. A model of sensor's longitudinal vibration and an equivalent electric circuit of the detection system were constructed to theoretically evaluate the coil design. In order to explain the reason for the different signal amplitudes, a theory of mutual inductive coupling between a vibrating sensor and the coil detectors was proposed. Agreement between the model and experiment was found to be excellent. There are two types of coil detectors for design and comparison: solenoid and planar spiral coils. Based on the sensor's longitudinal vibration and the structure of the coils, the planar spiral coil detector was found to be more sensitive at detecting the coupled magnetic flux changes and gave much larger signal amplitude at resonance. In addition, both

numerical simulation data and experimental results demonstrate that the planar coil detector has dramatically improved the detection distance, which is significant for surface scanning especially with large curvature or rough surfaces. Furthermore, the ability to simultaneously detect multiple sensors on surfaces has been demonstrated.

Proof in principle has been established for the direct detection of pathogenic bacteria on fresh fruits and vegetable surfaces by this new technique. A gradual change of the resonant frequency was observed over time during the reaction between an E2 phage-coated ME biosensor and *S.* Typhimurium on fresh food surfaces. Real-time, *in situ* detection was thus achieved with a ME biosensor. Unlike previous studies on the detection of bacteria in solutions, the methodology in this work employs direct placement of the biosensors on the contaminated food surface and eliminates any preceding sampling procedures facilitated by the wireless nature of detection. This new technique eliminates time-consuming and costly sample selection and preparation.

For the bio-experiment of *S.* Typhiumurium detection on food surfaces with handheld surface-scanning detector, the following conclusions were discussed:

1. The bacteria reaction and biosensor detection process depends on environmental humidity. A high humidity environment is desired for bacterial cells' movement and binding.
2. The curvature and roughness of the food surfaces need to be considered for the bacteria detection.

3. The LOD was statistically determined to be lower than 1.5×10^3 CFU/mm^2 with a confidence level of difference higher than 95 % ($p < 0.05$).
4. Detection distance and signal amplitude were improved by the planar spiral coil detector. In addition, multiple biosensors detection simultaneously was achieved.

With development of the new coil detector and ME biosensors, scanning of the surfaces of different foods *in situ* for surface bacterial contamination becomes a reality.